Materials, instrumentation and techniques for the detection of Special Nuclear Material and Radioactive Sources: EU project MODES_SNM

Direttore della Scuola: Ch.mo Prof. Andrea Vitturi
Supervisore: Ch.mo Prof. Giuseppe Viesti

Dottorando: Davide Cester

Contents

List of Figures

List of Tables

Executive summary

English

MODES_SNM project is part of the European Union effort to promote research and innovation in strategic topics; it includes seven participants from five different countries. The project aimed to carry out technical research in order to develop a prototype for a mobile, modular detection system for radioactive sources and Special Nuclear Materials (SNM). The project's main goal was to deliver a tested prototype of a modular mobile system capable of passively detecting weak or shielded radioactive sources with accuracy higher than that of currently available systems.

The R&D involved in the project aimed at designing, constructing and testing robust, safe, and lightweight high pressure cells with an advanced read-out system, to be used as basic components of the modular mobile system. These innovative cells use ^{4}He and Xe as scintillation materials, exploiting the potential of noble gases in the field of radiation detection. Furthermore, a patented technology enabled the simultaneous detection of fast and thermal neutrons in the same detector, providing additional information on the possible presence of shielding around neutron sources. The final detector configuration for MODES_SNM prototype includes 8 ^{4}He fast neutron tubes, 2 ^{4}He thermal neutron tubes, 1 xenon gamma ray tube and 1 NaI(Tl) gamma ray crystal.

A suitable Information System has been developed at Università degli Studi di Padova to manage the detectors, integrate and analyze the data, and provide to the user simple informations about the results of the inspections. The prototype was commissioned under laboratory conditions at NCBJ, a renowned European research establishment, then the detectors and the front-end electronics were mounted inside a van. Finally, a series of demonstrations took place in an on-field campaign driven by the end-user group established in the project.

I have been part of MODES_SNM collaboration from the kickoff meeting through to its successful conclusion. Since our group in Padova was responsible for the entire Information System I have been heavily involved in developing the prototype's system for acquisition and real-time analysis. During these months I had also the opportunity to participate to the first trials of the new detectors at Arktis in Zürich. Once this task was concluded I collaborated to the system commissioning, working two weeks at NCBJ laboratories in Warsaw, and then I followed the van to Rotterdam for the field tests, where I spent a couple of days deploying the system and inspecting real radioactive cargos and goods.

While working on MODES_SNM I also partecipated to other studies on detectors, electronics and data analysis, some of which resulted in publications.

Project MODES_SNM concluded with full success on June 30th, 2014. Not only all the project milestones were achieved, but the prototype was completed on time and showed good performances. The technical requirements defined at the beginning of the project have been fulfilled, and during the demonstration tour the end users showed great appreciation to the final result of the work, to the satisfaction of all the Consortium partners. The project has been positively evaluated by EU officials, from the point of view of both the organization and the results. The prototype is now being developed at an industrial level by one of the project participants; an agreement has been signed with Università di Padova for licensing the software written within the project.

Italiano

Il progetto MODES_SNM è parte dello sforzo da parte dell'Unione Europea per promuovere la ricerca e l'innovazione in settori considerati strategici; include sette partecipanti da cinque diversi paesi. Il progetto punta a sviluppare una attività di ricerca per lo sviluppo di un sistema mobile e modulare per la rivelazione di sorgenti radioattive e materiale speciale nucleare (SNM). L'obiettivo principale è la realizzazione di un prototipo funzionante capace di rivelare in modo passivo sorgenti deboli o schermate con precisione maggiore dei sistemi attualmente disponibili.

La ricerca e sviluppo svolta all'interno del progetto mirava alla costruzione di celle ad alta pressione robuste e leggere con un sistema di read-out avanzato, da usarsi come componenti di base del sistema mobile modulare. Queste celle innovative usano ^{4}He e Xe come scintillatori, sfruttando il potenziale dei gas nobili nel campo della rivelazione di radiazione. Inoltre una tecnologia brevettata consente la rivelazione simultanea dei neutroni veloci e termici, fornendo così informazioni aggiuntive sulla possibile presenza di schermi intorno alle sorgenti. La configurazione finale dei rivelatori del prototipo di MODES_SNM include 8 tubi ad ^{4}He per neutroni veloci, 2 tubi ad ^{4}He per neutroni termici, 1 tubo a xenon ed 1 cristallo NaI(Tl) per radiazione gamma.

Un apposito Sistema Informatico (IS) è stato sviluppato presso l'Università degli Studi di Padova per la gestione dei rivelatori, l'aggregazione e l'analisi dei dati, e per fornire all'operatore semplici informazioni riguardo i risultati delle ispezioni. Il prototipo è stato collaudato persso il centro NCBJ, una installazione di ricerca conosciuta in tutta Europa, quindi i rivelatori e l'elettronica sono stati installati dentro un van. Infine, una serie di dimostrazioni ha avuto luogo durante una campagna "sul campo" gestita dal gruppo di utilizzatori finali costituito all'interno del progetto.

Personalmente ho fatto parte della collaborazione di MODES_SNM dal meeting inaugurale fino alla sua felice conclusione. Essendo il gruppo di Padova responsabile per il Sistema Informatico sono stato fortemente coinvolto nello sviluppo del sistema di acquisizione ed analisi del prototipo. Durante questi mesi ho avuto anche l'opportunità di partecipare alle prime prove di qualificazione dei rivelatori presso la sede di Arktis a Zurigo. Una volta conclusa questa attività ho collaborato ai test di collauto, lavorando due settimane ai laboratori del centro NCBJ di Varsavia, quindi ho seguito il van a Rotterdam per i test sul campo, dove ho passato un paio di giorni attivando il sistema ed ispezionando carichi reali in transito attraverso il porto.

Durante il lavoro su MODES_SNM ho anche partecipato ad altri studi su rivelatori,

elettronica ed analisi dati, alcuni dei quali hanno dato origine a pubblicazioni.

Il progetto MODES_SNM si è concluso con pieno successo il 30 giugno 2014. Non solo ha raggiunto tutti gli obiettivi, ma il prototipo è stato completato per tempo ed ha mostrato delle buone prestazioni. I requisiti tecnici definiti inizialmente sono stati rispettati, e durante le dimostrazioni gli utenti finali hanno espresso grande apprezzamento per il risultato finale del nostro lavoro, con soddisfazione di tutti i partecipanti del Consorzio. Il progetto è anche stato valutato positivamente dai funzionari europei incaricati della valutazione, sia sotto il punto di vista della gestione che dei risultati. Attualmente il prototipo sta venendo sviluppato a livello industrial da uno dei partecipanti; è stato raggiunto un accordo con l'Università di Padova per la licenza del software scritto durante il progetto.

Chapter 1

Introduction

MODES_SNM project is part of the European Union effort to promote research and innovation in strategic topics; its goal is the design, construction, testing, and qualification of a mobile system for the detection of Special Nuclear Material (SNM). A short summary of the boundary conditions associated to nuclear threats is presented in this chapter; it is followed by an overview of the project and a description of my personal contribution to this research.

1.1 Motivation

Nowadays, the construction of a nuclear weapon does not pose strong technical problem, since the know-how has been in the public domain for several decades [1]. The only barrier preventing a terrorist group from performing a nuclear attack is the difficulty to access to a sufficient amount of special nuclear material (SNM) as highly enriched weapon-graded uranium (WGU) or weapon-graded plutonium (WGP), as defined in the next section.

Stockpiles of SNM should be stored in high-security facilities, but the "nuclear club" of nations who possess nuclear technologies and materials has widened compared to Cold War years, and a black market of procurement networks is being formed [2]. In such situation, the second line of defense will be the ability to detect special nuclear material (SMN) while in transit through the civilian transportation infrastructure.

Today's approach to nuclear detection relies primarily on fixed inspection portals placed at the national borders (the so-called "port of entry") or in other transportation nodes; while their presence still represents an advancement in security procedures, doubts have been rised about the possibility that highly shielded or masked SNM might not be detected by those portals. A real improvement would be reaching the capability to detect nuclear materials with improved detection systems anywhere within the transportation infrastructure; that would deter nuclear terrorist attempting to pursue construction and deployement of a nuclear weapon. Hence, last years have seen a large extension of research projects to the field of mobile instruments, to which this work belongs.

1.2 Definition of the threats

A great variety of items are considered to be *radiological* or *nuclear* threats; the nomenclature "radiological" refers to any radioactive material usable for radiological terrorism including

RDDs ("dirty bombs"), while "nuclear" refers specifically to neutron emitting materials, i.e. transuranic actinides such as uranium and plutonium isotopes. These items can be categorized in four classes:

1. Operative nuclear weapons

2. Improvised Nuclear Devices (IND)

3. Special Nuclear Material (SNM) that might be used to realize an IND

4. Radioactive material to be used inside Radiological Dispersion Devices (RDD)

Radioactive isotopes in each of the four classes emit gamma radiation. Neutron radiation may be emitted too, but not necessarily in substantial quantities. An RDD may contain radiological material emitting no neutron radiation at all, some uranium isotopes emit negligible amounts of neutron radiation, and most plutonium isotopes are known to be strong neutron sources.

Detectable signatures of RDD components

Generally speaking, RDD components (item 4 above) present no detection problems, even if shielded. In fact, in order to have a significant contamination potential, the activity of a Radiological Dispersive Device is expected to be at the 10^{13} Bq level.

Detectable signatures of SNM

SNM (items 1-3 above) may present non trivial detection problems. Special Nuclear Material is often characterized as:

- Weapons Grade Uranium (WGU), typically having a composition similar to the following:

$$^{234}\text{U } 1\%, \ ^{235}\text{U } 93\%, \ ^{238}\text{U } 6\%$$

   The IAEA defines 25 kg of WGU as a "significant quantity";

- Weapons Grade Plutonium (WGPu), typically having a composition similar to the following:

$$^{239}\text{Pu } 93\%, \ ^{240}\text{Pu } 6\%$$

   The IAEA defines 8 kg of WGPu as a "significant quantity".

Besides depending on the SNM composition and quantity, a nuclear device's radiation emission also depends on further factors such as geometry and tamper material.

The estimates presented here are related to the weapon model proposed by S. Fetter [3], more conservative with respect to the IAEA standards. The Fetter model is based on the assumption of a WGU loaded with 12 kg of highly enriched uranium or a WGPu with 4 kg of plutonium. The weapon model is illustrated in Fig. 1.1, where the radioactive core is surrounded by a first shell of 2 cm beryllium acting as reflector and a second shell of 3 cm tungsten or depleted uranium (DU) acting as tamper material. The tamper material has an influence on the emitted radiation rate, as can be seen from Table 1.1.

Tamper material	WGU n rate [n/s]	WGU γ rate [γ/s]	WGPu n rate [n/s]	WGPu γ rate [γ/s]
Tungsten	~30	~30	$\sim 4 \times 10^5$	$\sim 10^3$
Depleted uranium	~1400	$\sim 10^5$	$\sim 4 \times 10^5$	$\sim 10^5$

Table 1.1: Tamper material influence on the emitted radiation rate. From [3]
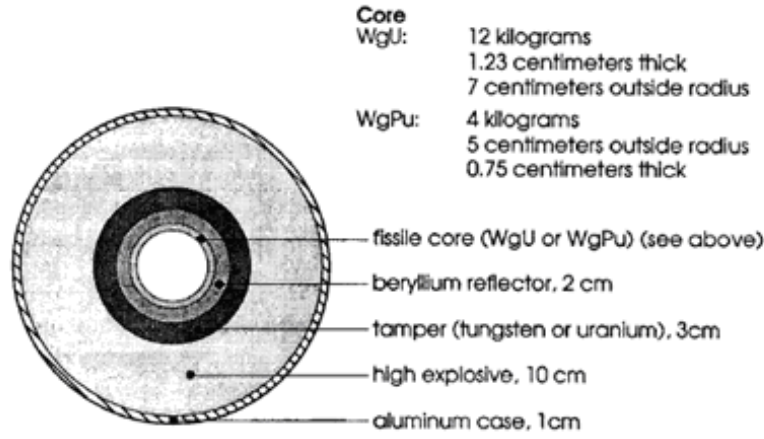
Figure 1.1: Weapon model used for signature estimation

Unless a genuine spectrometric capability is implemented, the gamma ray spectrum from WGU and WGPu can easily be masked by radioactive substances of common use in industry and by Natural Occurring Radioactive Material (NORM).

Irrespective of the high gamma ray flux, the detection of WGU and WGPu is often driven by neutron detection, essentially because natural neutron backgrounds are typically 3 orders of magnitude lower than natural gamma background. Moreover, the majority (>95%) of all neutrons emitted by SNM are so-called fast neutrons, with energies above 200 keV; the possibility to distinguish fast from thermal neutrons enhances the discrimination against natural background sources. This potential has been exploited during the project.

Neutron radiation signature

Neutron emission from the core material, including spontaneous fission and alpha particle induced neutron emission, is about 20 and 2×10^5 neutrons/second for the 12 kg and 4 kg of WGU and WGPu respectively. This is the characteristic neutron emission from bulk SNM. In case of an IND like that in Fig. 1.1, the neutron yield also depends on the type of tamper material. In the case of the device using 12 kg of WGU, the total emission at surface is about 30 neutrons/second when tungsten is used and 1400 neutrons/second when depleted uranium is used, due to neutron multiplication in these materials. Neutron emission remains very high in the case of WGPu devices for both tamper materials (about 4×10^5 neutron/second). Natural neutron backgrounds are typically three orders of magnitude lower than natural gamma backgrounds.

The majority (>95%) of all neutrons emitted by SNM are fast neutrons. Shielding generally has a thickness-dependent effect on the fast neutron component. Fig. 1.2 from

[4] shows the shielding dependency of the fast neutron fraction within the total neutron signature.
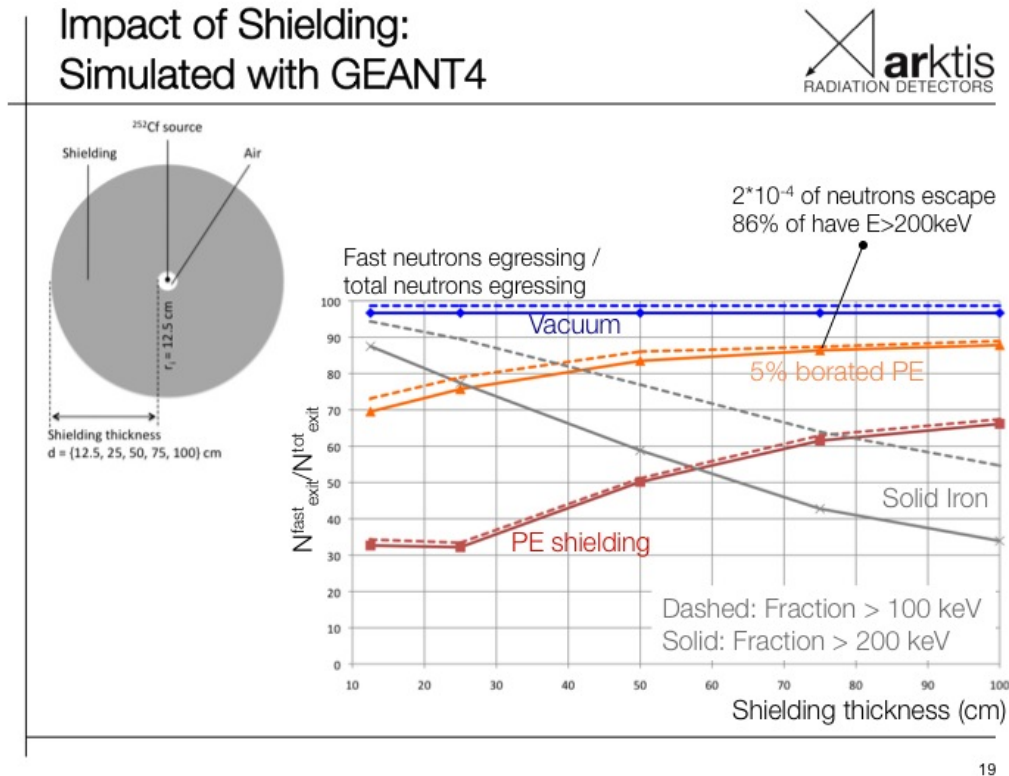
Figure 1.2: Plot showing the effect of shielding on the fraction of fast neutrons escaping an IND device described above based on simulations using GEANT4. From [4]

Gamma radiation signature

Neutron emission is accompanied by an important yield of gamma rays. As shown in [5], most of the isotopes of interest emit on average about 6.5 gamma rays of $\sim$1 MeV energy (per fission). The emission is high when DU tamper is used (about 10^5 gamma/second) for both WG materials, but it is significantly reduced when tungsten tampers are used, which act as a gamma ray shield and reduce emission to 30 gamma/second for WGU and 1000 gamma/second for WGPu.

Some characteristic gamma-rays are often used to identify each relevant isotope. For example, ^{235}U is normally identified by looking at the 186 keV transition. However, it has been reported that such low-energy lines are easily shielded or even masked by other radioactive substances of common use in industry (such as ^{137}Cs), thus making the identification of ^{235}U by only its gamma-ray signature difficult.

Signature strengths relative to background

The detection of WGPu is generally based on neutron emission. More difficult is the detection of WGU, especially when tungsten rather than DU tampers are utilized.

When searching for neutrons as the signature of SNM, the background due to neutrons produced in the interaction of cosmic rays at sea level is about 10^{-2} neutrons/second/cm^2,

increasing significantly with altitude.

In such background conditions and with a hypothetical neutron detector with 25% efficiency and 10 cm diameter, it is quite easy to detect the strong neutron yield from WGPu even at large stand-off distances (several meters), whereas the detection of WGU is more difficult, especially when the tungsten tamper is used. In the latter case it is only possible do detect the neutron yield at very close distance (at contact).

1.3 MODES_SNM: an EU FP7 Project

Framework Programmes are the European Union's main instrument to finance research and innovation [6]. Funding is determined on the basis of calls for proposals and a peer review process. The Framework Programmes for Research have two main strategic objectives:

- to strengthen the scientific and technological base of European industry;

- to encourage its international competitiveness, while promoting research that supports EU policies.

The *Seventh Framework Programme for Research and Technological Development* (FP7) ran from 2007 to 2013, with a budget of over 50 billion Euro. In order to complement national research programmes, activities funded from FP7 must have a "European added value". One key aspect of the European added value is the transnationality of many actions; research projects are carried out by consortia which include participants from different European (and other) countries, therefore fellowships in FP7 require mobility over national borders.

MODES_SNM proposal was submitted after the Security Research Call 4 (FP7-SEC-2011-1), and directly addresses the topic SEC-2011.1.5-1, "*Development of detection capabilities of difficult to detect radioactive sources and nuclear materials*". The project was selected and funded in 2011 as number #284842. It started on 1st January, 2012 and ended on 30th June, 2014; it featured a total budget of 3 282 051.20 Euro, of which 2 411 633.00 were the EU contribution.

The project aim was to carry out technical research in order to develop a prototype for a mobile, modular detection system for radioactive sources and Special Nuclear Materials (SNM). To maximize the detection capability for SNM the project developed new detectors for fast and thermal neutrons, as well as gamma-rays, based on the technology of high pressure scintillation cells. The project's main goal was to deliver a tested prototype of a modular mobile system capable of passively detecting weak or shielded radioactive sources with accuracy higher than that of currently available systems.

The R&D involved in the project aimed at designing, constructing and testing robust, safe, and lightweight high pressure cells (Chapter 2) with an advanced read-out system (Chapter 3) to be used as basic components of the modular mobile system. A suitable Information System has been developed to manage the detectors, integrate and analyze the data, and provide to the user simple informations about the results of the inspections (Chapter 4). Finally, the prototype was commissioned under laboratory conditions at NCBJ, a renowned European research establishment (Chapter 5), and demonstrated in an on-field campaign driven by the end-user group established in the project (Chapter 6).

1.3.1   Strategic impact

To date there is no coordinated European strategy for the interdiction of radiological and nuclear threats at the European border. The deployment of radiation screening technology in Europe is to an overwhelming extent driven by US strategies such as the Megaports Initiative, aimed at ensuring Port of Departure screening of goods destined for the United States. While some EU member states have developed their own radiological/nuclear screening strategies, these often rely heavily on the same technologies and architectures deployed in the US.

This lack of coordinated European effort is in part due to a lack of operationally viable technology: current technologies are prone to nuisance alarms caused by Naturally Occurring Radioactive Material (NORM), while at the same time having a low sensitivity for well-shielded Special Nuclear Material (SNM). European spending for R&D relevant to border protection technologies is substantially lower than equivalent spending in the US, reducing the likelyhood for Europe to develop and deploy proprietary technologies in this domain.

This project has three independent aspects that go one step away from European dependency on foreign technologies and strategies:

- development of a new technology capable of offering a substantially higher sensitivity for SNM by exploiting the fast neutron signature, in a novel technique originating in European fundamental research programs;

- development and testing of an ameliorated screening architecture. The technology will be tested for its capability of offering single stage screening, rather than conventional two stage screening with permanently installed portal monitors, and subsequent secondary screening with separate devices;

- reduction of EU technology's reliance on scarce and imported ^{3}He (Sec. 2.3.2).

1.3.2   Developed technologies

The state of the art in the detection of illicit radiological materials often includes two separate technologies for the detection of neutrons and gamma radiation. MODES_SNM developed a suite of detectors based on one common technology (pressurized noble gas) able to cover the full range of relevant radiation types (Table 1.2). In particular, the addition of fast neutron detectors to the system provides unprecedented sensitivity for shielded SNM.

	State of the art	**MODES_SNM**
Gamma rays	PVT or NaI(Tl)	Pressurized Xe scintillator
Thermal neutrons	^{3}He proportional counter	^{4}He scintillator with Li converter
Fast neutrons	none	^{4}He scintillator

Table 1.2: Detection technologies developed in MODES_SNM.

Sec. 2.2.3 and Sec. 2.3.4 are dedicated to the description of the detectors developed and used in MODES_SNM, while Sec. 3.3 describes the advancements made in the field of waveform digitizers and pulse shape analysis.

Together with the optimization of high pressure detectors, also R&D studies were performed on silicon photomultipliers (SiPMs [7, 8]) as viable replacement of standard photo-

multiplier tubes (PMTs). Within Work Package 2 Arktis and University of Insubria worked together in the development of a prototype based on SiPMs. The prototype was assembled and tested with very promising results, but due to the relatively tight time schedule it was decided not to incorporate this technology in the final MODES_SNM demonstrator. Therefore, SiPM application to MODES_SNM noble gas detectors are not described in this work; further details can be found in publications originated during MODES_SNM collaboration [9].

1.3.3 Project organization
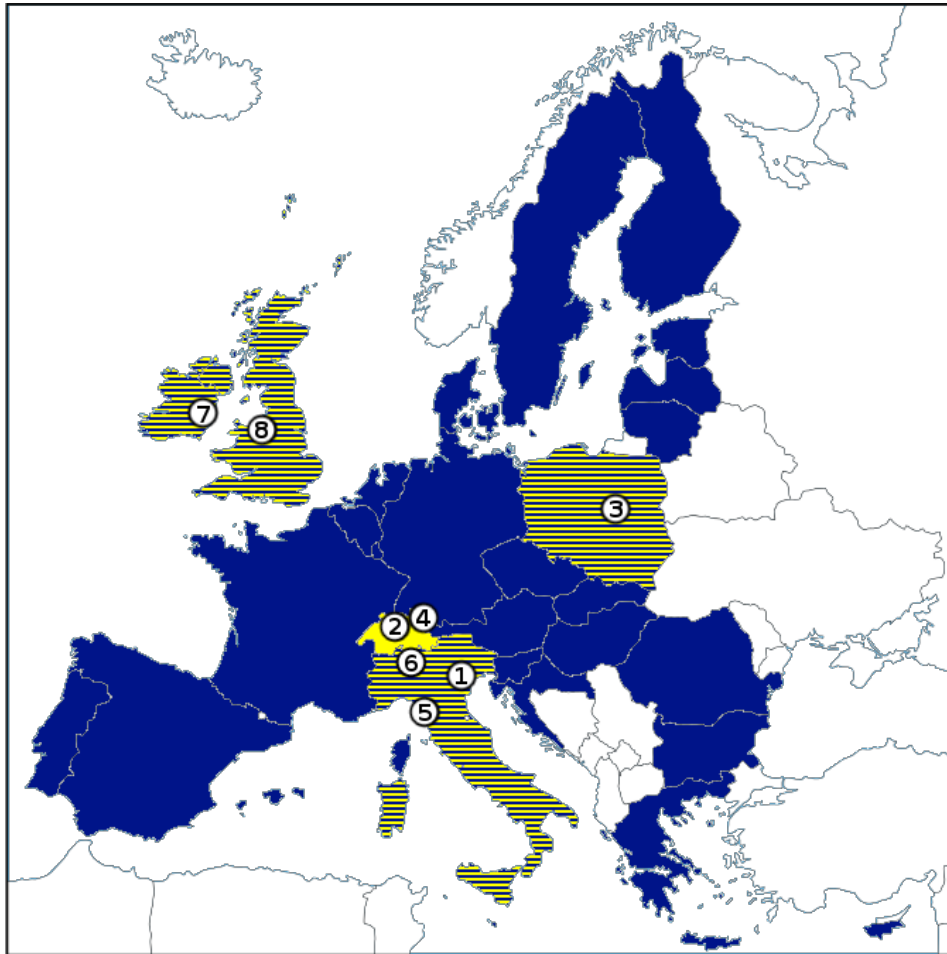
Figure 1.3: Map of MODES_SNM countries and participants. EU countries = blue, Consortium partner countries = yellow. Partners: 1) UNIPD, 2) ARKTIS, 3) NCBJ, 4) ETH, 5) CAEN, 6) UINS, 7) RC, 8) UNILIV

MODES_SNM Consortium includes seven participants from five different countries:

1. Università degli Studi di Padova - Group on Interdisciplinary Application of Neutron Physics (UNIPD, Italy)

2. Arktis Radiation Detectors Ltd. (ARKTIS, Switzerland)

3. Narodowe Centrum Badań Jądrowych - National Centre for Nuclear Research (NCBJ, Poland)

4. Eidgenössische Technische Hochschule Zürich - Physics Department (ETH, Switzerland)

5. Costruzioni Apparechiature Elettroniche Nucleari C.A.E.N. Spa (CAEN, Italy)

6. Università degli Studi dell'Insubria - Department of Physics and Mathematics (UINS, Italy)

7. Office of the Revenue Commissioners - Irish Tax and Customs authority (RC, Ireland)

8. The University of Liverpool - Physics Department (UNILIV, United Kingdom)

It was agreed that the most efficient way to perform the field demonstration was to prepare the MODES_SNM prototype as a van-mounted system that could be operated by end-user as a stand alone system as well as in comparison with existing portals or vehicle mounted system. An invitation was extended to members of the EU Customs 2013 Detection Technology Expert Group to participate in the field trials; Dutch, Irish and UK Customs agreed to participate.
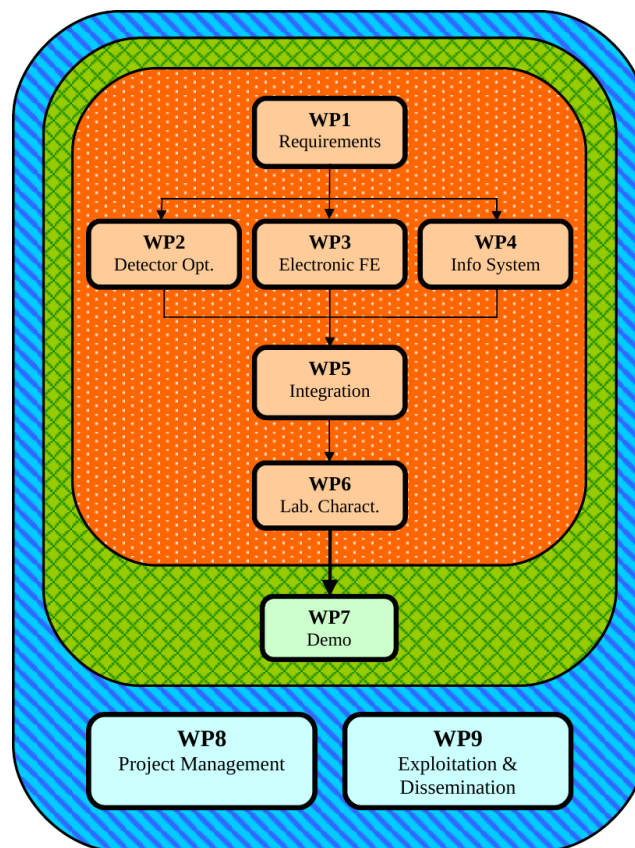
Figure 1.4: MODES_SNM PERT diagram

The structure of the project is mainly driven by the development and testing of the prototype. The project is divided into work packages (WPs) and tasks linked to the different parts of the prototype and to the different phases of its development. The highest level of division is based on the latter principle according to which five main classical stages can be identified: a) requirements specification, b) design & development, c) integration, d) laboratory tests and certification, and e) final field demonstration. The design & development

phase has itself been sub-divided into three parts corresponding to the three major components or modules of the prototype: i) Detector modules for the portable system, ii) Front-end electronics and data acquisition system, iii) Information System (IS) which is the software part of the prototype, including data integration, the decision-making algorithm, and the human interface. This leads to the first seven WPs of the MODES_SNM project, WP1 to WP7; WP8 includes the project management activities, and WP9 includes Exploitation & Dissemination activities (see Fig. 1.4 and Table 1.3).

	Work package	Leader	Duration (months)	
WP1	Requirements	ETH	3	(M1 - M3)
WP2	Detector optimization	ARKTIS	17	(M4 - M20)
WP3	Electronic Front-End	CAEN	17	(M4 - M20)
WP4	Information System	UNIPD	17	(M4 - M20)
WP5	Integration	UNILIV	9	(M15 - M23)
WP6	Laboratory Characterization	NCBJ	7	(M21 - M27)
WP7	Demonstration	RC	6	(M25 - M30)
WP8	Project Management	UNIPD	30	(M1 - M30)
WP9	Exploitation & Dissemination	ARKTIS	30	(M1 - M30)

Table 1.3: Details on MODES_SNM Work Packages

1.3.4 Objectives and performance requirements

The prototype detection system is the major deliverable of the project. It had to satisfy two major requirements:

- being usable by emergency responders in the field filling the gap between Radiation Portal Monitors and hand-held devices;

- improving the state of art in detection of radioactive and Special Nuclear Material in terms of sensitivity for shielded SNM.

While the former was easily addressed by working together with end-users since the early stages of the project, the latter involves a precise assessment of the system capabilities. Therefore, a detailed set of performance requirements was developed during WP1. These requirements include the sensitivity to radiation sources moving at walking speed; this will enable MODES_SNM prototype to be used to monitor travelling goods as well as to inspect static cargos, increasing the operational flexibility of the system.

International standards

To qualify the performance of a measurement system one must refer to international standards and guidelines. IAEA classification of the instruments [10] includes:

- fixed radiation portal monitors (RPMs);

- spectrometric Radiation Portal Monitors (SRPMs), like RPMs but with real-time radionuclide identification;

- personal radiation detectors (PRDs);

- hand-held radionuclide identification devices (RIDs);

- hand-held neutron search devices (NSDs);

- portable radiation scanners (PRSs).

MODES_SNM system is certainly close to the Portable Radiation Scanner (PRS), which is defined as a device designed mainly for covert detection of unauthorized or undeclared activities. In addition to covert detection, these instruments are useful for radiological security at locations where the standard approach for deployment of fixed installed and hand-held instruments is not feasible. This includes, as an example, major public events or other venues, as well as in patrolling green borders. The useful feature of this instrument is rapid radionuclide identification, providing advantages for monitoring at locations where the occurrence of radiopharmaceutical detections is high (e.g., major public events, airports, and other venues). For patrolling a green borders or urban areas, the embedded satellite navigation system is an essential feature of the instrument.

In addition to IAEA guidelines, IEC (International Electrotecnical Commission) defined a set of standard for detection systems dedicated to the monitor of ionizing radiations in various scenery. Two of them are of particular interest to our project: IEC 62244 (Installed radiation monitors) [15] and IEC 62327 (Hand-held instruments) [16]. The main difference between the two standards is that hand-held devices are required to detect not only the presence of a radiation source, but also to be able to identify it.

Work Package 1 was devoted to the quantitative definition of MODES_SNM performance requirements; since none of the official standards from IAEA, IEC or other institutions covered all the features foreseen for the prototype[1], the requirements have been elaborated by referring to several publications defining the state-of-the art for different types of radiation measurement devices (e.g. [10, 11, 12, 14, 15, 16, 17]).

What follows is a brief description of MODES_SNM requirements, as defined in WP1. The qualification tests are described in Chapter 5, while the results are summarized in Chapter 7.

Probability of detection (PD) and False alarm rate (FAR)[2]

IAEA defines for PRS devices a Probability to detect (PD, minimum acceptable number of alarms) of 0.9, or 96 per 100 trials, and a Probability of false alarm (FAR, Maximum acceptable number of alarms) of 0.001 (or 1 in 1 hour). MODES_SNM requirements incorporated both IAEA recommendations.

Gamma sensitivity

MODES_SNM prototype shall satisfy the IAEA requirement of generating alarms when the ^{241}Am, ^{137}Cs and ^{60}Co gamma ray sources are moving with a speed of 0.5 m/s (1.8 km/h) at a distance of closest approach between the source and the front face prototype of 1 m. The dose rate must be 0.05 μSv/h on the face of the detector; during laboratory tests the distance of closest approach can be varied to compensate the activity of available sources.

---

[1]One of the first known documents dedicated to van-mounted devices [13] was published in August 2013, 20 months after MODES_SNM kickoff.

[2]PD and FAR are defined in Appendix A.

For comparison, the IEC 62237 for hand held instruments is requiring that the instrument must alarm within 3 s when it is exposed to a radiation level of 0.5 μSv/h, ten times higher.

Neutron sensitivity

MODES_SNM prototype shall satisfy the IAEA requirement of generating a neutron alarm for a ^{252}Cf source emitting 1.2×10^4 neutrons/s and moving with a speed of 0.5 m/s (1.8 km/h) at a distance of closest approach between the source and a PRS of one meter. This requirement translate in a static fluence rate of 0.1 n/cm^2/s at one meter distance.

Single nuclide identification

The instrument shall be able to identify every nuclide in the instrument's library. If the nuclide is not in the instrument's library it should be reported as unknown. The time to acquire and analyse data should not exceed 60 seconds at an exposure rate from 0.05 μSv/h up to 5.0 μSv/h.

As a comparison, IEC 62327 is requiring for hand held instrument the identification of more than 20 single or mixed, unshielded or shielded radionuclides producing 0.5 μSv/h above gamma background. At least 90% of recognition trials shall be successful, with a measurement time of 1 or 2 minutes depending on the type of sources (un-shielded or shielded).

Radionuclide identification demonstrates the instrument's knowledge about specific signatures for radioactive materials to be identified. There are two important factors to consider when making the decision to include particular radioactive materials in the instrument library: the importance of the material from the Nuclear Security point of view (i.e., material posing potential threat if misused) and the frequency/probability of appearance at borders. Consequently, the two groups of radionuclides described below are those that are recommended by IAEA to be included into any instrument's library:

GROUP A) high concern nuclides:

- Special Nuclear Material and associated nuclides: ^{232}U, ^{233}U, ^{235}U, ^{238}U, ^{239}Pu, ^{240}Pu, ^{241}Pu, ^{237}Np;

- high activity industrial and medical sources: ^{238}Pu, ^{90}Sr, ^{60}Co, ^{137}Cs, ^{192}Ir, ^{75}Se, ^{241}Am;

- nuclides specific to spent fuel: ^{106}Ru/^{106}Rh, ^{134}Cs, ^{144}Ce/^{144}Pr, ^{152}Eu/^{154}Eu;

GROUP B) low concern nuclides. The Group B of low or no risk nuclides includes Naturally Occurring Radioactive Material (NORM), radiopharmaceuticals and/or those radionuclides that are not produced in quantities that allow their use as Radiological Dispersion Devices:

- industrial nuclides: ^{226}Ra, ^{109}Cd, ^{99}Mo, ^{57}Co, ^{133}Ba;

- radiopharmaceuticals, low dose sealed source radiotherapy sources and permanent implants: Positron Emission Tomography (PET) sources (^{11}C, ^{13}N, ^{15}O, ^{18}F), ^{51}Cr, ^{67}Ga, ^{99m}Tc, ^{123}I, ^{131}I, ^{133}Xe, ^{153}Sm, ^{201}Tl;

- naturally occurring radioactive material (NORM): ^{40}K and other natural radionuclides of ^{238}U- and ^{232}Th- decay series.

The identification library built for MODES_SNM had to be restricted to the sources available at NCBJ, where the commisioning tests were held. A list of the sources and their activities is reported in Table 5.6.

Multiple nuclide identification and masking

The MODES_SNM prototype should be able to identify the above indicated Group A nuclides under the above conditions with NORM or radiopharmaceuticals being simultaneously present. Partial exposure from the masking radioactive material should not exceed 1.0 μSv/h.

Radiation interference

Neutron detection instruments shall not misinterpret gamma radiation as neutrons. Neutron detectors must be insensitive to gamma radiation, as illicit trafficking incidents involving detection of neutrons require a higher level of response. Instruments featuring neutron detection shall not trigger a neutron alarm when exposed to a ^{60}Co gamma ray source producing a dose equivalent rate averaged over the face of the neutron detector of 100 μSv/h. The instrument shall continue to respond to neutrons as specified in the presence of gamma radiation. In case of ^{60}Co source and ^{137}Cs, the required dose rate is 4600 and 7800 photons/s/cm^2, respectively. MODES_SNM prototype shall satisfy this requirement.

1.4   My role within the project

I have been part of MODES_SNM collaboration from the kickoff meeting through to its successful conclusion. Since our group in Padova was responsible for the entire Information System (WP4) at the beginning I was heavily involved in developing the prototype's system for acquisition and real-time analysis (Chapter 4). During WP4's 17 months I had also the opportunity to participate to the first trials of the new detectors at Arktis in Zürich. Once WP4 was concluded I collaborated to the system commissioning, working two weeks at NCBJ laboratories in Warsaw (Chapter 5), and then I followed the van to Rotterdam for the field tests, where I spent a couple of days deploying the system and inspecting real radioactive cargos and goods (Chapter 6).

While working on the project I also partecipated to other studies on detectors, electronics and data analysis, some of which resulted in publications; they are described in Chapter 8.

Chapter 2

Detectors and materials

The detection of radiation and the identification of radioactive materials heavily rely on device performances; in the last years greats efforts have being made in the search for new materials and techniques, rapidly improving the state-of-the-art. MODES_SNM is part of this worldwide research, and its most innovative part is represented by gaseous detectors developed by Arktis.

The final detector configuration for MODES_SNM prototype includes the following devices:

- 8 ^{4}He fast neutron tubes

- 2 ^{4}He thermal neutron tubes

- 1 Xe gamma ray tube

- 1 NaI(Tl) gamma ray crystal

The first three types are new detectors; they are partly based on previous technologies, but have been developed to their present level within the project. They are described in Sec. 2.2.3 (xenon gamma detectors) and Sec. 2.3.4 (^{4}He neutron detectors).

2.1 Scintillators for radiation detectors

Scintillation is the process of converting the energy of ionizing radiation into light, typically in the visibile or UV ranges; the light emitted by a scintillator can easily be collected by a light sensor, generally a photomultiplier tube (PMT), and converted to an electric pulse suitable for electronic analysis.

Many scintillating materials have been discovered and studied, but only few of them have proved to be suitable for radiation detection; several properties contribute to qualify a good scintillator material. The conversion efficiency should be as high as possibile, and so the linearity between energy deposit and light yield over a range as wider as possibile; also the conversion process must be short enough in time to allow the generation of fast electrical pulses. In addition, the material must be transparent to its own scintillation light to avoid poor light collection, and it should be possibile to manufacture it in the typical sizes and shapes used in radiation detection application; lastly, its reflective index should match that of glass ($\sim$1.5) for good optical readout coupling.

Any material will hardly satisfy all of the aforementioned conditions; each scintillator is the result of a compromise between these requirements, depending on the specific application.

Many scintillators are based on organic molecules with special simmetry properties; their electron bondings are known as π-electron structure. For one of these molecules we can distinguish three different main processes that can lead to light emission:

- *fluorescence*: the prompt emission of visibile radiation from a substance following its excitation by some means; it is produced by deexcitation transitions between internal levels with the same multiplicity (singlet/triplet levels);

- *phosphorescence*: an emission slower than fluorescence. Corresponding transitions involve a change in multiplicity before the deexcitation can occur, thus the longer decay time;

- *delayed fluorescence*: has the same emission spectrum as prompt fluorescence, but is characterized by much longer emission time; corresponding transitions involve a double change in multiplicity, and for this reason they are suppressed.

Fig. 2.1 shows an example of gamma transitions in an organic molecule.
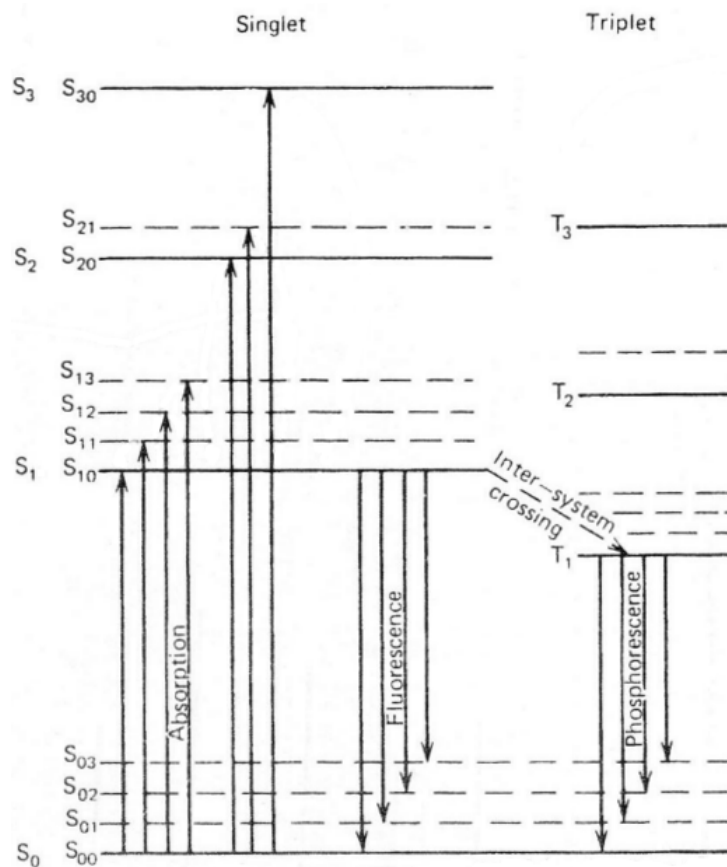
Figure 2.1: Energy levels of an organic molecule with π-structure. From [19]

Scintillating materials can be divided in *organic* and *inorganic* scintillators according to their chemical composition; the detectors that I have studied within my PhD activities are listed in table Table 2.1.

Detector	Family	Purpose
Xe	Inorganic noble gases	γ spectroscopy
NaI(Tl)	Inorganic alkali halide crystals	γ spectroscopy
^{4}He	Inorganic noble gases	**n** spectroscopy, **n**/γ discrimination
EJ-299	Organic plastics	**n** spectroscopy, **n**/γ discrimination
EJ-301	Organic liquids	**n** spectroscopy, **n**/γ discrimination
EJ-309	Organic liquids	**n** spectroscopy, **n**/γ discrimination

Table 2.1: List of detectors I have studied during my PhD thesis. Xe and ^{4}He are MODES_SNM developments

2.1.1 Organic scintillators

Scintillation phenomena in organics happen at a molecular level; Fig. 2.1 illustrates the level structure of an organic molecule with a π-electron structure. Single molecules maintain their scintillation properties without dependency on the physical state, and even when combined to other materials, provided the internal molecular structure is not altered. Therefore a scintillator may consist of a single homogeneous material, or even being a compound material.

In excited organic molecules, energy dissipation by means of thermal decay is an alternative channel to deexcitation; this has the effect of reducing the light output and may also affect the linearity of the response. Thermal decay and other radiationless deexcitations are grouped under the term *quenching*. To compensate for quenching, organic liquid scintillator detectors can be formed with a "binary" mixture of bulk solvent and a small concentration of an efficient scintillator; in this way the energy absorbed by the solvent is immediately converted into light once transferred to the scintillator molecule.

Quenching also accounts for the natural self-transparency of most scintillation materials. While absorption can bring the molecule in any of the excited states, excess vibrational energy inside a level is rapidly lost by means of thermal decay, and most of the radiative deexcitations involve only the lowest excited state. Due to this termal energy loss, the resulting emission spectrum is always shifted towards a low-energy region (and higher wavelenght) with respect of the absorption spectrum, an effect called *Stokes shift*. In most cases this wavelenght shift is sufficient to ensure that no self-absorption processes take place. In addition, in liquid or plastic scintillators another component can be added to serve as *wavelenght shifter*, absorbing primary scintillation light and reemitting it at a longer wavelenght. This can be useful to match the sensitivity of a particular light sensor, or to further reduce self-absorption phenomena in the main scintillator.

Gamma rays, charged particle and fast neutrons can be detected with scintillators. The problem of discriminating gamma ray events from neutron ones will be discussed in Sec. 2.3.3.

Two materials that have reached widespread use in the past are anthracene and stilbene; anthracene has the highest scintillation efficiency, while stilbene is used where neutron/gamma PSD analysis is applied. However, pure crystals of both materials are fragile and can't be easily manifactured in large sizes; their scintillation efficiency depends also on the relative direction on the incident particle with respect to crystal axis, with variations up to 30%. More often anthracene and stilbene are mixed in a solvent to make a liquid or plastic organic scintillator, sometimes with the addition of a wavelenght shifter.

Liquid scintillators represent one common type of scintillator for neutron detection on the market. They are sold in glass sealed containers, because oxygen is a strong quenching agent, and also their composition is often toxic, flammable or both. Despite these complications, the lack of a solid structure makes them very resistant to radiation damages, and also allows to build detectors as large as required.

Plastic scintillators are made of a solvent (e.g. styrene monomer) that can be polymerized to form plastic. Due to their solid structure they can easily be shipped, handled and operated without safety constraints, but they are generally more vulnerable to radiation damage.

2.1.2   Inorganic scintillators

Inorganic crystals with activators

Scintillation mechanism in inorganic crystals depends on the energy levels determined by the crystal lattice. Level structure is divided in energy bands: *valence bands* represent electrons bound at lattice sites, *conduction bands* represent free electrons, and *band gaps* represent regions forbidden to electrons in pure crystals. In this structure, the process of radiative deexcitation is inefficient, and considering the tipical energy values associated to transitions the resulting light would have a wavelenght out of the visibile spectrum. Moreover, since there is no intermediate level in the deexcitation process, absorption and emission spectra would be quite similar, and the scintillator would be heavy affected by self-absorption phenomena.

In order to build useable detectors, dopants are deliberately added to pure inorganic crystals. These materials are called *activators*, and their presence creates additional sites (*activation sites*) in the lattice where deexcitation can occur through intermediate states. An example of energy levels in an activated inorganic crystal is shown in Fig. 2.2.
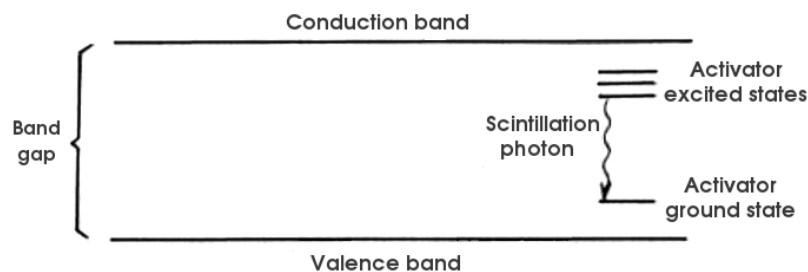
Figure 2.2: Example of energy levels in an activated inorganic crystal. From [18]

As in the case of organic molecules, the presence of intermediate levels causes a shift in the emission spectrum, addressing both the need for visibile light emission and the problem of self-absorption. Since typical lifetimes for the activator excited states are of the order of tens or hundreds of nanoseconds and migration time for the electrons inside the crystals is much shorter, the time characteristic of the scintillation light is dominated by the decay time of the activator states.

Noble gases

Noble gases represent a less known family of scintillation materials and their use has been limited to special applications. Scintillation in noble gases follows the same principles of

other materials: gas molecules are excited by the incoming particle, and photons are emitted during deexcitation from the two lowest molecular excited states to the ground state. Transitions are generally much faster than any other detector (a few nanoseconds) and the typical emission peak lies in the ultraviolet region; sometimes a second gas, nitrogen for example, is added as a wavelenght shifter, at the price of a reduced light output. Temperature and pressure are two additional variables that affect gaseous detector performances, resulting in the need of a more complex characterization.

In order to properly correlate energy measurements with the incident photon, no energy must escape from the detector; while a complete absorption can be obtained for most solid and liquid detection materials, this might become an issue in the case of gas cells. In addition, energy may be lost in interactions of radiation with the walls of the containing vessel. The development of noble gas detectors must address these issues with proper choice of size, pressure and enclosing material.

Among the noble gases, xenon and ^{4}He (natural helium) are used as scintillator materials. MODES_SNM exploits the latest advancements in the use of both types of gas: xenon tubes for gamma rays and ^{4}He tubes for neutron detection (Sec. 2.2.3 and Sec. 2.3.4, respectively).

2.2 Gamma detectors

2.2.1 Gamma ray interactions with matter

Gamma ray photons have no charge and can not cause direct ionization in the absorbing material; instead, in order for a photon to be detectable, it must transfer all or part of its energy to an electron. The electron energy is subsequently lost through ionization and excitation of atoms. Gamma ray spectroscopy at low energies relies on three main interaction mechanisms: *photoelectric absorption*, *Compton scattering* and *pair production*.

Photoelectric absorption it is the process in which the photon transfers all of its energy to a single electron; the resulting free electron will have a kinetic energy equal to the original photon energy minus the binding energy of the bound electron. Assuming that the incident radiation has the energy $h\nu$, the resulting structure in the ideal spectrum is a single peak at $E = h\nu$ called *photoelectric peak*; it is also known as *Full energy peak* because it might also be originated by multiple interactions in large volume detectors. Cross section for photoelectric absorption varies approximately as $Z^{4.5}$ [18], therefore this interaction channel is more relevant in high-Z materials.

Compton scattering represents the case in which there is only a partial energy transfer between the photon and the electron assumed to be free; the fraction of the transferred energy depends on the scattering angle and results in a continuum distribution whose shape is described by the formula of the Klein-Nishina cross-section:

$$\frac{dN}{dE}(E) = 2 + \frac{(E/E_0)^2}{(E_0/m_ec^2)^2(1-(E/E_0))^2} + \frac{(E/E_0)}{(1-(E/E_0))}\left((E/E_0) - \frac{2}{E_0/m_ec^2}\right)$$

where E_0 is the energy of the incident radiation and m_0c^2 the mass energy of the electron; the normalization factor has been omitted. The high energy border of this continuum is called *Compton edge*; it corresponds to the maximum energy transfer (when the photon is scattered at 180°) and in the limit of $E0 >> m_0c^2/2$ it tends towards the value of

$E_0 - m_0c^2/2$. Compton edges are used as reference structures for energy calibrations when using materials that do not present strong photoelectric effect such as organic scintillators. In the limit of very large detectors, all scattered photons will interact multiple times with the medium, until all the initial energy has been released, contributing to the Full energy peak.

Pair production is the creation of an electron-positron pair in the surroundings of a nucleus. This process can occur only when $h\nu > 2m_0c^2$; the excess energy $E_0 - 2m_0c^2$ is equally shared by the two particles and they are emitted in opposite directions. Then they lose their kinetic energies in the medium: the amount of released energy is $E_0 - 2m_0c^2$, corresponding to the original energy minus the mass energy of the electron-positron couple. If the positron annihilates with an electron of the medium, two 511 keV photons are emitted in opposite directions. If they both interact with the medium, all the original energy is detected, and the event contributes to the Full energy peak; if one of the photons does not interact and "escapes" the detector, the event will contribute to the spectrum with an energy of $E_0 - m_0c^2$ (*Single escape peak*); if both photons escape the detector, then the measured energy will be $E_0 - 2m_0c^2$ (*Double escape peak*). The probability for single and double escape events is directly influenced by the size of the medium.
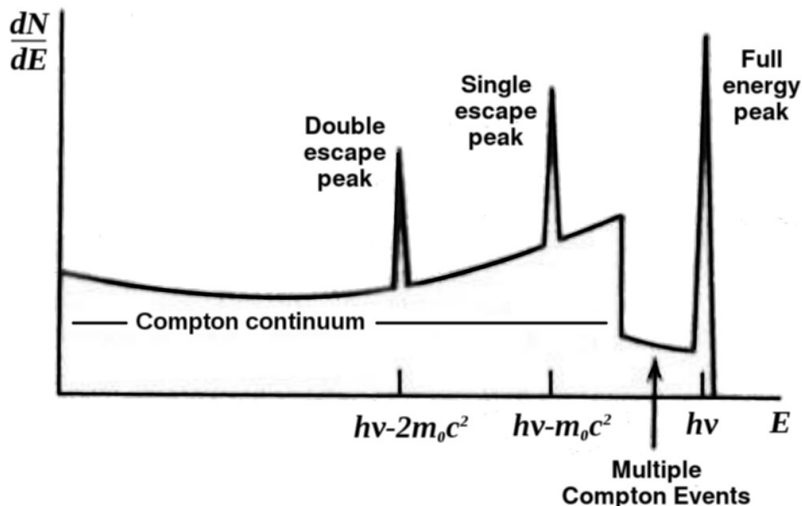
Figure 2.3: *Theoretical spectrum of a monoenergetic radiation with E >> 1 MeV. From [18]*

Fig. 2.3 illustrates the resulting spectrum when all three mechanisms take place in a detector, considering a monoenergetic incident radiation of a few MeVs.

When using real detectors, the detector response function is complicated by other effects due to the surrounding materials.

The energy resolution of a gamma ray detector is usually defined as the ratio between the full width at half maximum (FWHM) and the centroid of a peak. The use of the Compton Edge for energy calibration is discussed in Sec. 8.2.

2.2.2   NaI(Tl) crystals

One of the first and the most famous inorganic scintillator is NaI(Tl), crystalline sodium iodide with thallium used as activator. The atomic number of iodine (Z = 53) provides a good photoelectric cross-section resulting in reasonable full-energy peak efficiencies. It was

first described in 1948 by Robert Hofstadter and rapidly became the standard reference detector for gamma spectroscopy, a status that still holds despite the discovery of modern materials with better light output or energy resolution. Nowadays it can be manifactured in many different sizes and shapes at a reasonable cost. Its major drawbacks are mechanical fragility, non-linear energy response and hygroscopicity: it deteriorates quickly when exposed to any level of humidity, so it needs to be enclosed in airtight containers. Also with a decay time of about 230 ns its timing response if rather slow compared to modern scintillators.

Table 2.2 lists NaI(Tl) detector's most relevant properties; the typical waveform of a NaI(Tl) detector is shown in Fig. 2.4. One NaI(Tl) detector has been used in MODES_SNM, as described in Sec. 5.3.

NaI(Tl) gamma-ray detector (typical values)	
Density	3.67 g/cm^3
Emission Maximum	415 nm
Decay Constant	0.23 μs
Refractive Index @ maximum	1.85
Hygroscopic	yes

Table 2.2: Properties of a typical NaI(Tl) detector. From [20]
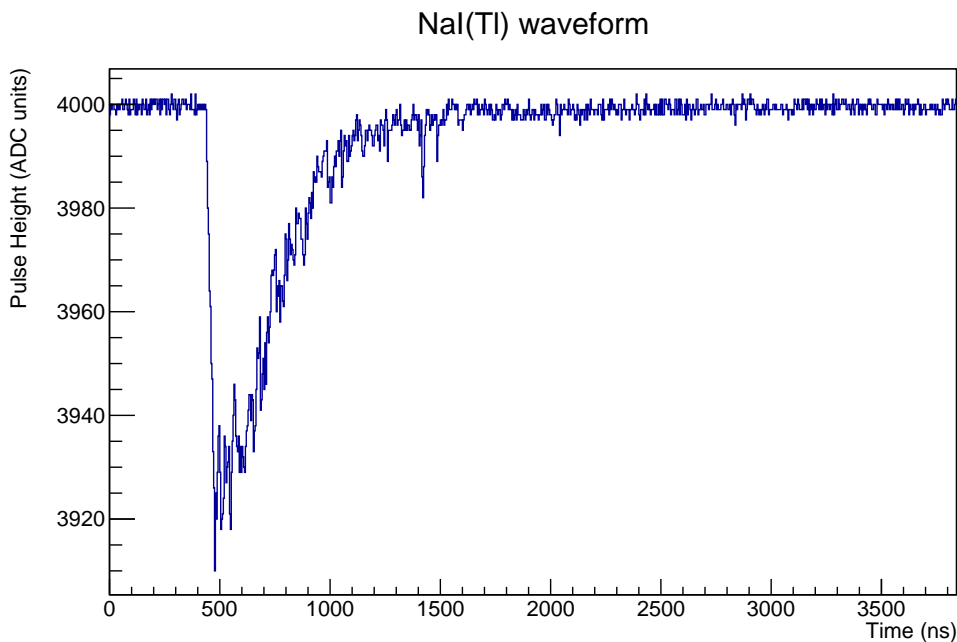
Figure 2.4: Signal waveform for a NaI(Tl) scintillator

2.2.3   MODES_SNM xenon detectors

Xenon is an attractive material for gamma ray detection, mainly because of its high atomic number (Z = 54) and large cross-section for photoelectric absorption (photoelectric cross-section dominates up to around 300 keV); it is also a rather dense material (0.4 g/cm^3 for gaseous xenon at 50 bar and 293 K). The emission peak is located in the VUV region at 175 nm, outside the visibile spectrum.

High-pressure xenon detectors have been used mostly as ionization chambers, but in recent years their potential in the field of gamma-ray spectroscopy has gained increasing attention [21, 22]. Within the MODES_SNM collaboration a study has been performed on the properties of high-pressure xenon as a scintillator, and a few tubes have been manifactured and used in the prototype. Preliminary studies resulted in an article [23] describing the light yield and energy resolution for a high-pressure Xe tube, together with the dependency on thermodynamic conditions.

Figure 2.5: The xenon gamma-ray detector used in MODES_SNM

The tube described in [23] is of the same family of those later integrated in MODES_SNM first prototype; it uses a stainless steel high-pressure tube (designed to withstand pressures up to 200 bar) filled with high purity xenon, having a length of 200 mm and a diameter of 44 mm, with UV transparent windows at both ends. The inner surface of the tube is lined with a reflector combined with a wavelength shifter, that shifts the VUV light from xenon scintillation into visible light.

The scintillation light from the high-pressure tube was read out using two Hamamatsu R580 (quartz window) photomultiplier tubes (PMTs). The data were taken using a CAEN V1751 digitizer (1 GS/s, 10 bit). The two PMTs were digitized independently, and the trigger, directly programmed on the digitizer, required the coincidence of the two PMTs. Energy information has been extracted by means of an off-line analysis of each waveform and summing the contribution of both PMTs.

MODES_SNM xenon gamma-ray detector					
Total length	600	mm	Active volume	1.9	l
Maximum diameter	130	mm	Weight	$\sim$10	kg
Active length	200	mm	Pressure @ 20°C	45	kPa
Active diameter	110	mm	Resolution @ 662 keV	6.7	%

Table 2.3: Specifications of MODES_SNM xenon gamma-ray detector

Fig. 2.5 represents one of the final xenon detectors used in MODES_SNM; its main characteristics are listed in Table 2.3.

Fig. 2.6 shows an example of digitized waveform: the difference with traditional scintillators (e.g. Fig. 2.4) is clear.
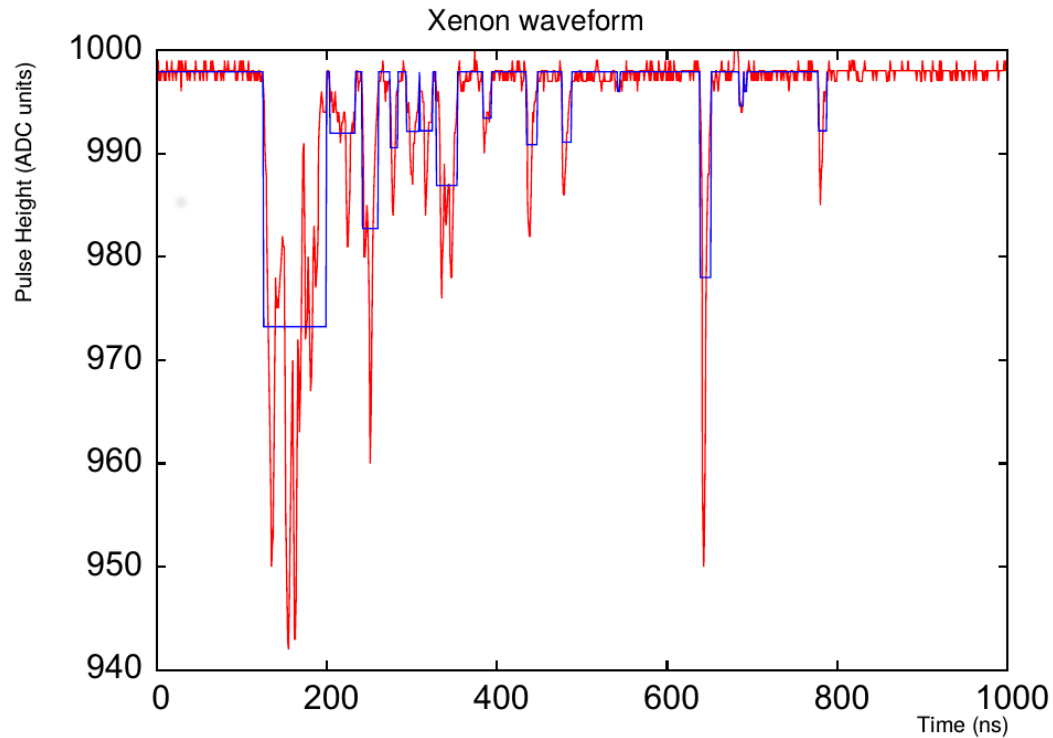
Figure 2.6: Signal waveform for a xenon scintillator. Integration windows are superimposed to identified peaks. From [23]
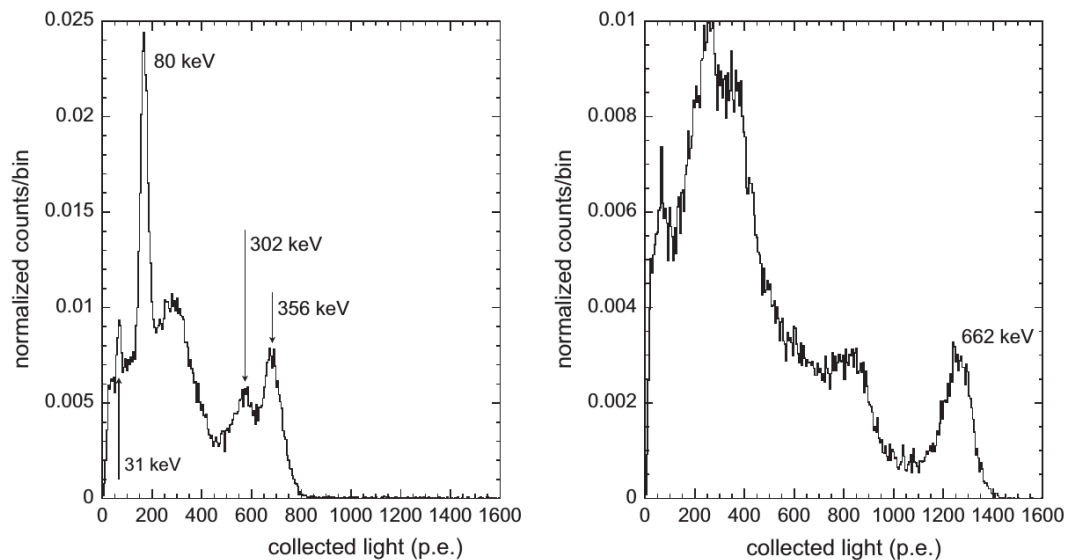
Figure 2.7: ^{133}Ba and ^{137}Cs spectra taken with xenon detectors

An off-line peak-search algorythm is applied to define the integration windows for energy estimation; Fig. 2.7 shows spectra for ^{133}Ba and ^{137}Cs as obtained during the first test measurements. In both cases the radiation was collimated to the center of the tube by lead

bricks to exclude asymmetries in the light collection. ^{133}Ba gives lines at 31 keV (X-ray), 80 keV, 302 keV and 356 keV. At ~30 keV several X-ray lines from iron and lead are also possible; ^{137}Cs gives a line at 662 keV (and 32 keV X-ray line), while other measurements with a ^{22}Na source gave lines at 511 and 1275 keV. Measured energy resolution is 9% FWHM at 662 keV, with a light yield of 1.9 p.e./keV.
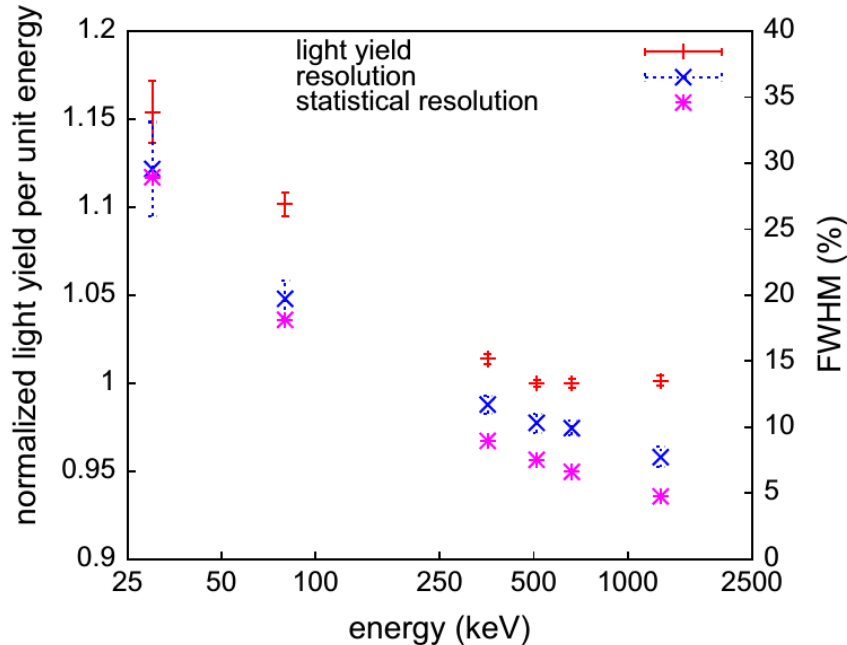
Figure 2.8: Normalized light yield, energy resolution, and limit to the energy resolution from photostatistics

Fig. 2.8 shows the dependency of light yield and energy resolution on absolute energy. Light yield is normalized as 1 at 662 keV and appears to be lower at higher energies, due to non-contained electrons.

Energy resolution is compared to that expected from statistical consideration; not only resolution is lower at higher energies, but also is higher than predicted values; these discrepancies increase with the energy and are explained again with non-containment effects and the dominance of the Compton effect at higher energies which spread the light production over a larger volume.

Fig. 2.9 shows the dependency of resolution and collected light on gas pressure, showing the best working condition in the range 40-45 bar.

The results reported in [23] are related to the first test campaign; the detector and the readout used in [23] differ from the ones used in MODES_SNM final configuration, which implements a different digitizer with a sampling rate of 500 MSamples/s and a resolution of 14 bits (more details in Sec. 3.3.5). Moreover, the size of the final detectors is 100 mm in diameter × 200 mm in length.

Fig. 2.10 shows a spectrum of ^{137}Cs obtained with the final configuraton of MODES_SNM system. Energy resolution is now about 6% at 662 keV.

The MODES_SNM xenon gamma ray system is therefore capable of reaching energy resolutions typical of the standard NaI(Tl) scintillators but with larger volumes and lower costs so that it can be adapted easily to specific geometrical requirements.
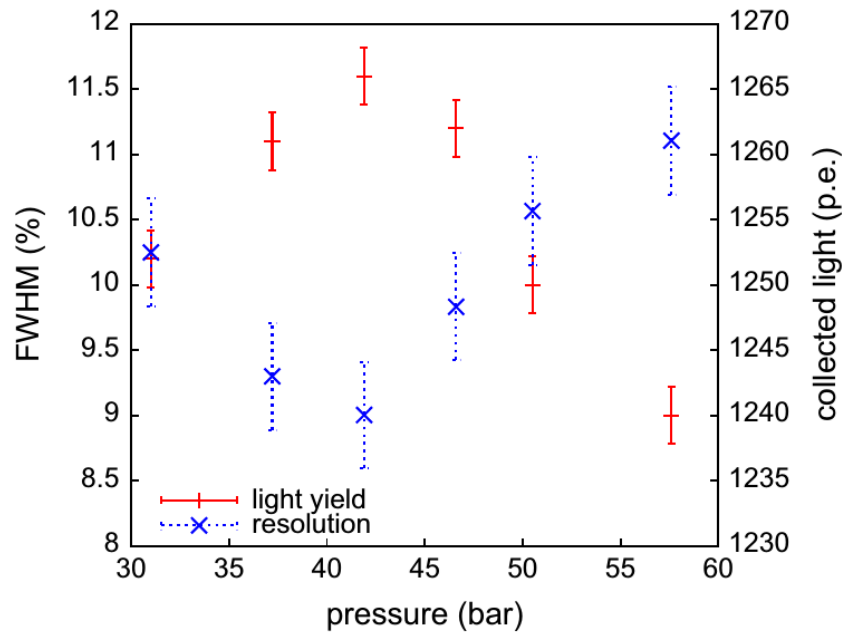
Figure 2.9: Light yield and energy resolution as a function of the xenon pressure
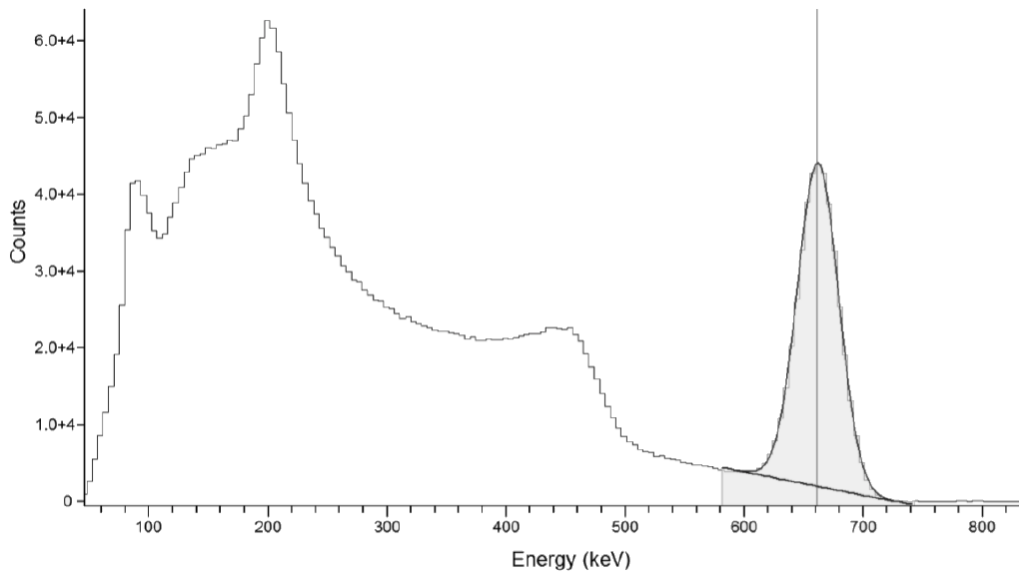
Figure 2.10: ^{137}Cs spectrum taken with MODES_SNM xenon detector

2.3   Neutron detectors

2.3.1   Physics of neutron detection

Since neutrons carry no charge, they are not influenced by the Coulomb force of the electron cloud and they can penetrate many centimeters of matter before interacting. The only possibile interaction is with a nucleus of the detector material with production of secondary radiation, including charged particles. Neutron detectors exploit this conversion process.

Several types of nuclear interactions are possibile; their relative probability depends on the incoming neutron energy; neutrons are thus classified following this convention:

- Thermal neutrons: E $\sim$ 0.025 eV

- Slow neutrons: E < 0.5 eV

- Fast neutrons: E > 0.5 eV

The border between slow and fast neutrons is defined by arbitrarily taking as a reference the *cadmium cutoff*, the energy at which the absorption cross-section of neutrons in cadmium has a significant drop. The neutrons in thermal equilibrium with the absorber medium are called thermal neutrons; they represent a subset of slow neutrons and their average energy at room temperature is 0.025 eV.

Slow and thermal neutrons

One of the possibile interaction of neutrons with nuclei is elastic scattering. Since the energy that a slow neutron can transfer through elastic collisions is very low, it is impossibile to use this process for slow neutron measurements. However elastic scattering still plays a significant role in slow neutron detection, since the relative probability of this interaction is very high resulting in the thermalization of slow neutrons.

Nuclear reactions are also possibile, but for energetic reasons only those with a positive Q-value are likely to occur; some reactions used to detect slow neutrons result in the production of heavy charged particles with energies determinated by the Q-value rather than the initial energy of the neutron. In most materials the dominant reaction is the radiative neutron capture (n,γ) but its secondary gamma radiation might be difficult to detect. Reactions which produce charged particles, such as (n,α), (n,p) and (n,fission) are generally used.

Fast neutrons

As the energy of neutrons increase, the probability of neutron-induced nuclear reactions rapidly decreases; at the same time, since the maximum amount of energy that can be transferred is higher, elastic scattering processes dramatically increase in importance. In this case secondary radiation is made by the recoil nucleus itself. The process of slowing down a fast neutron via elastic scattering on nuclei is called *moderation*. Moderation cross-section is higher at low mass numbers, with the highest value corresponding to hydrogen, since a single collision can lead to a complete transfer of the neutron initial energy, whereas for heavier nuclei only partial energy transfers are possibile.

If energies are high enough, inelastic scattering processes can take place, leading to nuclei excitation and deexcitation with emission of gamma rays. In this case the maximum energy transfer is greater than the corresponding elastic interaction.

In security applications, fast neutrons are generally detected directly in scintillators or by slow neutron detectors surrounded by an appropriate amount of moderation materials.

2.3.2 Classic solution: ^{3}He proportional counters

Proportional counters are a type of gas-filled detectors, based on the phenomenon of gas multiplication. While other detectors are often preferred in spectroscopic applications, they are very useful in revealing radiation and its relative intensity.

A proportional counter typically consists in a cylinder, often made of stainless steel, with an anode wire running along its axis (see Fig. 2.11). A high voltage (hundreds of volts) is applied to the wire, with respect to the tube that is grounded. Ions and electrons are produced inside the tube by incident radiation; then they are attracted and drifted towards their respective collecting electrodes. If the average energy provided from the electric field is strong enough to overcome ionization potential, each ion can produce additional ionization while colliding with other gas molecules; this process takes the form of a cascade known as *Townsend avalanche.*
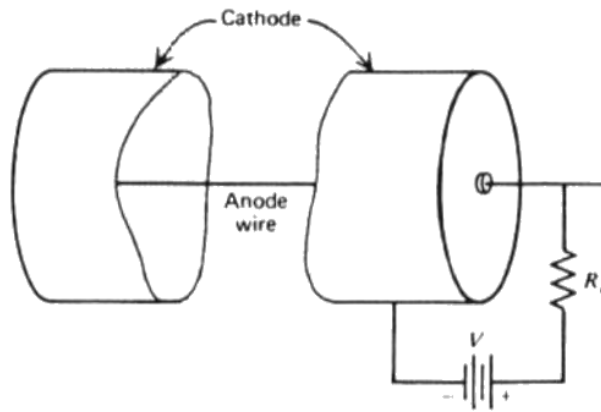
Figure 2.11: Scheme of a proportional counter

Under proper conditions, the number of secondary ionization events can be kept proportional to the number of primary ion pairs formed, but the total number of ions can be multiplied by a factor of many thousands, reducing the demand of external amplifiers.

^{3}He proportional counters exploit the ^{3}He(n,p)^{3}H reaction for the detection of thermal neutrons with Q = 764 keV. The energy dependency of cross section in case of ^{3}He follows the relation 1/v (v = neutron velocity) up to 0.2 MeV, resulting in greater efficiency at lower energies, the value of cross section being 5330 barns for thermal neutrons.

In addition of having a large capture cross-section for thermal neutrons, ^{3}He sensitivity to gamma rays is negligible and pileup effects can often be neglected.

The "gold standard" of thermal neutron detection is therefore composed by a proportional counter filled with a suitable gas, ^{3}He being the most effective choice due to the aforementioned reasons. If the counter is surrounded by a layer of a hydrogen-rich material of the appropriate thickness, the sensitivity of the detector will be extended to include also the fast neutron energy range. ^{3}He proportional counters proved to be mechanically stable over a wide range of environmental conditions, and do not degrade over years of operation.

The problem with ^{3}He is that its rarity is increasing even quicker than the demand for
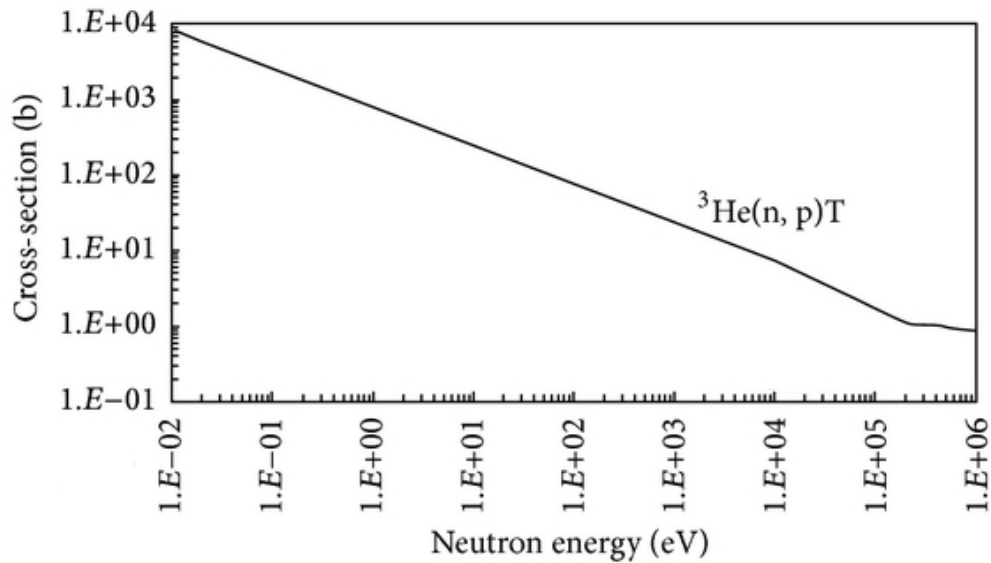
Figure 2.12: Cross section versus neutron energy for $^3He(n,p)^3H$ reaction. From [24]

it. ^{3}He is a byproduct from the beta decay of tritium (t(1/2) = 12.3 y), and it is separated from tritium as part of the tritium purification process. Tritium is mainly used in the manifacturing of nuclear weapons, which are periodically processed to remove the excess of ^{3}He to maintain the desired tritium concentration [25]. U.S. Department of Energy has made the resulting ^{3}He available on the western commercial market, but with the reduction in the nuclear weapons stockpile the production of ^{3}He from tritium decay has heavily declined.

The only other significan supplier of ^{3}He has been Russia. Tritium is also produced in the CANDU heavy water reactors used in Canada and elsewhere, and is regularly extracted by Ontario Power Generation (Toronto, Canada). However, the extraction of ^{3}He from this source would represent a substantial investment [26]. At the same time, following 11/09/2001 events, the demand for neutron detection to be used in security application has risen, leading to the world shortage of this isotope. It is estimated that the total ^{3}He demand is ~65.000 l/y, while total supply is ~15.000 l/y [27]. As a result, an extensive research effort is currently being made to find a suitable replacement as a reference neutron detector.

2.3.3   Organic scintillators and neutron-gamma discrimination

Scintillator materials described in Sec. 2.1.1 are sensitive to any type of ionizing radiation or particles, including not only gamma rays but also charged particles resulting from neutron interactions. Almost any type of scintillator can be used to detect neutrons, although in most cases signals generated by neutron events can not be distinguished from those originated by gamma rays. To separate neutron and gamma ray events, one must implement additional techniques. Time-of-Flight (TOF) is one of the most popular and reliable ones, but requires detectors with fast timing performances, a suitable flight path and a more complex analysis.

Among the usual organic scintillators, liquid scintillators are of special interest since they allow to separate neutrons from gamma rays by means of the so-called Pulse Shape Discrim-

ination (PSD) technique [28]. One of the first commercial liquid scintillators was NE213, followed by other similar commercial products [18]. Common features of this generation of liquid organic compounds include their intrinsic chemical hazard, toxicity, and fire hazard due to their low flash point. Consequently liquid scintillation detectors have been largely used in research laboratories, where the required safety procedures are easily implemented even in the presence of large volume of liquid, but much less in field applications such as in Homeland Security, where, besides the operator safety, the presence of general public is a primary concern [27].

As of today, the need of new neutron detectors to replace standard ^{3}He proportional counters generated a large effort in trying to remove or diminish the hazards related to the use of traditional liquid scintillators. This can be achieved in different ways:

a) producing new liquid scintillators with good pulse shape capabilities but with reduced hazards. This is the case of EJ-309, a liquid with lower chemical and fire hazards [57]; its study is described in Sec. 8.3;

b) producing new solid organic scintillators with pulse shape capabilities [29, 30]; solid scintillators are particularly appealing since they are mechanically easier to work compared to liquid scintillation cells with optical windows. Sec. 8.4 describes our characterization of EJ-299-33, the first commercial plastic scintillator with PSD capability [32];

c) decreasing the cost and improving the effectiveness of organic crystals as stilbene [31];

d) developing new types of scintillators. MODES_SNM proved the effectiveness of gaseous neutron detectors based on ^{4}He, as described in Sec. 2.3.4.

Pulse Shape Discrimination (PSD)

As discussed in Sec. 2.1, scintillation light is composed of two main components, one faster than the other. The fast component is due to prompt fluorescence, and is characterized by a decay time in the nanosecond range. The slow component corresponds to the delayed fluorescence, and has a typical longer decay time. The ratio between fast and slow components depends on the kind of particle which causes the ionization; higher ionization density will lead to higher fraction of slow component light. Taking into account the fact that a neutron produces protons when interacting with scintillator, while a gamma ray produces electrons, the produced light shows a different distribution as demonstrated in Fig. 2.13. The analysis of the signal slope provides the possibility to discriminate between neutrons and gammas; this technique is called Pulse Shape Discrimination (PSD).

The PSD parameter used for discrimination is normally defined as the ratio between the tail and the total charge integral:

$$PSD = \text{tail integral} / \text{total integral}$$

The more relevant the tail of the signal, the higher the PSD value. Consequently, theoretical PSD values lie in the range [0,1]; this is true only when integrating digitized waveform, while the use of splitters, delay gates and QDC modules might lead to values up to 1.3 due to signal distortions induced by the analog chain.

Plotting the PSD parameter over the energy of the particle results in a plot with the structure of Fig. 2.14. The events are grouped in two populations centered around two
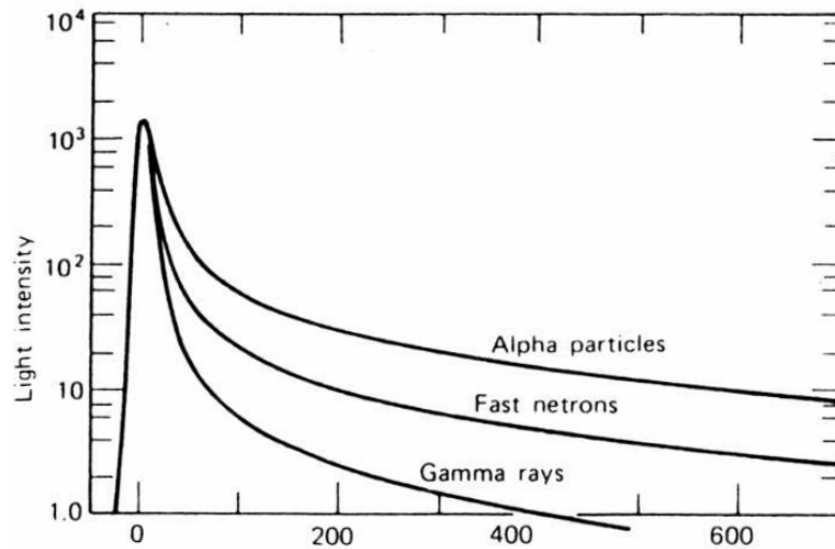
Figure 2.13: Different pulse shapes in stilbene. From [19]

relatively constant values of the PSD parameter; the lower one is that of gamma rays, the higher contains neutrons. There is often an overlap of the two populations in the low energy range (0 to 200 keV): this is the region where noise and other fluctuations of signal baseline have the biggest impact on digital charge integration; such effects decrease as energy goes up.
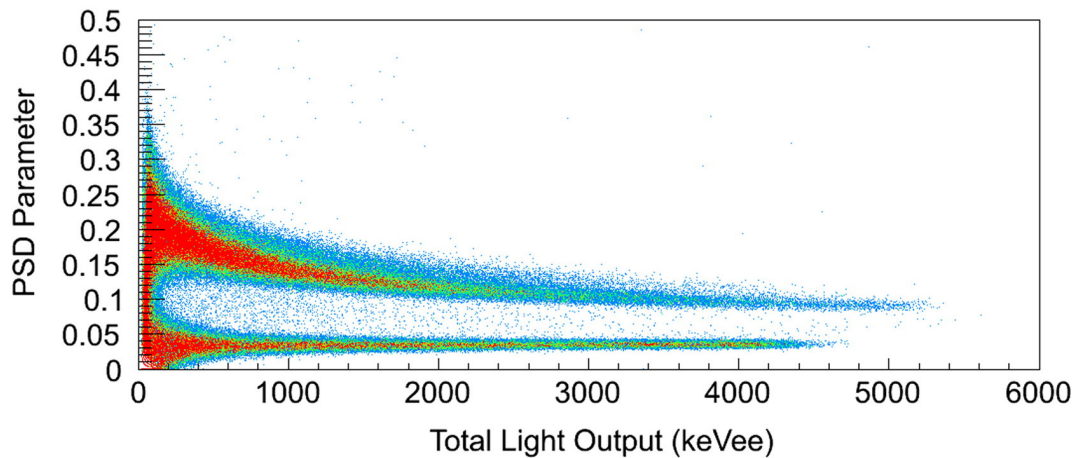
Figure 2.14: Example of PSD scatter plot

The relation between particle energy and light output depends on both the particle type and the scintillation material; consequently gamma rays and neutrons have different energy calibrations in the same detector. Since the neutron-gamma discrimination is done before separate calibrations could be applied, only gamma ray energy calibration is performed, and the same energy scale is used for both gamma rays and neutrons. Therefore, the common X axis unit is *keVee*, where "ee" stands for *electron equivalent*: it is the energy that would have been deposited to generate that amount of light if the particle were an electron. In most nuclear security application the use of this unified scale is sufficient to count neutrons and identify neutron sources, without the need to perform a separate neutron energy calibration.

The implementation of Pulse Shape Discrimination is described in Sec. 3.3.3 (electronic set-up) and Sec. 4.2.3 (software analysis).

Figure of Merit (FoM)

While PSD parameter is used to separate gamma ray events from neutron ones, an additional parameter can be defined to estimate the quality of this separation, the Figure of Merit (FoM). If the events of Fig. 2.14 are projected on Y axis, for a given window in total light output, the resulting plot will have the structure shown in Fig. 2.15.
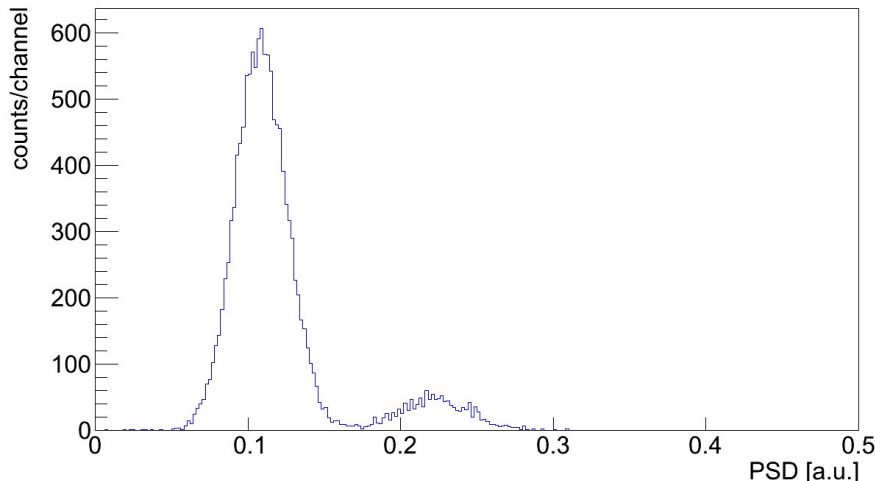
Figure 2.15: Example of FoM plot

With reference to Fig. 2.15, FoM is defined as follows:

$$FoM = \frac{Mean(n) - Mean(\gamma)}{FWHM(n) + FWHM(\gamma)}$$

where $Mean$ and $FWHM$ refer to the parameters of the two curves that fit the peaks corresponding to the two populations.

FoM value is therefore an estimation of the distance of the two populations compared to their width. Typical values of FoM range from 10^{-1} to 10^1: the higher the value, the better the separation. Values around 1.2 are often taken as a sort of reference threshold for modern scintillators [29].

The Figure of Merit can be calculated over different energy ranges. Looking at Fig. 2.14 it is clear that FoM values calculated over the entire energy span of the detector will be lower than FoM values calculated excluding the low-energy overlapping region. More generally, FoM improves at higher energies; sometimes this dependency is explicited by calculating FoM values over narrow energy windows and plotting the values over the window centroids. An example of this study is presented in Sec. 8.4.

2.3.4 MODES_SNM ^{4}He detectors

Within MODES_SNM project, ^{4}He detectors have been developed not only to replace ^{3}He counters but also to overcome their performances. The sensitivity of a ^{3}He counter is limited to slow neutrons; fast neutrons can be detected over a wide energy range but only after being

moderated with complete loss of informations about their original momentum. Instead, ^{4}He detectors can detect both fast and thermal neutrons preserving energy information.

^{4}He, like most noble gases, is a fairly good scintillator; its emitted light, with a wavelenght of the order of 70 nm, is in the vacuum ultraviolet (VUV) and requires to use a wavelength shifter. Approximately 18 000 VUV photons are produced per MeV deposited by neutrons in 200 bar ^{4}He cell [33].
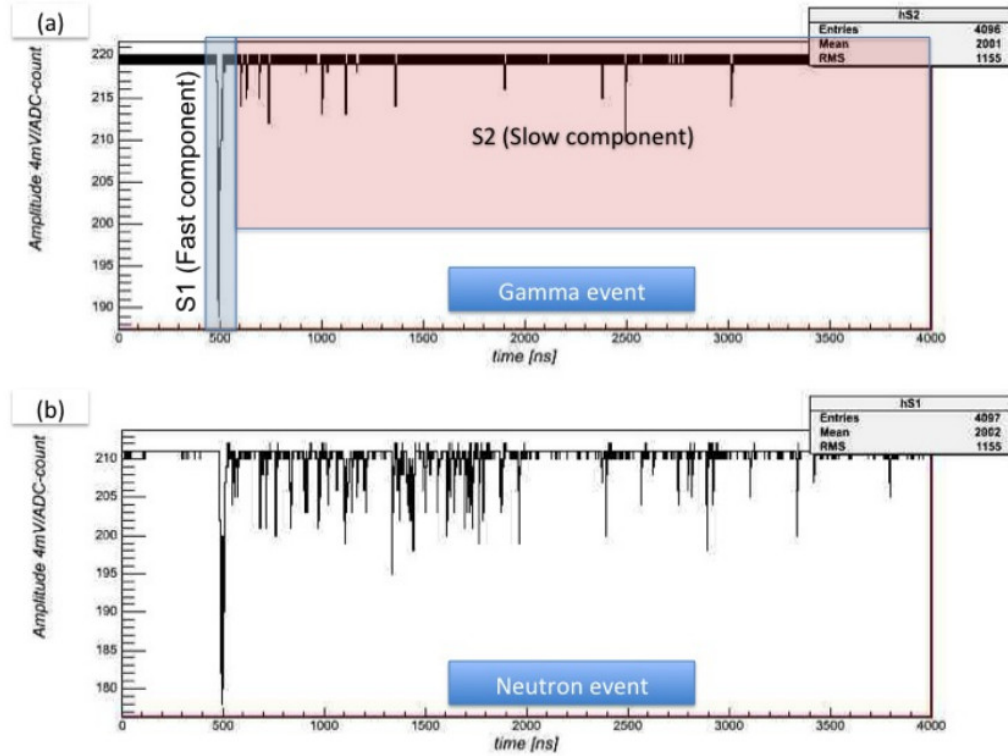
Figure 2.16: Examples of ^{4}He scintillation signals: they consist of a fast component with a decay time of a few nanoseconds and a slow component of the order of a microsecond. Depending on the type of interaction the relative strength of the two scintillation components are different: (a) shows a gamma ray event, while (b) shows a neutron event.

.

Gamma rejection

Gamma rejection is a key factor for a neutron detector. ^{4}He shows good gamma rejection performances, the physics reasons being essentially three:

1. gamma rays have a low interaction probability, due to the low electron density of helium;

2. gamma rays interactions produce low energy deposit, caused by the low material density; it is estimated that average energy loss of Compton scattered electrons in ^{4}He at 200 bar is 40 times lower than in a liquid scintillator;

3. ^{4}He scintillation signals are suitable for PSD analysis

As in the case of liquid organic scintillators, scintillation signals can be divided in two components. Depending on the type of interacting particle, the relative strengths of the

two scintillation components are observed to be different, allowing their discrimination. An example is shown in Fig. 2.16. In this example, while the amplitude of the fast component is of the order of 120 mV for both signals (gamma and neutron), the number of photoelectrons detected in the slow component is approximately a factor 3-4 larger for the neutron event.

Therefore, standard PSD techniques apply to ^{4}He signals too, and cuts can be made to isolate neutron events and further increase the natural gamma-ray rejection capabilities of these detectors. An example of PSD cut applied to ^{4}He detectors is presented in Fig. 4.3.

Energy resolution and relative calibration

To perform an accurate energy calibration of a ^{4}He detector is not an easy task.

A relative calibration can be obtained considering that gamma interactions lead to recoil electrons, which in these ^{4}He detectors deposit only tens of keV per centimeter of trajectory; therefore the maximum energy deposited by a gamma ray is limited by the detector size. When the energy of the incident gamma ray is greater than a certain threshold the exceeding energy is not detected, resulting in an energy cut-off in the spectra. The value of this cut-off depends only by the detector parameters and can be use as a reference point; however this procedure will only lead to a relative calibration. Fig. 2.17 illustrates this method in the case of a ^{60}Co source placed on top of the detector.
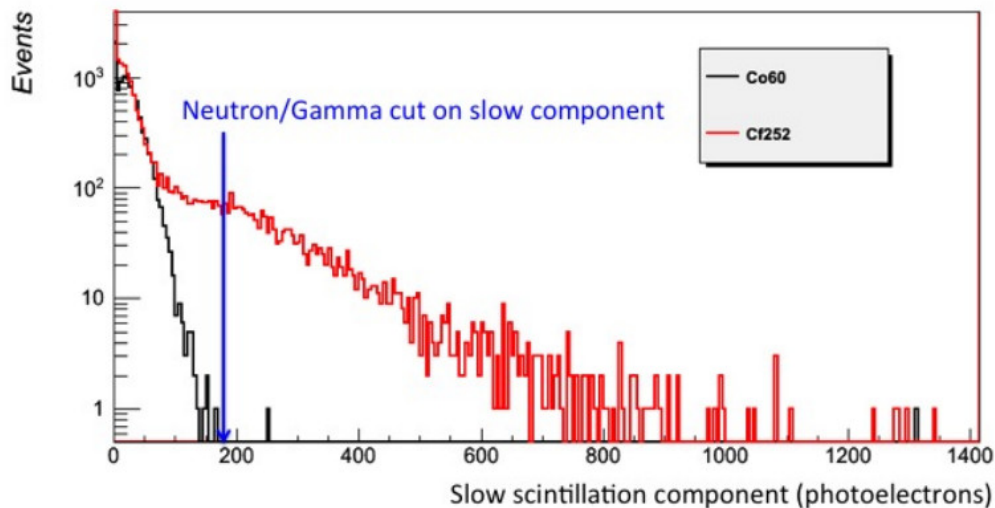
Figure 2.17: Histogram of the number of detected slow component photons from a ^{60}Co gamma source placed in contact with the detector (black entries) and a ^{252}Cf source (red entries)

A more practical and accurate way to perform the energy calibration exploits trace quantities of ^{222}Rn, inadvertently introduced during the gas purification process. The decay chain of ^{222}Rn features the emission of alpha particles of a few MeV; long measurements (at least 12 hours) can be carried out to obtain a calibration peak from these alpha decays, as shown in Fig. 2.18.

The detector's energy resolution has been estimated by the manifacturer placing a 3 Bq ^{241}Am alpha source inside a detector; the results are depicted in Fig. 2.19. The width of the line is measured to be approximately 10% for the 5.48 MeV alpha particles, a value in agreement with the expected statistics of scintillation photons [33].
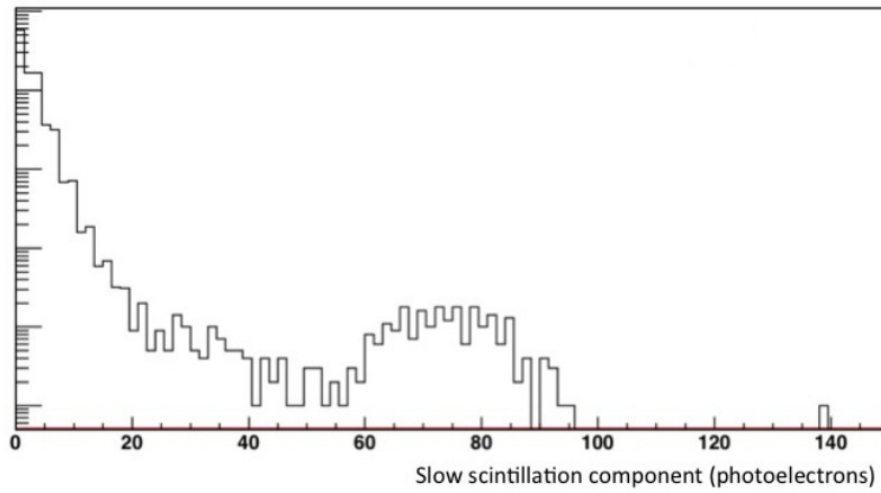
Figure 2.18: Histogram of the number of detected slow component photons take in a 15 hour background run. A clear peak can be seen, attributed to the three alpha emission lines of the ^{222}Rn decay chain; it can be used for energy calibration
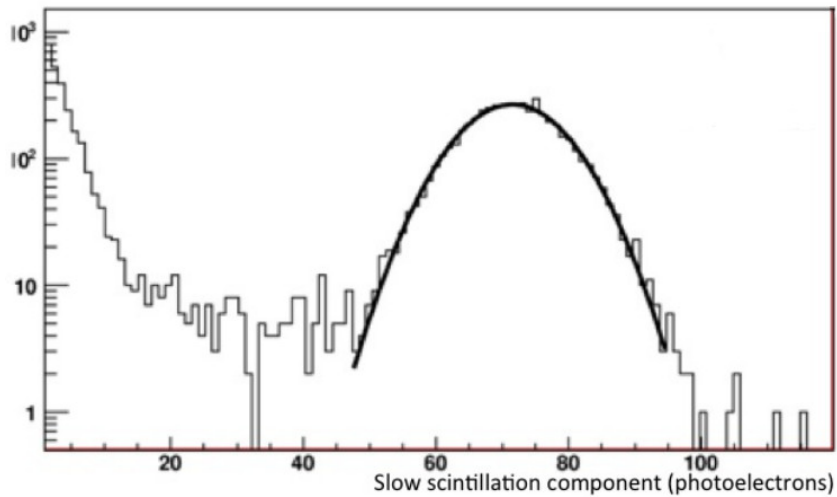
Figure 2.19: Histogram of the number of detected slow component photons in a measurement carried out with a 3 Bq ^{241}Am alpha source placed inside a detector

Fast neutron detectors

Fig. 2.20 compares the neutron capture cross-section of ^{3}He with the elastic scattering cross-section of ^{4}He. ^{3}He has a high capture cross-section for low energy neutrons, while the elastic scattering cross-section of ^{4}He is substantially smaller in the low energy region; however, this cross section exhibits a peak that is located at roughly 1 MeV, matching the energy range of fission neutrons.
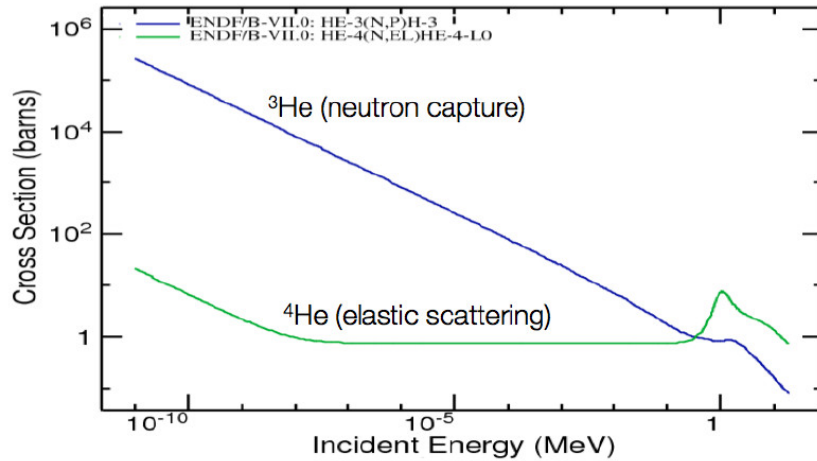
Figure 2.20: Elastic scattering cross-section for ^{4}He: it exhibits a peak at around 1 MeV, matching the emission spectrum of fission neutrons rather well. From [33]

The development of fast neutron ^{4}He detectors exploits this relatively large elastic scattering cross section in the energy range of fission neutrons. In an elastic scattering interaction, energy is transferred from an incoming neutron to a ^{4}He nucleus; the neutron is not absorbed in the process. For kinematic reasons, the maximum energy transfer from an incoming neutron to a ^{4}He nucleus is 64% of the initial neutron kinetic energy.
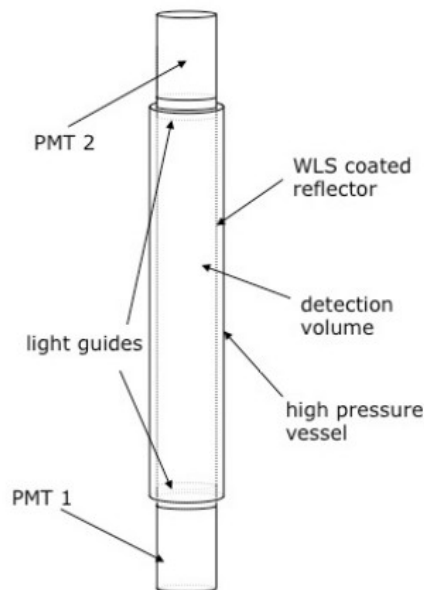
Figure 2.21: A schematic drawing of ^{4}He scintillation detectors

Fig. 2.21 shows a schematic view of the detectors used. A cylindrical high-pressure vessel, sealed by windows at both ends, is read out by two standard 1.5" PMTs encapsulated in a stainless steel extension of the main vessel. Due to the short wavelength of ^{4}He scintillation light, the walls of the detection volume are coated with a wavelength shifting material (WLS). Fig. 2.22 is a photo of 4 fast neutron tubes. Specifications for the fast neutron detectors used in MODES_SNM are listed in Table 2.4.

Figure 2.22: ^{4}He fast neutron tubes used in MODES_SNM

MODES_SNM ^{4}He fast neutron detector

Total length	1000	mm	Active volume	1	l
Maximum diameter	70	mm	Weight	4.9	kg
Active length	470	mm	Pressure @ 20°C	180	kPa
Active diameter	50	mm	Efficiency	5.7	cps/μSv/h

Table 2.4: Specifications of MODES_SNM ^{4}He fast neutron detectors

A typical pulse shape discrimination (PSD) plot for the ^{4}He fast neutron detector is shown in Fig. 2.23. As already reported, the gamma ray sensitivity of this detector is lower with respect to liquid scintillators so that neutrons are more easily detected also in presence of a very strong gamma ray background, as required in case of Homeland Security applications.

Thermal neutron detectors

Once the primary neutron inspection is performed in the MODES_SNM prototype by the fast neutron detectors, additional information is obtained from the thermal neutron detectors. Fast neutrons and thermal neutrons are usually detected with different types of detectors, as described in Sec. 2.3.1. If a slow neutron is surrounded by moderating material, fast neutrons can thermalize enabling their detection. When this technique is used, a single
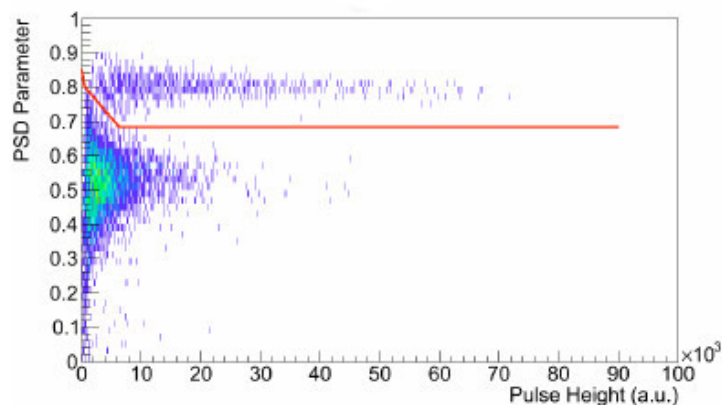
Figure 2.23: Typical PSD plot from the ^{4}He detectors showing the discrimination between neutrons (above the red line) and gamma rays (below the red line) from a ^{252}Cf source

detector can count both types of neutrons, but any information about the initial energy is lost.

MODES_SNM thermal neutron detectors are a special version of the ^{4}He detectors specifically developed to detect both fast and slow neutrons. These modified detectors are very similar to the fast neutron ones described above, the main difference being an internal coating layer of ^{6}LiF which acts as a converter. Details about this detector structure are covered by a patent registered by Arktis Radiation Detectors Ltd. and will not be described here. Since these detectors work without moderator, the measured fast-to-thermal neutron ratio brings information on the presence of shielding around the neutron source. The capability of providing information on the type of neutron source and on its eventual shielding is a peculiar characteristic of MODES_SNM system.

Specifications for the modified thermal neutron detectors used in MODES_SNM are listed in Table 2.5.

MODES_SNM ^{4}He thermal neutron detector

Total length	700	mm	Active volume	1	l
Maximum diameter	70	mm	Weight	4.9	kg
Active length	200	mm	Pressure @ 20°C	130	kPa
Active diameter	50	mm	Thermal neutron det. eff.	4.6	%

Table 2.5: Specifications of MODES_SNM ^{4}He thermal neutron detector

Slow neutrons are discriminated from the fast component by a variation on the PSD standard technique. Instead of plotting the slow component versus the total light, for thermal discrimination structures become evident when plotting the fast component versus the slow component (Fig. 2.24 and Fig. 4.4):

- gamma ray signals feature both a small slow component (as for gammas in other scintillators) and fast component (due to gamma rejection properties of ^{4}He); therefore gamma ray events are confined in a small region near the origin of the axis;

- fast neutrons have a rather small fast component (see Fig. 2.16) but bigger slow component with respect to gammas; they can be isolated in the region near the Y axis;

- thermal neutrons can have the same values of the slow components as fast neutrons, but due to the presence of lithium their interactions result in bigger fast component values, placing their events in a separate region of the plot.
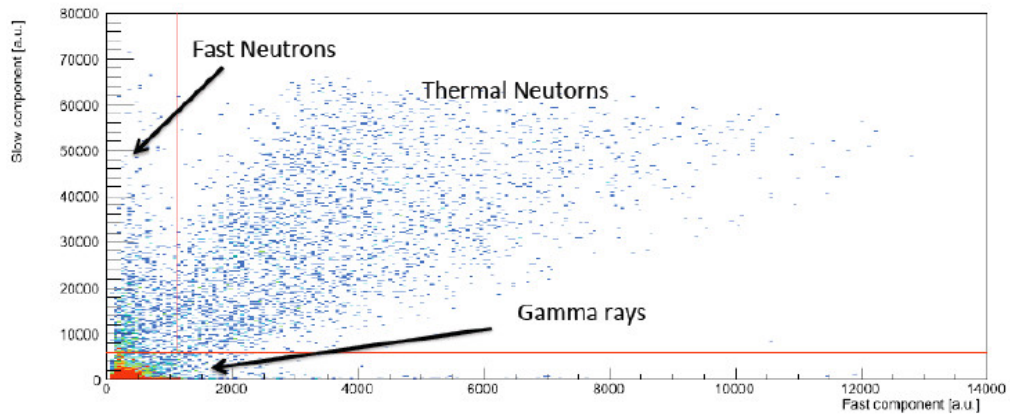
Figure 2.24: Fast and thermal neutron discrimination in a ^4He detector

Chapter 3

Electronic front-end and IS hardware

According to the original project specifications, the radiation-sensitive part of MODES_SNM was to be made up of 12 different high pressure cells: 8 fast neutron detection ^{4}He tubes, 2 thermal neutron detection ^{4}He tubes and 2 Xe gamma detectors. Each tube is coupled to a PMT at both ends, to maximize the collection of light. Every PMT has its own output line, but to reduce the number of connections both PMTs are powered by the same HV line through a splitter inside the detector box. Later in the project one of the Xenon detectors has been replaced by a NaI(Tl) gamma detector with a single negative-powered PMT. The final configuration accounts for a total of 12 HV channels (10 positive for the ^{4}He tubes and 2 negative for the gamma ray detectors) and 23 signal channels.

Power management and signal processing are handled by six CAEN desktop modules, three HV power supplies and three waveform digitizers, daisy-chained through an optical fiber connection. The desktop configuration has been chosen to eliminate the need for a VME rack, and to maximize flexibility and modularity in the system designs.

Front-end modules are managed by the Information System (IS) computer unit, together with a set of USB-controlled devices providing monitoring and positioning functions. The front-end modules, the computer unit and the auxiliary systems are integrated inside the Electronic Box (see Sec. 5.1.1).

3.1 Computer unit and related devices

In order to comply with the concept of a modular and relocatable system, characterized by a reletively light weight and the possibility to operate with battery power, MODES_SNM IS hardware was designed to feature low power consumption, small dimensions, the necessary computational speed and a given number of different connection interfaces.

According with the general features outlined above, at first a group of main specifications were identified for the hardware components:

- small Mini-ITX motherboard with embedded graphics, low-power processor and essential connections;

- solid-state hard drive, quick boot-on-power BIOS;

- PCI-Express interface with optical cables to communicate with front-end electronics;

- commercial devices for GPS localization and Wi-Fi communications, using USB connections wherever possible. As a backup choice also Bluetooth interface could be considered: this type of interface offers a standard and cheap protocol, but involves more components (both HW and SW).

The limited number of moving parts makes the system more suitable for mobile field operations, while the low consumption results in a lower heat production and weaker cooling requirements.

A direct connection to the computer for maintenance and/or for expert operations had to be provided. This is possible at anytime by connecting the motherboard to an external monitor and keyboard through the waterproof connectors mounted on the rear panel.

As far as the communication and remote controls are concerned, the proposed solution was to configure the device for operating as a Wi-Fi hotspot, providing access to a secure network for monitoring and operating the system. The main advantage of using such a configuration is that almost any existing device with networking tools and basic screen resolution could be used to remotely control the system. Thanks to the large diffusion of the web-based applications, such an interface was also expected to be more familiar and easy-to-use by the end users. On the contrary the choice of developing custom "control station" for the remote device would have resulted in larger costs producing a more "device-dependent", and therefore less flexible, system. For this reason, an additional basic requirement for the hardware was a wireless device that other devices would be able to connect to.

3.1.1 Computer unit

The core of the IS hardware is a small personal computer with specific features and connection devices. The final hardware configuration is based on the commercial Mini-ITX standard with an x86-64 architecture; the core of the system is represented by the Sapphire PURE White E350 motherboard, featuring an embedded AMD E350 APU (*Accelerated Processing Unit*); a 320 GB Solid-State Drive (SSD) and 4 GB of RAM are installed on top of it, providing enough memory for data buffers and operation logs. Computational resources of this machine may be limited compared to a recent laptop, but with a tailored software configuration this low-consumption setup is able to drive the operations of the MODES_SNM prototype for a reasonable operating time while battery-powered.

3.1.2 Communication and positioning

Communication between the components of the system and with the users is a crucial issue. Data transfer between the electronics and the computer units is carried through a CAEN PCI-Express controller mod. A3818 (Fig. 3.1). This family of controllers can hosts up to 4 different optical channels; each channel has a maximum data transfer rate of 85 MB/s and is capable of handling 8 different boards in daisy-chain configuration, for a total of 32 boards.

The position is provided by an additional card (RF Solutions GPS Eval Kit with GPS-1513R embedded module, Fig. 3.2) working as GPS receiver: it is a platform aimed to the development of hardware and software GPS solutions, and it can be controlled via USB with standard protocols and data formats. An external magnetic GPS antenna will be placed in the most exposed position possibile according to the operational conditions.
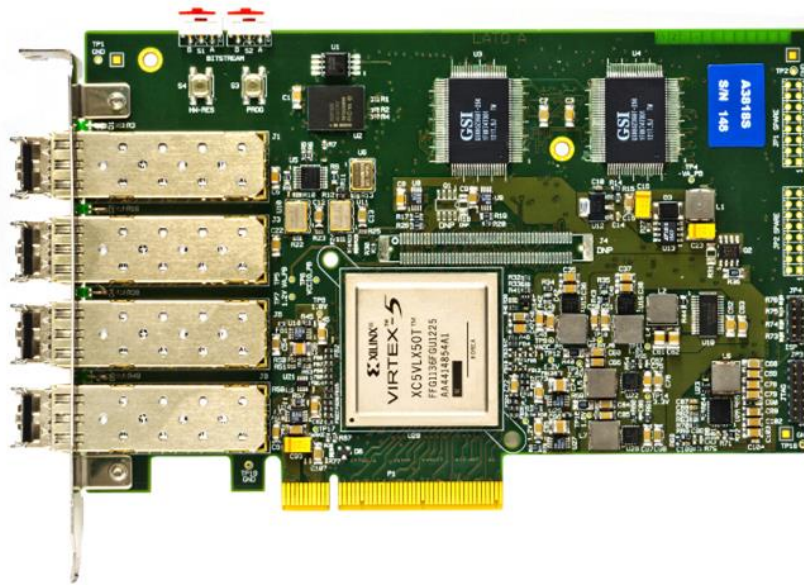
Figure 3.1: CAEN A3818 Optical controller (PCI-Express x8)
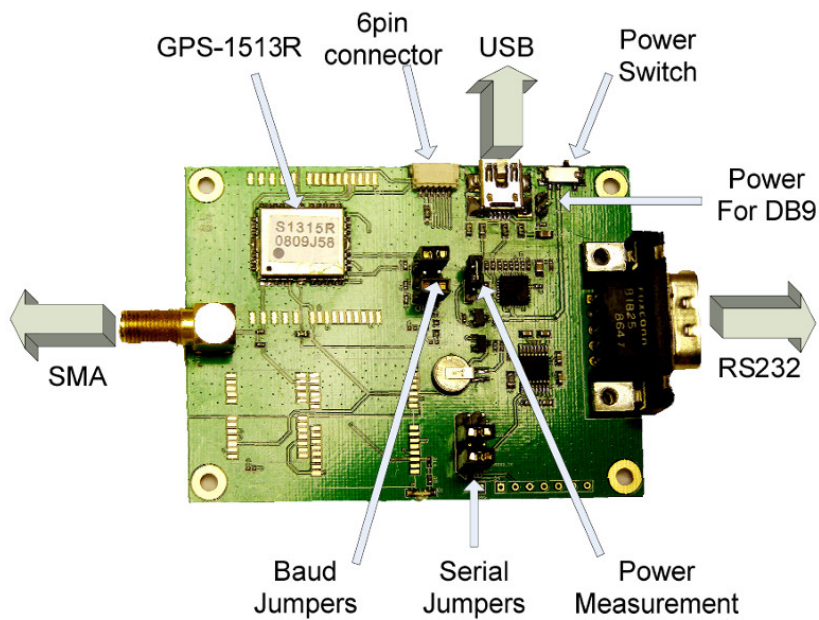
Figure 3.2: RF solutions GPS module

To provide system access to the operators, a commercial Wi-Fi router is used (TP-LINK W8960N); it provides both wireless and cabled connection, by means of an external Wi-Fi antenna and an Ethernet port mounted on the side of the Electronic box. All commercial security protocols are available to enforce the proper protection on the data link.

3.1.3   Monitoring devices

To monitor and log the status of the core components, a dedicated USB device was installed, Powerlog 6S by Progressive RC (shown in Fig. 3.3). Table 3.1 shows its datasheet.

Figure 3.3: Powerlog 6S logger

The Powerlog 6S is designed to be connected in series within the input DC power line, sampling the voltage/current values and integrating the used charge; it also features an embedded temperature sensor used to prevent overheating inside the electronic box. Values can be monitored via the LCD screen or downloaded via USB with an open protocol.

Input Voltage Range	4.5 ÷ 60 V DC
Current Measurement Range	-130 to +130 A (-40 to +40 A continuous)
Cell Voltage Range	0.05 ÷ 28.0 V DC
External Temperature Meas. Range	-55 to +125 °C (-67 to +257 °F)
Pulse Measurement Range	10 ÷ 999999 μs
Steering Gear Pulse Output Range	0 ÷ 20 ms (0.5 μs step)
RPM Measurement Range	0 ÷ 999999 rpm
Voltage Display Resolution	1 mV
Current Load of Test	12 mA
Maximum Voltage for Alarm Port	50 V DC
Current Drain for Alarm Port	<500 mA
Log File Storage	16 Mbit (33 hours @ 2 second interval)
Logging Interval	0.25 ÷ 60 seconds
Weight	28 g
Dimensions (L × W × D)	85 mm × 40 mm × 13 mm

Table 3.1: Technical data sheet for Powerlog 6S USB logger

MODES_SNM detectors feature embedded sensors for pressure and temperature; they

are read through a serial RS-485 daisy-chain configuration ending with a USB controller. All the components of this Slow Control system were developed by Arktis Radiation Detectors Ltd. during WP2 and WP5.

3.1.4 Connections

The connection scheme for the different components, according with the final prototype integration layout, is shown in Fig. 3.4.
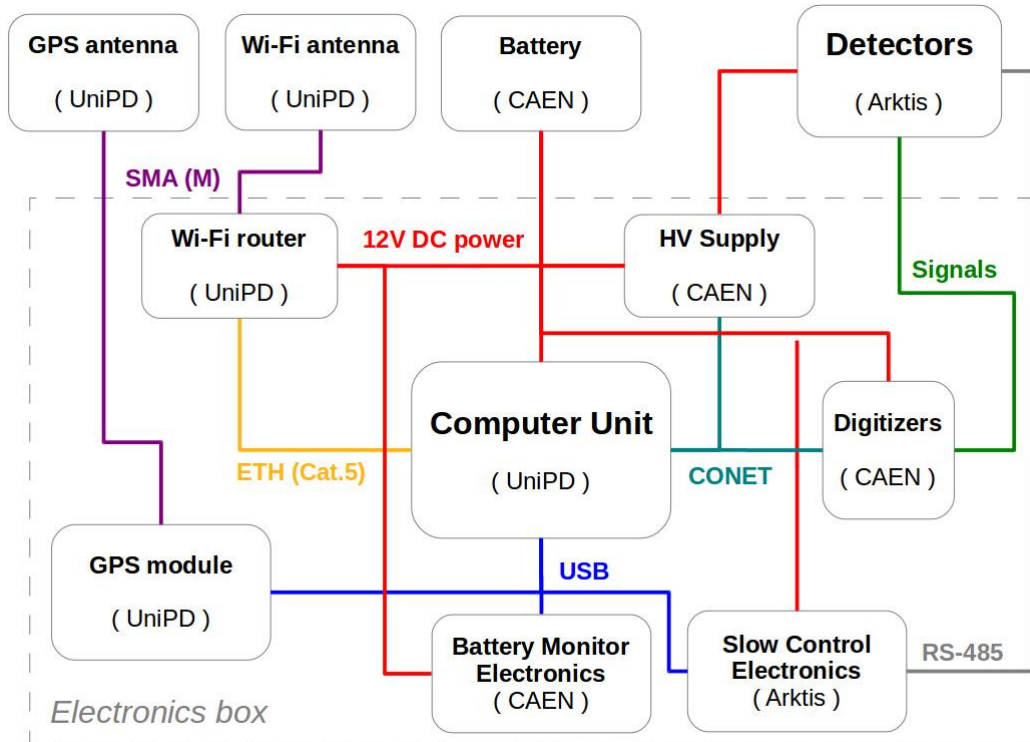
Figure 3.4: Connection map for Electronic Box in the final configuration

The computer unit is connected to the front-end electronics (digitizers and HV power supplies) through the CAEN proprietary CONET optical connection. ARKTIS slow controls, battery monitor and GPS module use standard USB and RS-485 transmission protocols, while the router for the hot-spot functionality is connected to the Ethernet port. A 12 V bus connected to the battery socket distributes the DC power supply to all the commercial components of the system. Finally, external antennas make use of SMA coaxial cables.

Additional connectors, not shown in the drawing, provide sealed connectors for the operators to inspect the system without opening the Electronic Box; they consist of 2 USB plugs, one Ethernet socket and a female VGA connector.

3.2   HV power supply

High voltage power to detector boxes is supplied by three CAEN DT5533N desktop modules, shown in Fig. 3.5.

Figure 3.5: CAEN HV Desktop Module mod. DT5533

These modules have been developed during Work Package 3 of the project; the result is a HV card with increased output power and lower electrical noise with respect to existing models. DT5533N datasheet is presented in Table 3.2.

Dimensions	154 mm × 50 mm × 164 mm (W × H × D)
No. of Channels	4
Polarity	Positive or Negative (factory set)
Output Voltage	0 ÷ 4 kV
Max. Output Current	3 mA (4W max)
Voltage Set/Monitor Resolution	100 mV
Current Monitor Resolution	50 nA (high range) / 5 nA (low range)
Current Set Resolution	50 nA
Current Set Maximum Value	3100 μA
VMAX hardware	0 ± 4100 V common to all board channels
VMAX hardware resolution	20 V
VMAX hardware accuracy	2% of FSR
Ramp Up/Down	1 ÷ 500 Volt/sec, 1 Volt/sec step
Vmon vs. Vout accuracy	±0.05% of read ±1 V
Vset vs. Vout accuracy	±0.05% of read ±1 V
Imon vs. Iout accuracy	±2% of read ±100 nA
Iset vs. Iout accuracy	±2% of read ±100 nA
Maximum output power	4 W per channel (software safety limit)

Table 3.2: Technical data sheet for DT5533N HV power supply

The three cards are software operated by means of a custom developed library, and share the same controller and optical chain link of the digitizers.

3.3   Waveform digitizers

3.3.1   Traditional set-up for radiation detection experiments

There are many ways in which a measurement setup can output its data, ranging from mechanical indicators to photographic emulsions. However, due to the huge developments

in the field of electronics, almost every instrument of the last decades has been designed to output one or more electrical signals. Radiation detectors make no exception, and most of the physical analysis is achieved through the processing of these signals.

Different protocols have been developed during the years to accomplish this task in a standardized and flexible way. They all obey to the logic of splitting the analysis in a sequence of simple operations, each one handled by an independent module; modules are then connected according to the sequence of steps required by the analysis. Every module is therefore provided with input and output connectors, and each standard specifies cabling, connectors, impedances and levels for logic signals, to ensure compatibility between modules of different manifacturers. Modules can be stand-alone or, more often, hosted in crates providing cooling and power supply.

The typical layout for a spectroscopic experiment is represented in Fig. 3.6:
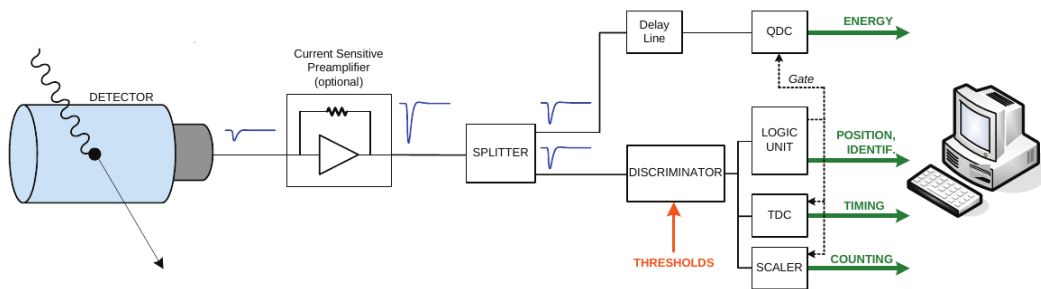
Figure 3.6: The analog chain required to extract charge and timing information from signals. From [34].

Signals coming from the detectors must undergo several passages before the physical information is extracted. The first one is usually a pre-amplifier stage, to improve signal-to-noise ratio (S/N); a splitter is likely to follow immediately after the preamplifier, to distribute copies of the original signal. As an example, the procedure for validating a signal with a threshold discriminator is as follows:

1. signal is splitted in signals A1, A2;

2. signal A1 is delayed by the time corresponding to steps 3 and 4;

3. signal A2 is fed into the threshold discriminator;

4. gate signals AG is generated in correspondence to events in A2;

5. AG is used to validate A1 and B2.

Since this entire sequence may require up to 5 different modules for the sole purpose of validating a signal, it is clear that space and cost issues will easily arise when building the entire setup for any experiment with more than few channels.

Moreover, even for the simplest operation the corresponding module relies on a certain number of analog components, each one introducing its own contribution to signal distortion. The more modules are used, the more distortion is introduced in the analysis, resulting in loss of linearity, signal attenuation and other undesired effects. Therefore the need to reduce the number of modules has often a significant impact on the final layout of a system, posing limits to the types of analysis that can be performed.

At the present time, there are at least three standards widely used in physics experiments: NIM, CAMAC and VME. They are all based on crates (or bins) designed to fit into the standard 19-inch relay rack; however the size of the single modules is different, as is the number and type of connections provided by the crate.

- **NIM - Nuclear Instrumentation Module (1964)**
  Defined by the U.S. Atomic Energy Commission, it was the first modular standard for scientific experiments. Module width is a multiple of 34.4 mm, and each crate can accommodate up to 12 modules, providing standard DC power supply through back connectors. Signals are transmitted by means of coaxial cables with BNC connectors, while SHV standard is used for high voltage connections. NIM modules cannot communicate with each other through the crate backplane; as a consequence, NIM-based ADC modules are nowadays uncommon in nuclear and particle physics. NIM is still widely used for amplifiers, discriminators, nuclear pulse generators and other logic modules that do not require digital data communication. Data connection to computers is very uncommon, and can happen only on a single-module basis.

- **CAMAC - Computer Automated Measurement And Control (1975)**
  One CAMAC crate is divided into 25 stations spaced 17.2 mm apart, and can host up to 24 single-width modules; the reduced size compared to NIM was made possibile through the development of printed circuit boards with integrated circuits, resulting in a higher module density inside a crate. The backplane provides DC voltages to modules like its NIM counterpart, but a dataway (or communication bus) with 48 lines is also present. The extreme right-hand station is reserved for the crate controller, a special module required to control the dataway and handle data communication between the modules. The controller provides also an interface to communicate with other crates or computers. Signal links are often provided through ribbon connectors instead of BNC due to space constraints.

- **VMEbus - Versa Module Europa bus (1987)**
  Originally developed as a computer bus for the Motorola 68000 CPU, it is now a common alternative to CAMAC systems. Newer versions of the standard are VME64 (1994) and VME64x (1997): they increased the speed and the number of the available connections both for power supply and data transfer, and each version is backward compatible. The size unit for modules is 20.32 mm, allowing crates to accommodate up to 21 single-unit modules. Due to the limited space on the front panel, LEMO 00 or ribbon connectors are often used instead of BNC. VMEbus modules perform the same operations of CAMAC modules, but their configuration is more often controlled by software rather than by front panel switches, allowing the complete automation of system operations. VME modules can even host embedded computers running custom software - as is the case of Waveform Digitizers. Connection to computer is possibile by means of modern interfaces and protocols such as USB, PCI and Ethernet.

As can be seen, computers soon began to become ubiquitous in all kinds of experiments. Initially they were placed as the last element of the hardware setup of experiments; this allowed to store the data in a digital format, to be copied, shared, and analyzed as many times as needed. Further improvements and module updates allowed single components to

be managed by computers, eventually leading to the automatization of data acquisition, and the new standards have been explicitly designed to be connected to computers and controlled by software through a variety of standards and protocols.

Despite this widespread use of digital equipment, in most cases the first stage of analysis still relies on independent analog modules, each one performing one specific function (amplification, shaping, integration, discrimination...). This choice is made to ensure compatibility with existing equipment and optimize investments. In addition, there is often the need to reduce the amount of data to a scale that could be handled by available ADC speed and computing power: until a few years ago, limitations in the performances of digital DAQ systems represented a serious bottleneck for almost every experimental set-up.

3.3.2 Introduction to waveform digitizers

Nowadays, the constant increase in computer speed and the availability of very fast and high precision ADCs (*Flash ADCs*) permits to design acquisition systems in which the analog-to-digital conversion occurs as close as possible to the detector. The digitizer signal is stored in memory and the entire analysis is performed in the digital domain, a process known as *Digital Pulse Processing*, or DPP [34].
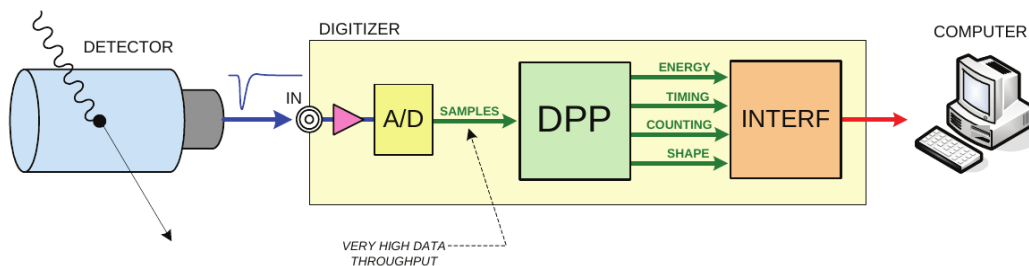
Figure 3.7: The digital chain required to extract charge and timing information from signals. From [34].

The use of ADCs in Physics started to spread in the early 1990s, with the development of new high-speed components with good resolution; the digital processing of pulses from detectors was applied to spectroscopic systems with performances at least comparable to analog solutions.

The main advantages of digital processing are essentially two: *flexibility* and *stability*.
Flexibility: since all the processing is performed through software routines, the modification of a parameter is simply a matter of changing a number in the source code, while the same change in an analog module would require the substitution of physical circuit components. Even the most sophisticated analog module can provide only a limited choice of parameters to be set from the panel switches; digital systems can use infinite combination of values, and new algorithms can be implemented in the software at almost any time.
Stability: once the data has been converted to a digital format, there is no further change in that information. Digital time delays introduce no distortion in the signals, and processing is immune by temperature drifts, voltage fluctuations or signal interferences.

Waveform digitizers further exploit the advantages of digital processing, combining the performances of fast ADCs with embedded computers for real-time analysis of the signals. Signal properties such as Energy, Pulse Height or Time reference can be calculated on-line,

instantaneously incrementing counters or filling spectra; in addition, a large variety of filters can be applied (pile-up, coincidence...) to reject events before transferring the data.

Modern digitizers can easily handle input rates of the order of 10^4 analyzed events/s per channel, with a maximum of 16 or 32 channels in a single module. Moreover, the possibility to embed most typical processing functions inside a single front-end module eliminated the need for racks and controllers; it is now possibile to build standalone modules with the so-called "Desktop" form factor. These improvements not only greatly reduce the hardware requirements in large experiments, but also make possibile to build complex but compact, real-time analysis systems, such as relocatable radiation monitors like MODES_SNM.

How does a digitizer work?

The principle of operation of a Waveform Digitizer (also known as Transient Recorder or Flash ADC) is the same as the digital oscilloscope: the analog-to-digital conversion is performed continuously, and when the trigger occurs a certain number of samples (the "acquisition window") are saved into one memory buffer.
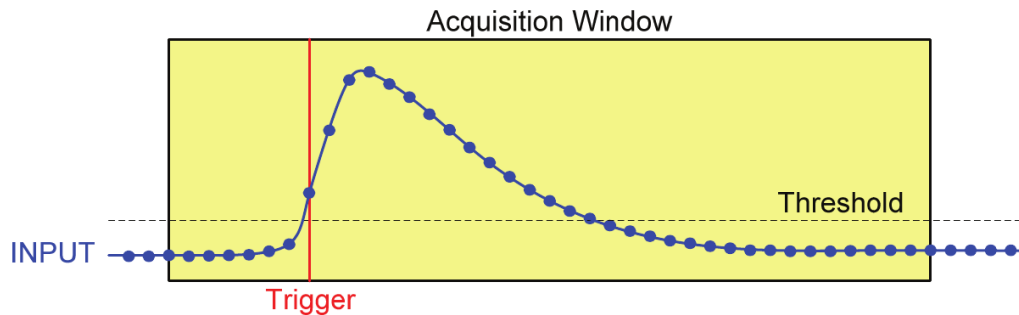
Figure 3.8: Digital sampling of signals and the acquisition window

However, the digitizers present some important differences with respect to digital oscilloscopes:

- triggered events are stored in a temporary buffer; while the acquired samples are copied in the buffer, a new trigger can occur and the two overlapping windows will originate two different events in the buffers. Provided that the readout rate is high enough to avoid the memory to go full, there is no dead-time between triggers and no events are lost;

- different waveform digitizers can be connected in chains and synchronized, allowing for system scalability;

- they have high bandwidth data readout links (VME, optical links, etc...);

- digitizers embed FPGAs or DSPs to do on-line data processing and data reduction.

Most waveform digitizers feature three different operating modes:

- *Oscilloscope mode*: no calculations are performed and only the waveforms are transferred; this mode has the higher data transfer requirements and the analysis relies completely on off-line software routines;
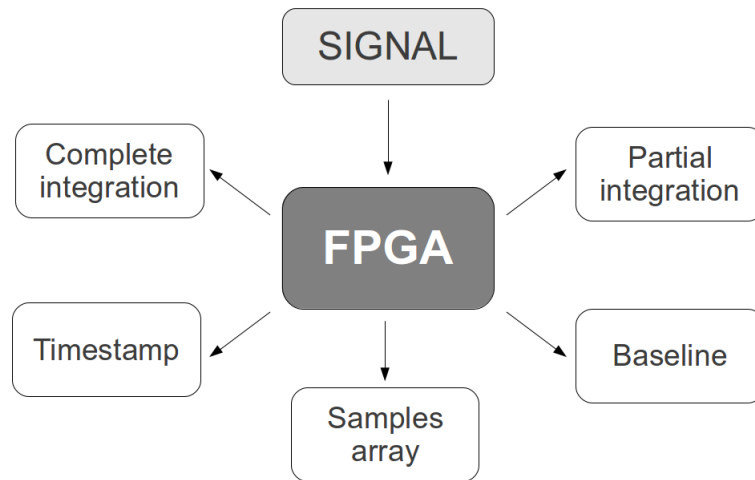
Figure 3.9: Possible outputs of on-line FPGA processing

- *List mode*: only the DPP outputs are transferred (timestamp, charge...); the size of the transferred data is the smallest, allowing for a greater input event rate; no further analysis on individual signals is possibile and this is the typical solution for real-time setups with little computing power;

- *Mixed mode*: output events contain both calculated values and part of the original waveforms; this is a compromise between the need for real-time analysis and the possibility to perform further corrections based on selected regions of the waveforms.

Comparison with analog chains

Fig. 3.10 depicts the comparison of analog and digital acquisition chains in a practical case: a NaI(Tl) detector exposed to gamma radiation, when both charge and timing informations are produced.

The use of waveform digitizers has many advantages over that of chains made of analog modules:

- one single board can do energy, timing and pulse shape analysis: there is a dramatic reduction in module number, resulting in simpler systems, lower costs and improved reliability;

- performing all the analysis in the digital domain increases linearity and stability;

- the dynamic range is wider, and also the uniformity of the performances over the range;

- digital techniques allows better correction of pile-up, and baseline fluctuation effects;

- pulse information is preserved;

- all the channels can easily be kept synchronized and correlated; coincidence and anti-coincidence filters can be applied both in real time or after the acquisition (off-line);

- the dead-time in the acquisition is very low, resulting in a higher counting rate;
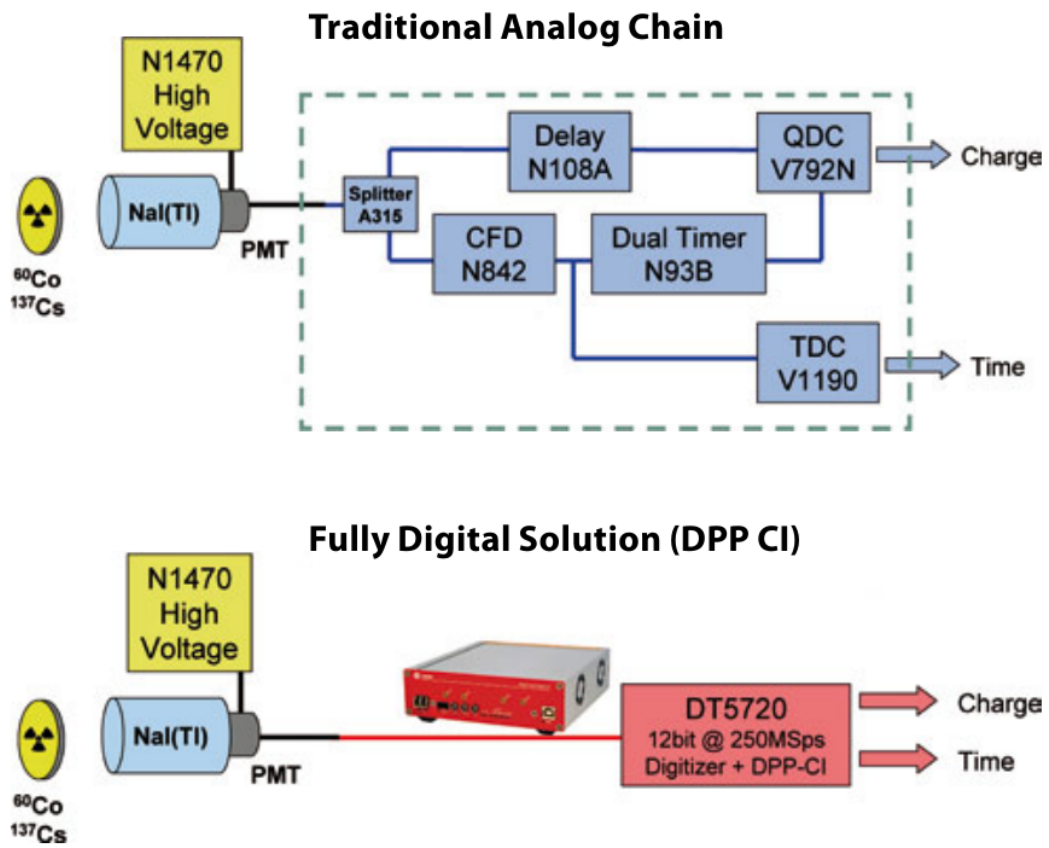
Figure 3.10: *Comparison of analog and digital chains for charge integration of signals*

- the use of FPGAs enables the users to change and adapt the algorithms, easily tailoring the digitizers to the specific application;

- the system is tuned and calibrated through register programming instead of manual regulations; these operations are faster and can be fully automatized.

However, the increased flexibility of a digitizer comes at the price of greater complexity concentrated in a single module. In addition, it is difficult to reuse existing and well-known tools and techniques, making the use of waveform digitizer a paradigm shift in the approach to acquisition systems.

3.3.3 Digital techniques for signal analysis

In waveform digitizers, like digital oscilloscope, the analog-to-digital conversion is performed in a continuous way; in principle this could lead to the so-called "fully digital approach", where the signal samples are recorded at any time for the entire duration of the acquisition. However, the resulting data transfer rate would be difficult to sustain with present technology.

As an example, considering an 8-channel digitizer with 12 bit resolution and 250 MS/s sampling rate, the transfer rate for continuous acquisition would be 3 GB/s, completely filling 1 TB hard drive every 6 minutes. Instead, with a threshold trigger that selects 5 kHz of events, each one made by 512 samples (corresponding to an acquisition window of about 2 us) the required transfer rate drops to 30 MB/s, a value that can be sustained by a single USB cable.

Therefore it is essential for every digital acquisition system to have a trigger mechanism to select interesting events. Sometimes additional filters are required to achieve a sustainable data rate, depending on the experimental conditions.

Trigger

Usually, the digitizers and the oscilloscopes feature a self-trigger based on a programmable voltage threshold, being generated as soon as the input signal crosses that threshold. Unfortunately, this technique is not suitable for most physics application because of the baseline fluctuation, pulse pile-up, noise, etc. However, the ability in finding all the good pulses and discriminating them from the noise is very important. In fact, missing pulses or false triggers can cause loss of important events, bad pile-up rejection, errors in the statistics and other undesired effects. The digital filters are able to reject the noise, cancel the baseline and make shape and timing analysis for this purpose.

In Fig. 3.11 two different situations are illustrated: in the upper panel, a standard threshold trigger fails to select events due to noise and baseline fluctuations, while in the lower panel the trigger operates after the signal has been filtered to address these issues. Trigger filters are developed by manifacturers and embedded in the digitizer firmwares.

Some digitizers allow the user to switch between two different trigger modes: *Edge mode*, equivalent to an analog threshold discriminator, or *Peak mode*, which automatically senses peak structures over the baseline. In Peak mode, the threshold is used to arm the trigger, but the trigger is fired only when the signal reaches its top; this kind of trigger is less

sensitive to walk effects and less dependant on the signal amplitude that triggering directly
at the threshold-crossing point.
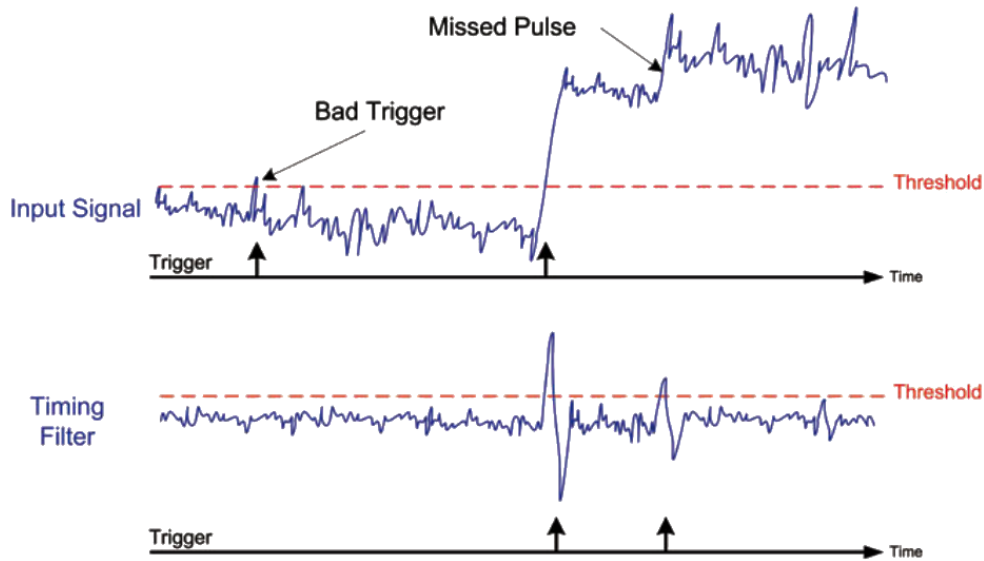
Figure 3.11: Examples of triggers operating on distorted signals (upper panel) and ideal signals (lower panel)

Baseline calculation

The baseline of an acquisition system can be defined as the input level that the system
would see in absence of noise fluctuations or signals. Baseline is often treated as a constant
reference, noise as a random alteration of the baseline (its average being zero) and signals
as structured alterations. However, this is only a conceptual approximation: since elec-
tronic circuits are always interacting each other, baseline level is influenced by both noise
and signals, not including other possible fluctuations within the conversion stage. Baseline
calculation is therefore an essential feature for DPP systems: not only its evaluaton has a
direct impact on trigger performances, but it also affects integration routines, leading to
wrong charge estimations, and possibily other analysis routines.

The typical solution to address this problem is to perform a dynamic evaluation of the
baseline, averaging N points inside a moving window, where N is a value defined by the
user depending on signal dynamic range. This dynamic evaluation must freeze some time
before trigger occurs, or the leading edge of the signal will contribute to the calculation;
for the same reason, there must be a hold-off period after the trigger before the baseline
evaluation could start again, considering in the mean value also the points before the freeze.
This technique allows to have almost no dead-time due to the baseline calculation. Fig. 3.12
illustrates this mechanism; *Long gate* is the interval in which the signal is integrated.

Timestamp

There are many types of timing and triggering filters. Inside its digitizers, CAEN has devel-
oped $RC - (CR)^N$ filters able to reject the high frequency noise (RC filter = mean filter),
restore the baseline and cancel the low frequency fluctuations (CR^N filter = derivative) and
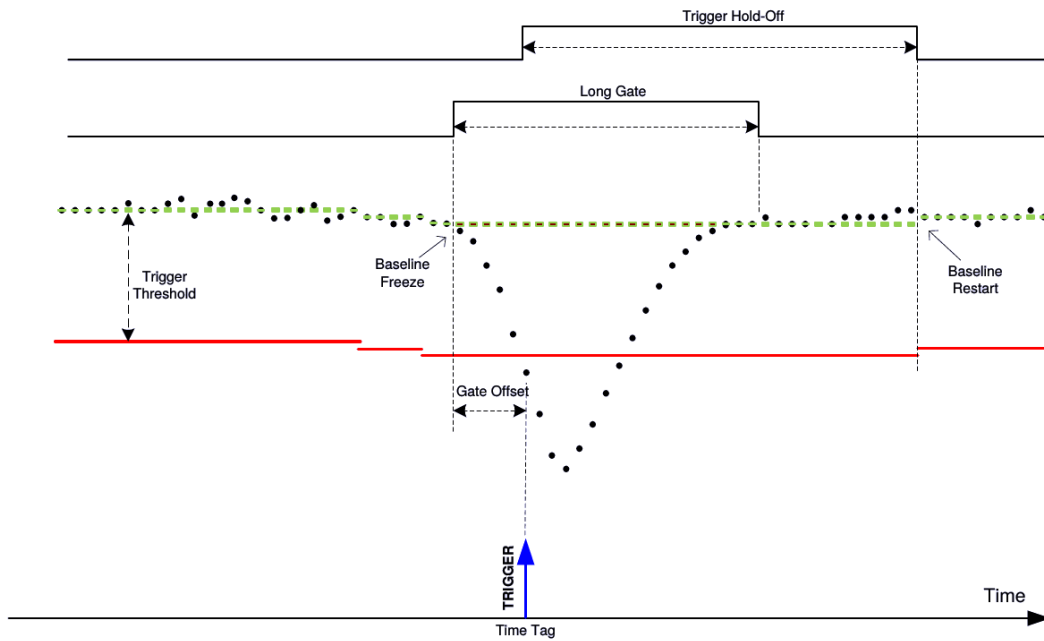
Figure 3.12: Example of continuous baseline calculation

transform the pulses into bipolar signals whose zero crossing (which is independent from the pulse amplitude) can be used for the determination of the timestamp.
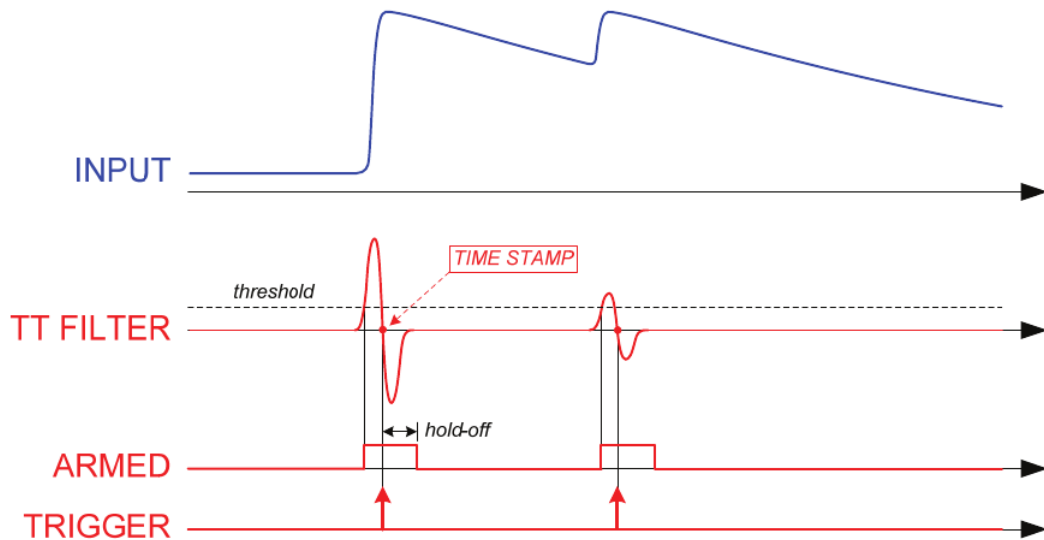
Figure 3.13: Signal filters to determine time reference of pulses

The sampling period of the ADC reflects in a granularity of the timestamps; in order to increase the timing resolution beyond this limit, it is necessary to use two or more samples around the zero crossing and make some kind of interpolation. The simplest choice is the linear interpolation (segment between two points).

The presence of a timestamp reference for each event allows to easily perform off-line coincidence analysis on the data with arbitrary logic, provided that the required coincidence window is compatible with the timestamp uncertainty (usually a few nanoseconds). On-line coincidence filters do not make use of timestamps; instead, they work at a lower level.

On-line coincidence filters

One of the most useful tecniques used to reduce data output and select events is the coincidence method. The analog sequence to perform the coincidence of two events is described in Sec. 3.3.1; with a waveform digitizer the procedure is very similar, but it is completely performed inside the module.

While the implementation may vary depending on the manufacturer, the mechanism often relies on a programmable logic matrix for the cross-validation of triggers. As soon as it occurs, every channel's trigger is spliced: one copy is fed to the matrix and the other is put in a digital delay line. For each channel the matrix performs the logic combination of all the channel triggers, and then outputs a logic signal used for validate (with an AND operation) the original trigger.

Although the matrix can handle only one logical operation (AND, OR, majority) at the time, each channel usually has its own validation, and it is possibile to limit the affecting channels to a subset of the available ones; acting on the delay line and the length of the validation signals it is also possibile to define custom coincidence windows.

In all the cases in which a more sophisticated coincidence logic is required, panel connectors can be programmed to output individual non-validated triggers and receive back a valid trigger signal calculated by an external logic module.
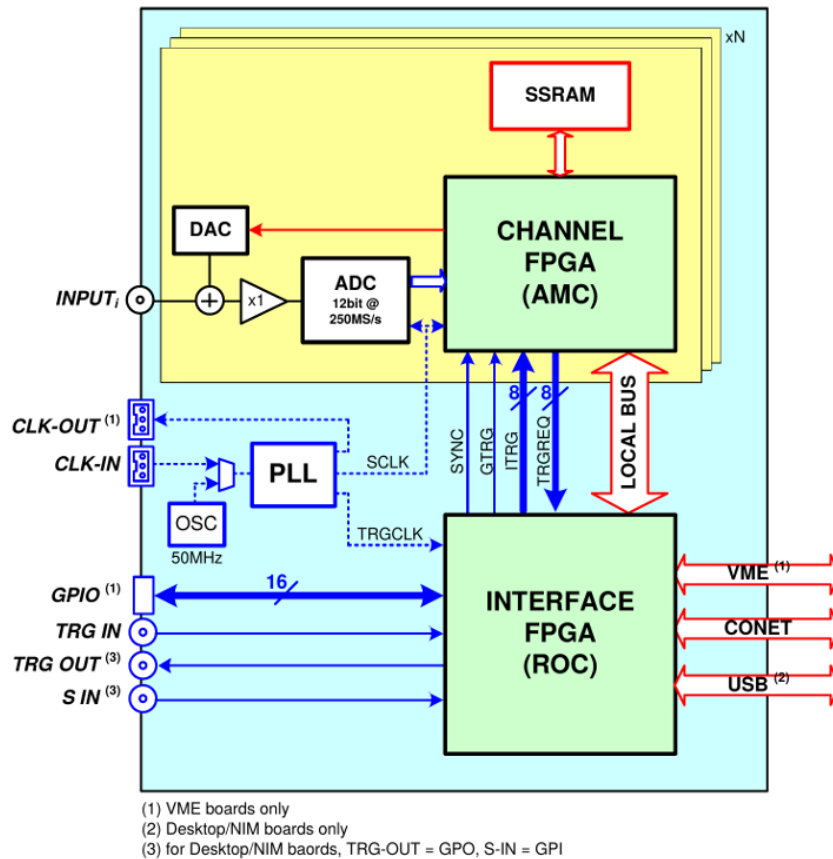
Figure 3.14: Block diagram of a digitizer including an FPGA. From from [35]

Real-time analysis of signals and FPGAs

FPGA (*Field Programmable Gate Array*) is a particular type of integrated circuit that offers the possibility to be configured after being manufactured ("in the field"). They typically provide a large amount of logic gates and memory blocks; the configuration of the FPGA consists essentially in the linking of the logic gates to perform more complex functions, and it is done via special programming languages called *Hardware Description Languages* (HDL) of which VHDL is one of the most common representatives. Together with the ADC stage, FPGAs (or equivalent components) are the distinctive components of a waveform digitizer, handling all the digital processing between the conversion and the transfer of data.

By programming a new firmware inside an FPGA, DPP functions can be added to the on-line analysis stage of the digitizer. Most common firmwares implement pile-up rejection filters, timing routines, coincidence and integration functions, but in principle any kind of function can be programmed, the only limit represented by the available memory. Of course, processing speed will be affected by the complexity of the firmwares.

Fig. 3.14 taken from CAEN documentation illustrates the internal block diagram of a generic digitizer using an FPGA. Actually the card is hosting many FPGAs: one for each channel, to handle individual processing, and one "global" FPGA, providing communications between channels and interfaces to the outside.

Pile-up

When the spacing in time between two signals is lower than the typical duration of a signal, an interference occurs and the effect is called *pile-up*.
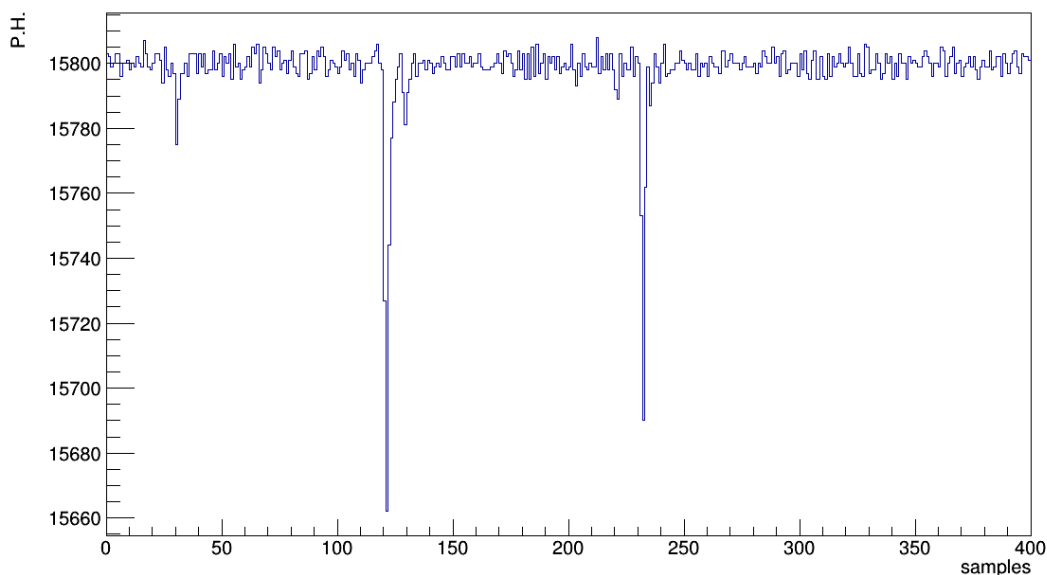
Figure 3.15: Example of tail pile-up

There are two possibile types of pile-up:

- *Tail pile-up*: it involves the superposition of a pulse over the tail of a precedent pulse. Since tails can persist for a relatively long amount of time, this kind of pile-up effect is the most common and can be significant even at relatively low counting rates. On the other side, since the two pulses are clearly distinguishable, tail pile-up can be detected

by on-line DPP algorithms; the event can either be rejected or marked and transferred: off-line deconvolution routines are available to separate the two pulses and completely reconstruct the original events;

- *Peak pile-up*: it happens when the two pulses are sufficiently close together and the system treats them as a single event. It is very difficult to recognize peak pile-up from the shape of the waveform, and only off-line corrections are possibile in selected cases. When applying integration routines, the energy of this event will be roughly the sum of the two original energies; if the measured spectrum is composed by few lines of defined energy (e.g. a calibration spectrum with ^{22}Na) the sum peaks can be easily spotted, allowing to correct the number of events, as shown in Fig. 3.16.
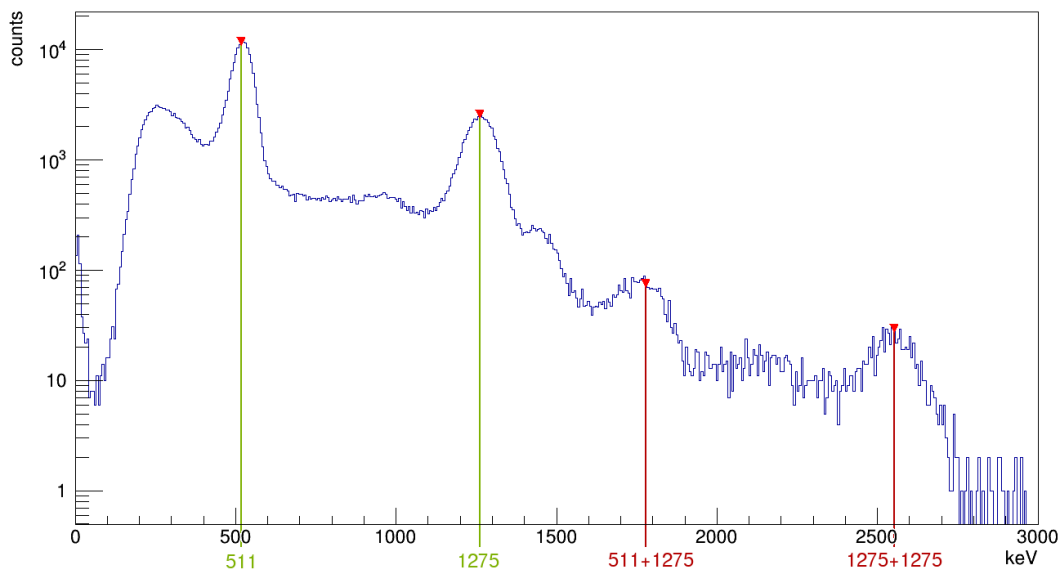
Figure 3.16: Sum peaks appearing on a ^{22}Na spectrum due to peak pile-up

Pile-up is of course directly related to the input event rate: the interval between pulses must be greater than the effective pulse width. The probability to observ an interval greater than T is

$$P(> T) = exp(-nT)$$

where n is the true rate of events [18].

One of the applications where a correct managing of pile-up effect is of paramount importance is the detection of SNM. Since there are many legal commercial uses for gamma-ray sources, one possibile way to illicitly export neutron emitters is to hide them in the middle of authorized radioactive cargo. Provided that the gamma rate is sufficiently high, pile-up effects are sufficient to create "fake" neutron events in a number that completely hides real neutrons (see Fig. 3.17). A second example involves nuclear accidents in power plants or industrial installations, where the detection of neutrons in a high-rate gamma field is essential to understand the reactions taking place in the areas that can not be directly reached by human operators.

In 2012 our group investigated the capability to identify weak neutron sources in a high gamma-ray background, using two different liquid scintillators (EJ-301 and EJ-309) and a

waveform digitizer (CAEN V1720) [36]. The possibility to correctly identify neutrons has been demostrated by developing an off-line pile-up rejection filter compatible with a future implementation inside an FPGA.

Working on the stored data file, the filter detected the presence of pile-up looking at multiple minima in the digitized signal. In addition, event-by-event, the FPGA parameters were compared with the same parameters derived off-line from the digitized signals. The filtering action resulted in the rejection of about 2% of events labelled as pile-up but an additional 5% of the events were discarded since they did not fulfill the quality control performed off-line on the FPGA calculations. This means that at this count rate some FPGA integrations (Peak or Total integral) are not correct. As an example, some events had the correct total energy but not the peak integration, resulting in a wrong determination of the PSD parameter (for details on PSD see Sec. 2.3.3). The result of this filter is shown in Fig. 3.17 where the distribution of accepted and rejected events after the filtering is reported.
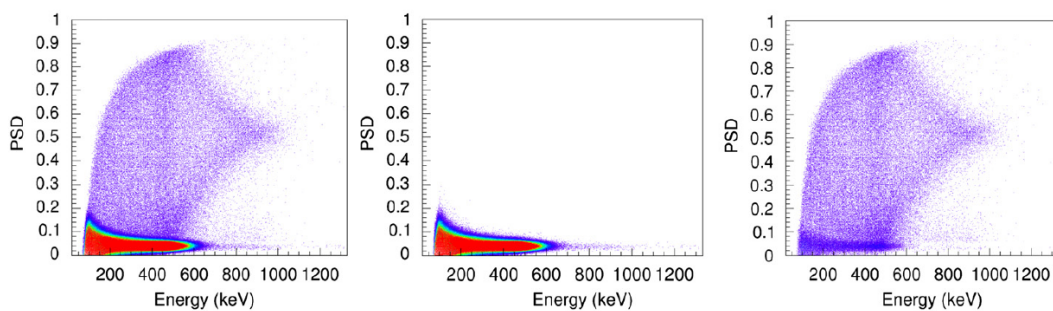
Figure 3.17: PSD scatter plot from EJ-301 scintillator irradiated with a ^{137}Cs source at the dose rate of 100 mSv/h. Left: scatter plot obtained from the FPGA processed parameters; centre: scatter plot after the off line event filtering; right: rejected events. Rejected events represent only about 5% of the total

The application of the off-line software filter largely improves the situation, removing almost completely both pile-up signals and faulty values generated by the FPGA. When such filter is applied, a weak neutron source in conditions described by the IEC62327 standard for hand-held instruments is detected with 95% probability at 95% confidence level with both types of scintillators.

The computing time needed for the software filter is compatible with real time operations. For 10 s of acquisition, the time needed to process all data (about 0.5 Mevents) is of the order of 15 s. The computing time is reduced to 2 s when only the events in the neutron region are filtered, which represents presumably the most interesting situation for nuclear security applications.

Charge integration

Charge integration is the key digitizer utility for spectroscopy applications. In the digital domain the integration process is reduced to the sum of the samples contained in the integration window; the result is then baseline-subtracted and stored inside the event buffer. The integration is controlled by two parameters: the *Gate Width*, corresponding to the size of the integration window expressed in sampling units, and the *Pre-Gate*, that sets the beginning of the integration window with respect of the trigger position. Another parameter, the *Trigger Holdoff*, inhibits the trigger for the time required by the integration.

Moreover, the *charge integration method* is one of most used Pulse Shape Discrimination techniques; it relies on the principle that neutron signals in scintillators have a bigger tail than gamma ray signals, as described in Sec. 2.3.3. The discrimination parameter expresses this difference and is defined as the ratio between the tail integral of the input signal and the total integral.

In the analog processing the tail integral is measured directly with one of the following methods:

- a second QDC unit operating on a copy of the original signal with a different gate

- a second QDC unit operating with the same gate on a delayed copy of the signal [37]

Both methods may introduce relevant errors in the comparison of the integrals.

Inside a digitizer the *total integral* and the *peak integral* are calculated on the same sample sequency and starting from the same starting point, with the *Short (Peak) integration* stopping earlier than the *Long (Total) integration*. Only one new parameter, the duration of the *Short gate*, must be provided in addition to those of the single integration method. The *tail integral* is then computed as the difference of the total and peak integrals:

$$PSD = (total\ integral - peak\ integral) / (total\ integral)$$
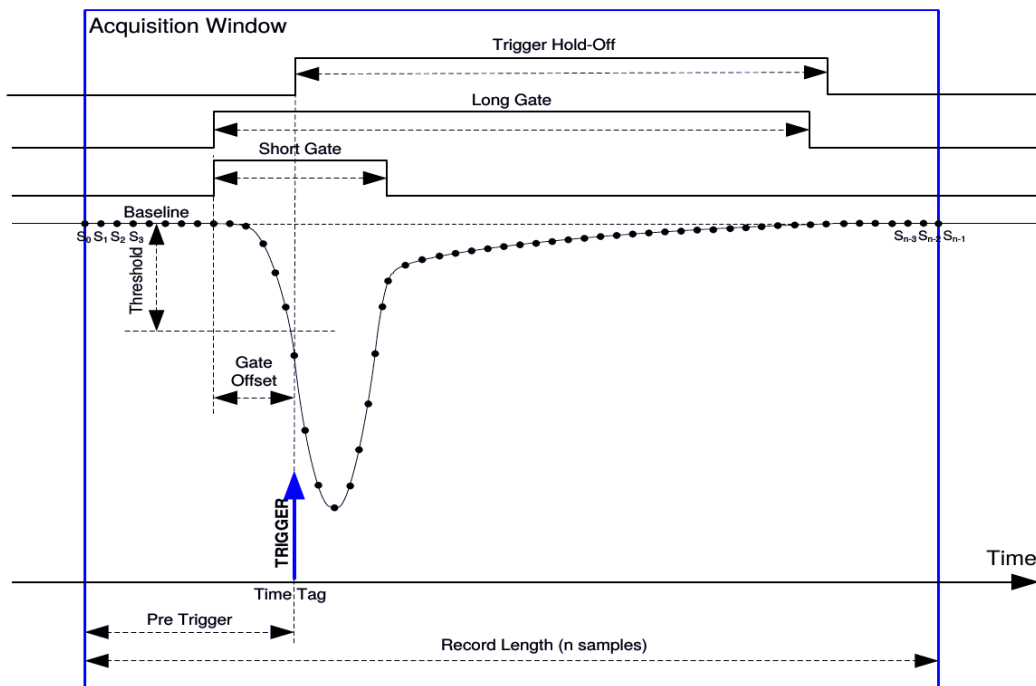
Figure 3.18: *Double-gate integration in the digital domain, and parameters involved*

Thanks to the stability properties of digital processing, the relative positions of the integration gates are fixed, reducing errors and improving the performances of the method.

Fig. 3.18 shows the different parameters involved in a double-gate digital integration: *Short Gate* is the size of the peak integration window, while *Long Gate* is the size of the total integration window.

3.3.4 Influence of parameters on discrimination performances

Two major parameters that define the performances of a waveform digitizer are the *sampling rate* and the *bit depth*.

The **sampling rate** is the frequency at which the input signal is sampled and stored. According to the Shannon-Nyquist sampling theorem [38], a digitized signal can be univocally reconstructed when sampled at twice the frequency of its highest frequency component. Therefore, the sampling frequency of a digitizer should be strictly correlated to the timing properties of the output signal of each type of detector. The analysis reported in [39], related to a reference liquid scintillator (BC501A), demonstrated that the highest frequency component is at about 100 MHz. This results in a lower theoretical limit of 200 MSamples/s for a digitizer to be effective in reconstructing the signals; the typical lower value used with this family of detectors is 250 MSamples/s.

The **bit depth** is a parameter describing the resolution of the ADC. A 12-bit ADC can output $2^{12} = 4096$ different integer values; since the uncertainty resides in the Less Significant Bit (LSB), this ADC would offer a "digital resolution" of 1/4096, less than 0.025% for voltages lying near the upper limit of the accepted range. This resolution is actually nominal, since it does not take into account noise. Any ADC suffers from a certain amount of electronic noise that introduces fluctuations in the conversion process; when this effect becomes relevant, the uncertainty may affect more than one LSB, reducing their significance. To consider this effect the concept of *effective number of bits* (ENOB) has been introduced; ENOB is defined as

$$ENOB = N - log_2(RMS_{noise}/\epsilon)$$

where N is the number of bits and ϵ is the quantization error. ENOB mainly depends on the average noise amplitude: high-fluctuating noise will significantly lower the ENOB, while as noise approach the ideal quantization error the ENOB will shift towards the nominal bit depth.

Applications that require precise timing measurements are more oriented to the use of high sample frequency digitizers, while acquisitions where high energy resolution is a prerequisite will typically rely on digitizers with high bit depth. Typical sampling rates used in radiation detection are 250 - 500 - 1000 MS/s, while the available bit depth can vary from 8 to 14 nominal bits.

During 2013 our group studied the dependance of neutron-gamma discrimination performances on the digitizer sampling rate and bit resolution, for three different values of both parameters [40]. The pulse shape discrimination capability has been studied using a 51 mm diameter × 51 mm depth cylindrical cell filled with a standard EJ-301 liquid scintillator. The scintillator was coupled to a H1949-51 Hamamatsu linearly focused 12 dynode photomultiplier (PMT). The PMT was operated at a bias between 1380 and 1650 V depending on the dynamic range to be studied. The PMT anode signal was directly processed by a set of CAEN fast digitizers:

- V1720 (250 MHz sampling rate, 12 bit resolution);

- DT5751 (1 GHz sampling rate, 10 bit resolution);

- DT5730 (500 MHz sampling rate, 14 bit resolution).

The x730 digitizer family has been developed within MODES_SNM project to maximize performances in radiation detection applications with scintillators.

In addition to the analysis of the waveforms output by the three digitizers, the off-line analysis of the DT5730 was performed converting event by event the data in order to simulate a lower sampling rate (250 MHz) and lower resolutions (10 and 12 bits). All of the digitizers were equipped with DPP-PSD firmware that implements the double-gate integration feature described in Sec. 3.3.3 and were operated in *Mixed mode* to allow both on-line and off-line analysis.

To characterize the neutron-gamma discrimination capability we used the *Figure of Merit* (FoM) discussed in Sec. 2.3.3.

Initially, FoM values have been extracted from the DPP data for different energy windows on the total light output. Data are reported in Fig. 3.19.
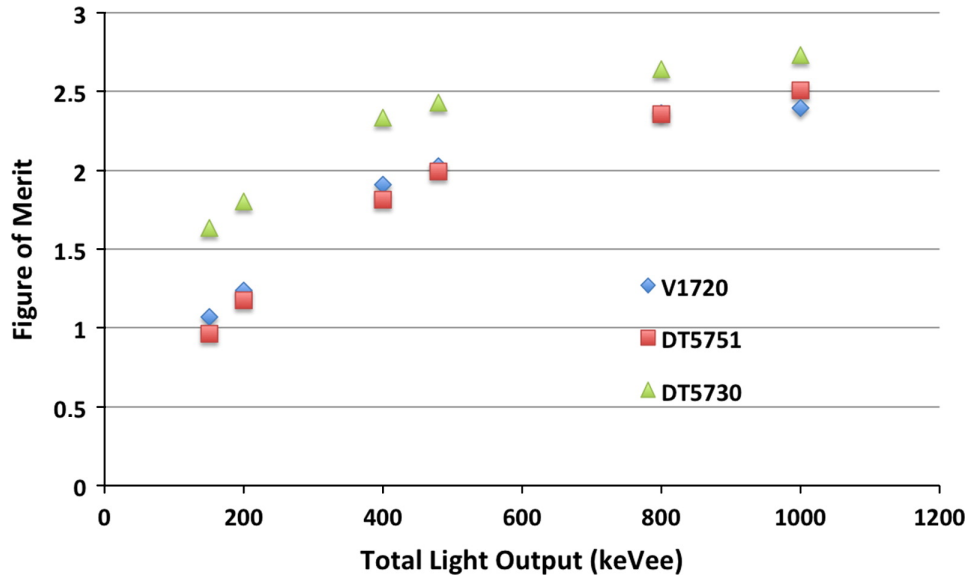
Figure 3.19: *FoM values measured on-line by the different digitizers for narrow windows on the total light output. Windows were defined as ± 70 keVee with respect to the X axis value, with the exception of the lower window which was defined as 150 ± 50 keVee*

It is clear that the PSD capability is normally increasing with the total scintillation light, as expected, due to the improvement of the signal/noise ratio. Moreover, the DT5730 provides significantly better FoM values compared to DT5751 and V1720. The improvement obtained with DT5730 is important especially for the lower Total Light Output windows, i.e. those associated mainly with lower energy neutrons. This allows one to lower the energy thresholds in the data analysis thus increasing the neutron absolute detection efficiency. The lower window in Fig. 3.19 is associated with the cut 150 ± 50 keVee.

To further investigate the digitizer performances, effects due to sampling rate and resolution need to be disentangled. A detailed study of the parameters' role in determining the overall neutron-gamma ray discrimination capability has been obtained by analyzing off-line the data taken with the DT5730 digitizer. In this case it is indeed possible to study the FoM and the detector resolution by changing the sampling rate between 500 and 250 MHz and/or the resolution in the range 10-14 bits.

As a first step, the detector energy resolution is determined directly from the spectra collected with a ^{22}Na source using the procedure described in Sec. 8.2. In particular, the

resolution σ/E was extracted from the Compton Edge of the 511 keV photons (see Fig. 8.4).

By looking at the energy resolution plot (upper panel of Fig. 3.20), it appears that the energy resolution thus obtained is independent from the sampling rate but increases significantly from 10 to 12 bits and then saturates above that value. This shows the limit represented by the intrinsic resolution of the detector, essentially governed by the scintillation statistics.
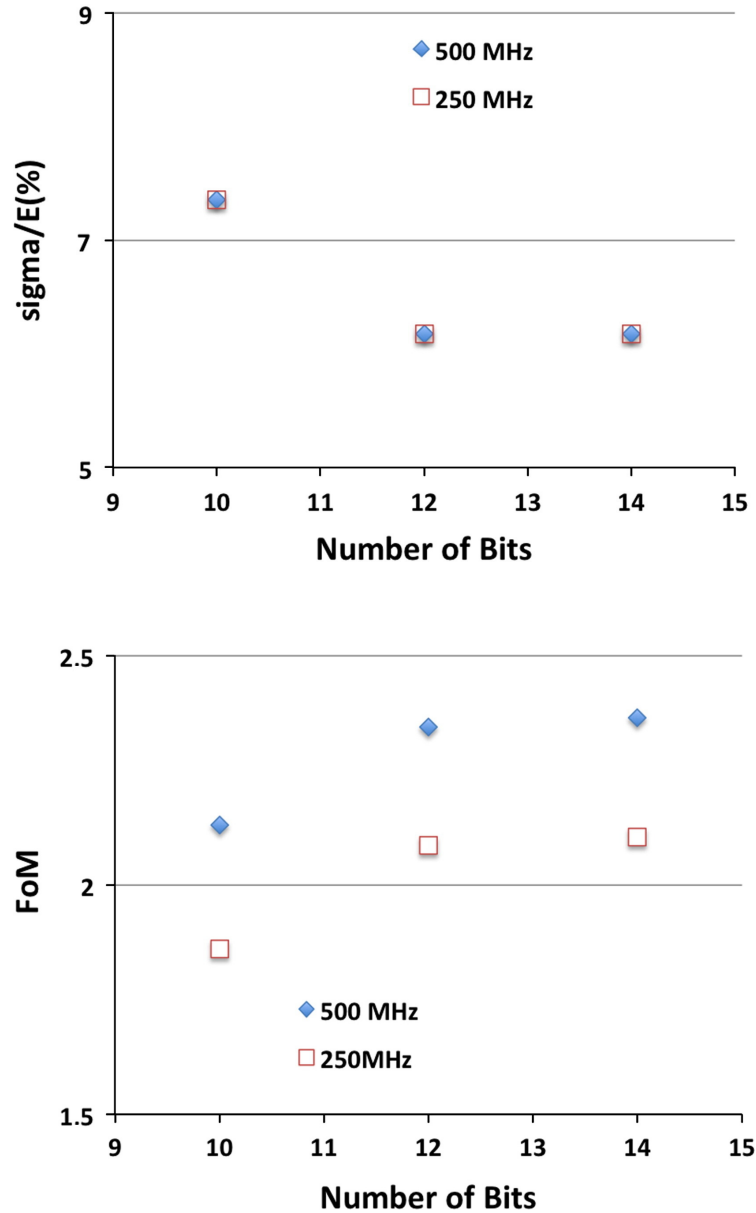
Figure 3.20: Energy resolution (upper panel) and Figure of Merit (lower panel), for different sampling rates and bit depth. Energy resolution was calculated on the 511 keV Compton Edge; FoM is related to the energy window 480 ± 75 keVee

On the other hand, the plot of FoM values for the total light window 480 ± 75 keVee (lower panel of Fig. 3.20) shows a sizeable increase of the FoM from 250 MHz to 500 MHz sampling rate and also by increasing the resolution from 10 to 12 bits. Moreover a very small gain (about 1%) is evidenced increasing the resolution to 14 bits.

These results also include the effects of the time jitter in the position of the integration gates that is important when the number of samples is small with respect to the rise time of the signal; the effect is higher at lower sampling rates.

As a conclusion of the study, the use of 500 MHz sampling rate produces a sizeable improvement of the PSD capability that is further improved in going from 10 to 12 bits resolution. As evident from Fig. 3.19, a further improvement of the sampling rate to 1000 MHz is not effective to compensate for a low resolution (10 bits). Also the advantages of using 14 bits resolution seemed to be not completely assessed.

3.3.5   MODES_SNM digitizers

MODES_SNM uses three digitizers of the new family (x730) developed by CAEN within the project; one DT5730 is shown in Fig. 3.21. It features a depth of 14 bit with a dynamic range of 2 Vpp, and a sampling rate of 500 MS/s (Table 3.3).

Form Factor	154 mm × 50 mm × 164 mm (W × H × D) Desktop	
Power consumption	2.8 A @ 12 V (typ.)	
Digital conversion	**Resolution**	14 bits
	Sampling rate	500 MS/s simult. on each channel
Clock source	Internal (50 MHz loc. oscillator) or external	
Analog input	**Channels**	8 channels, single ended
	Connector	MCX
	Impedance	50 Ohm
	Full Scale Range	0.5 or 2 Vpp, SW selectable
	Offset	Programmable DC offset, range ± 1 V
	Bandwidth	250 MHz
Digital I/O	**CLK-IN (AMP)**	AC coupled differential input clock
		LVDS, ECL, PECL, LVPECL, CML
		Jitter < 100ppm
	TRG-IN (LEMO)	External trigger in NIM/TTL 50 Ω
	GPO (LEMO)	General purpose out NIM/TTL 50 Ω
	GPI (LEMO)	General purpose in NIM/TTL 50 Ω
Memory	640 kS/ch or 5.12 MS/ch	
Trigger	Channel self trigger, external trigger, software trigger	
Synchronization	**Propagation**	One-to-many clock distribution
	Acquisition sync.	Sync Start/Stop through digital I/O
ADC & FPGA	Altera Cyclone EP4CE30 (one FPGA serves 4 channels)	
Comm. interface	**Optical Link**	CONET, 80 MB/s, daisy chainable
	USB	USB 2.0 compliant, 30 MB/s
Firmware	Digital oscilloscope (factory provided) or DPP	

Table 3.3: Technical data sheet for DT5730 Desktop digitizer

Digitizers used in MODES_SNM run the DPP-PSD firmware, implementing the double-gate integration mechanism described in Sec. 3.3.3; a pile-up filter is also implemented but

not used, due to the nature of the signals (see Fig. 2.6 for an example). Since the gas detectors are read by two PMTs at both ends of vessels, a coincidence filter with AND logic is activated for each couple of channels corresponding to the same vessel.

Figure 3.21: CAEN Desktop Digitizer mod. DT5730

Chapter 4

Data acquisition and analysis

4.1 General overview

Within MODES_SNM project, Work Package 4 was dedicated to the Information System (IS); this included all the software required to run the final system, from the acquisition engine to the control interface. The group at University of Padova was leader of WP4, and within my collaboration to the project I devoted part of my work in the development of the control, acquisition and analysis modules.

MODES_SNM Information System is made of different specialized modules; a central program coordinates the actions of the modules and handles all the communications with the hardware and the users. The three main modules are the Acquisition Engine (AE), the Decision Tree (DT) and the Man-Machine Interface (MMI):

- The **Acquisition Engine** is the lowest level module and manages the data transfer from the electronic front-end to the computer unit. Inside the AE also the first stage of the analysis takes place; raw data are merged to reconstruct physical events, labelled with timestamp, energy values and particle type flags;

- The **Decision Tree** is the high-level analysis; starting from counting and energy data, its algorithms can detect alarm situations and identify a given set of gamma ray and neutron sources;

- Finally, the **Man-Machine Interface** provides human access to the system, with controls to operate the prototype and the display of all the relevant physical informations; it is a web-based client-server application.

The first two of these modules are embedded inside a single main program, called "MODES_SNM server program"; it also contains a few smaller modules to configure the electronics, calibrate the system and log informations from the hardware sensors. The main language used for the server-side software is C/C++, with the addition of the Apache web server with PHP module; the client part of the MMI is made of plain HTML, Javascript and AJAX paradigm.

All the modules have been written by me, with the exception of some interface libraries that have been provided by other project partners for their respective hardware. CERN ROOT Libraries [41] have been used for data organization, plot management and analysis.

Together with the detectors, the Information System provides the bigger contribution to the final performances of the prototype; the results of the characterization tests are presented in Chapter 5, while field tests will be described in Chapter 6.

4.2   Acquisition engine

The Acquisition Engine (AE) is responsible for the first stage of the analysis, converting the data stream coming from the electronics to a more structured format, related more to the detector geometry than to the front-end layout.

Speed is an essential factor of any acquisition engine; not only it must be able to manage the highest possibile trigger rates, but it should also have some extra resources for base-level analysis, validation filters and data writeout. Although the amount of generic computing power of modern computers largely overcomes that of embedded FPGAs, the task of building an effective acquisition engine is still a challenging one; this is due to the much lower level of optimization of a software that is written in a high-level language and runs on general-purpose designed Operating Systems and CPUs. Depending on the system load, the typical bandwidth of a fiber connection (80-100 MB/s) can be greater than the effective disk writeout rate sustainable by the system.

In addition, MODES_SNM implementation of the AE is particularly sensitive to speed issues, since the aim of the project is to provide a real-time radiation monitor device. A temporary delay in the data stream, even of the order of 10^{-1} s, and the consequent misalignment of the time labels, could result in either missing the trigger of a real alarm (*false negative*) or causing the trigger of a false alarm (*false positive*), heavily affecting the performances of the entire system.

Speed concerns are made even worse by the requirement that the system must be relocatable and battery operated, thus requiring low-consuption components including the computer unit. The computer itself is the result of a delicate compromise between computational needs and several design constraints regarding size, power and heat management.

Considering all these aspects, and given the importance that timing has in MODES_SNM, it is clear that the Acquisition Engine is a critical component of the project. While the use of FPGAs and DPP inside the digitizers sensibly reduce the burden on the IS, this software module has to be designed with a lean and lightweight structure as much as possibile, to allow for a seamless flow of the data towards the operator.

4.2.1   The acquisition loop

The acquisition loop is based on the libraries provided by CAEN; since the library operates on a digitizer basis, the three MODES_SNM digitizers are handled by three independent processes. Each process runs a loop that continuously polls the associated digitizer for new events; the events are then collected by the main process and reorganized from being ordered by digitizer and channel to a more meaningful classification by detectors and PMTs. The reorganized data are then instantaneoulsy transferred to the first stage of analysis, where particle events are reconstructed from the single PMT signals; this is done through a class that describes system detectors.

Front End Electronics

SIGNALS
ordered by digitizer, channel

polling loop

Acquisition Engine (AE)

acquisition loop
assigns timestamps and geometry labels to signals

EVENTS
ordered by detector, PMT

direct fill

`Detector` **class**
reconstructs particle events from PMT signals
manages time buffers and rate counts

PARTICLES
ordered by detector, type

timed poll

Decision Tree (DT)
merges the data to describe the radiation source

ALARMS & SOURCE ID

polling loop

Man-Machine Interface (MMI)
displays the processed data to the operator

Figure 4.1: Data flow between MODES_SNM software modules

4.2.2 First analysis stage: the `Detector` class

The algorithms underlying the Decision Tree stage are based on informations about *incident particles* in relation with the detector type and geometry. Therefore PMT signals must be processed to reconstruct particle events, discriminating between particle types, and putting the resulting events inside time-sized buffers. The `Detector` class performs this conversion; Fig. 4.2 shows its internal structure.

Each instance of the class represents one physical detector tube inside the program; it must be initialized with a value representing the type of the corresponding detector. The internal flow of the data is modified accordingly: gamma detectors do not need a coincidence filter, and the discrimination algorithm is obviously different for the three detector families.

Input buffers

Each acquisition loop is connected to one digitizer, corresponding to 4 physical detector tubes and 8 PMT outputs; pointers to four different instances of the class are provided at startup, and the loop continuously fills the buffers corresponding to the eight PMTs. These buffers are organized as *First-In, First-Out (FIFO)* structures: the events are extracted in the same order as they are inserted, preserving the chronological sequence.

Data process

After each readout cycle, a method is called to process events in the input buffers. At first, the absolute time of events is reconstructed by summing the machine time of the acquisition start to the timestamp provided by the digitizer, for which t = 0 corresponds to the start command.

Xenon detectors are built in a way so that each half of a tube works as an independent detector with his own PMT; after the timestamp reconstruction, events are directly put in the output buffers. Neutron detectors are made of a single tube with readout at both ends, each PMT collecting part of the light output. Therefore, to reconstruct an event one must perform the coincidence of the two signals and combine the information of both channels. A concidence filter is activated inside the digitizers, but a small fraction (2-3%) of the events can escape the validation, probably due to jitter problems. For each of the PMTs, the software filter discards events that have no counterpart in the other buffer, compensating this issue.

At this point, pulse height values are combined to calculate discrimination parameters. Performing the energy calibration of a ^{4}He detector is a complex procedure (see Sec. 2.3.4); since discrimination is based only on the signal shape and no spectroscopy is performed, uncalibrated values can be safely used. Dedicated tests during the characterization of the system further validated this assumption. Discrimination algorithms are described in Sec. 4.2.3. Once the particle has been tagged as gamma ray, fast neutron or thermal neutron, the event is transferred to the output buffer associated to that particle family.

Output buffers

Since the maximum number of detectable particle types is three, every detector features three FIFO buffers. Gamma detectors use buffer 0 and 1 to store the events of PMTs A and B, respectively. Fast neutron detectors use buffer 0 for gamma ray events and buffer 1
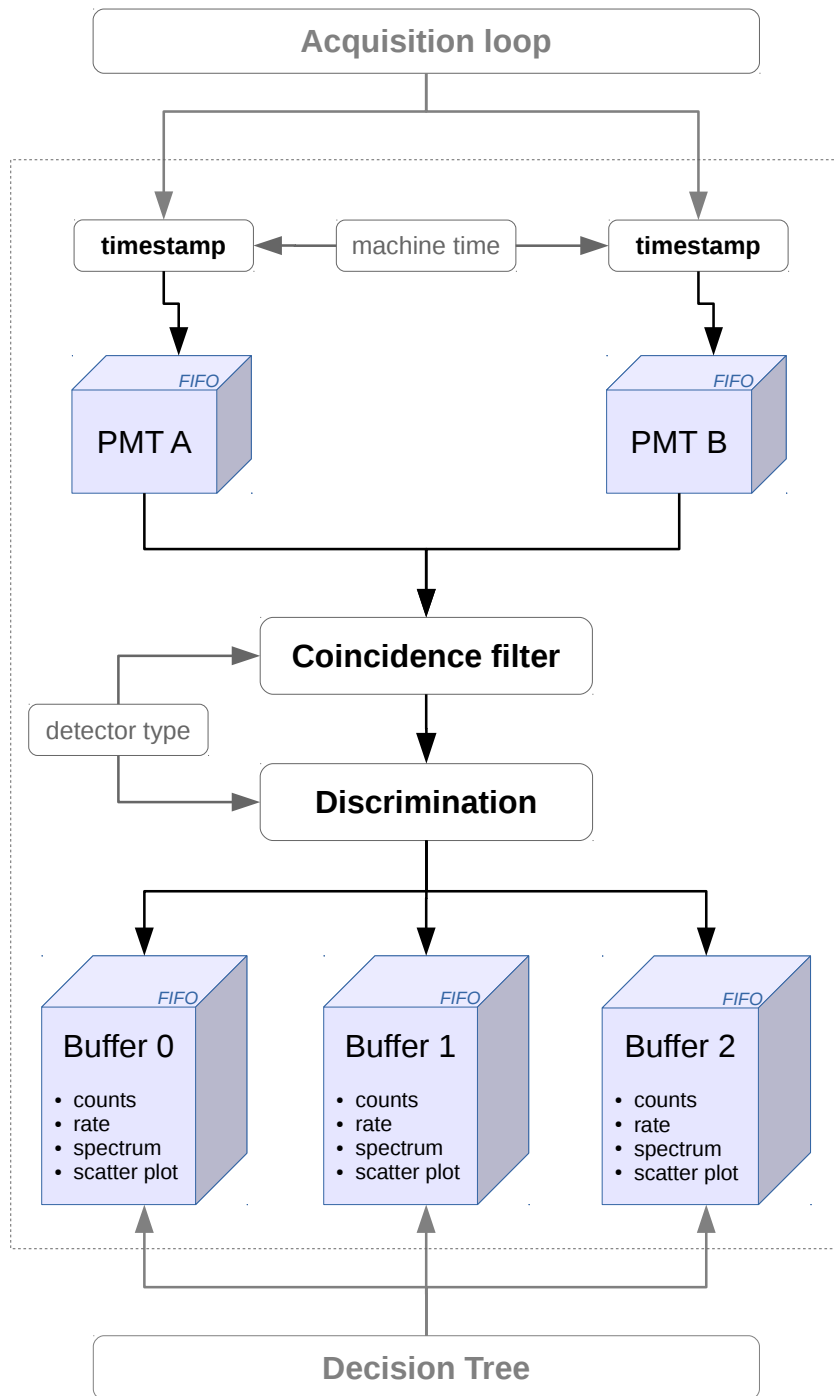
Figure 4.2: Internal structure of `Detector` class

for neutron events; as for gamma detectors, buffer 2 is not used. Thermal neutron detectors use buffer 0 for gamma rays, buffer 1 for fast neutrons and buffer 2 for thermal neutrons.

Each buffer has a fixed time size of N seconds; values used are $N = 2$ s for gamma rays and $N = 10$ s for neutrons. After each readout, which happens at a recorded time t, all events with a timestamp older than $t - N$ are discarded; all the statistics (counting, average counting rate) are then updated, as well as energy spectrum and scatter plots. In this way, every time the Decision Tree polls refers to these values, they always reflect the last N seconds of operation.

4.2.3   Discrimination algorithms

Neutron - gamma discrimination

Neutron - gamma discrimination in fast neutron detectors is performed through PSD techniques (Sec. 2.3.3); neutron signals have a higher value of the PSD parameter, and can be separated from gamma rays by means of a simple threshold on that value. The use of a single threshold for the entire energy spectrum corresponds to a horizontal cut in the scatter plot as shown in the upper panel of Fig. 4.3.

The discrimination efficiency can be greatly improved using a variable threshold that is function of the particle pulse height; the simplest way to do so is replacing the horizontal line with a poligonal chain as in lower panel of Fig. 4.3. With this method, the threshold T is a linear function of the particle pulse height E; the X axis range is divided in intervals, and the slope $m = T/E$ is defined separately for each interval. Events above the line are labelled as neutrons, otherwise they are treated as gamma rays.

The actual position of this poligonal chain affects both the neutron detection efficiency and the False Alarm Rate. To rise the discrimination line leads to a lower number of gamma rays mislabelled as neutrons and therefore lowers the FAR; but it also reduces the overall sensitivity to neutrons. The final positions of the vertices have been empirically determined by analyzing the scatter plot of a pure ^{60}Co source (middle panel of Fig. 4.3). The source was set-up to produce a dose equivalent rate averaged over the face of the detector of 100 μSv/h as prescribed by international standards (Sec. 1.3.4), then the line was adjusted to meet the requirements for radiation interference and FAR.

Fast neutrons and thermal neutrons

Thermal neutron detectors are sensitive to all three types of particles, including gamma rays. As shown in Sec. 2.3.4, discrimination between the three families is done by defining three windows in the scatter plot. The size of the windows is empirically determined by analizing the plots of a pure gamma ray source and of a pure neutron source, with and without a heavy polyethylene shield (Fig. 4.4); the events from the three measurements are mostly confined to only one of the discrimination regions, allowing to define boundaries between them.
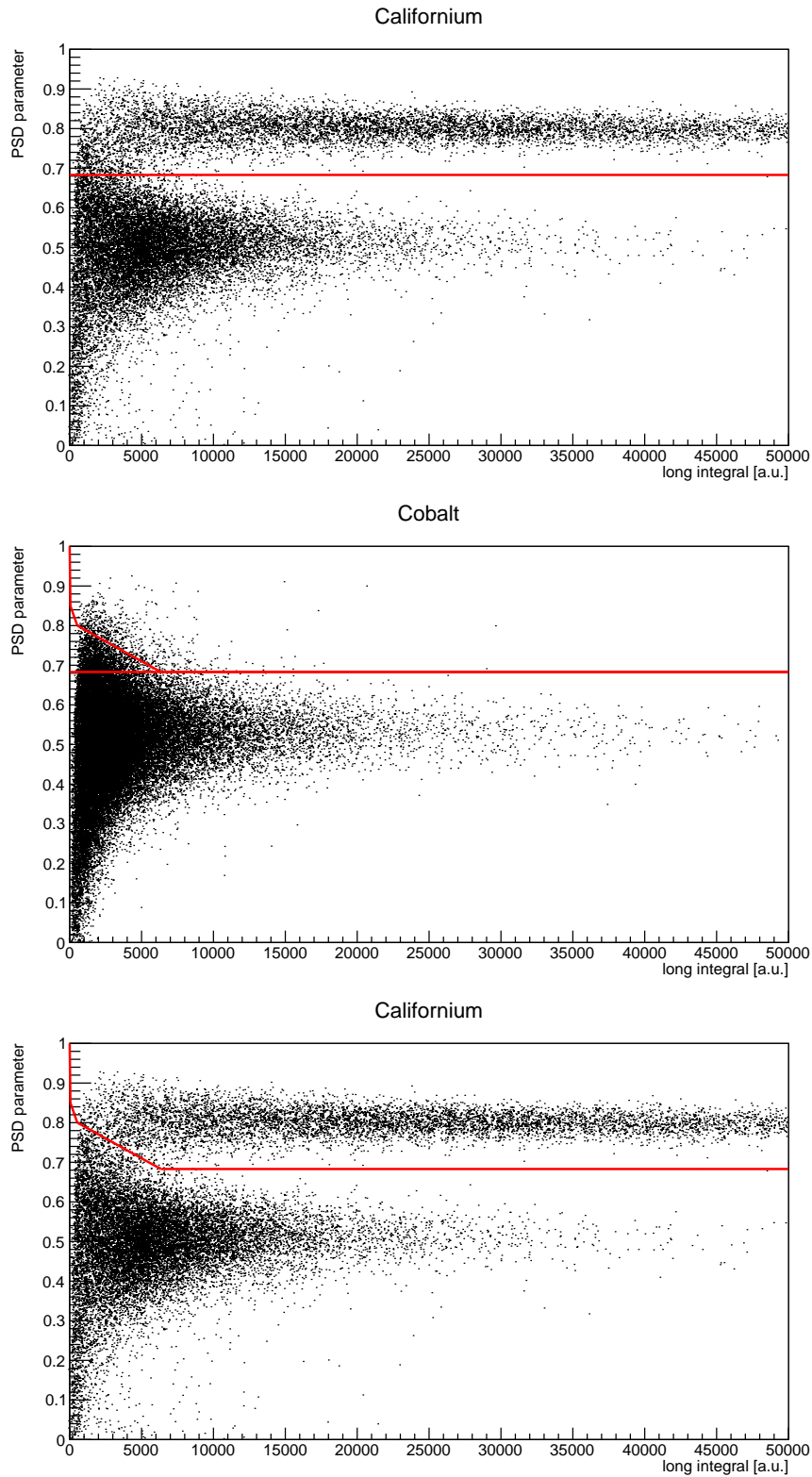
Figure 4.3: Different cuts for neutron-gamma discrimination: a simple linear cut on the PSD parameter might look efficient when applied to a californium spectrum (upper panel), but when applied to a gamma source it clearly leads to identify too many gamma rays as neutrons; a smarter cut can be tailored on the gamma profile (middle panel) and then applied back to the californium spectrum for comparison (lower panel)
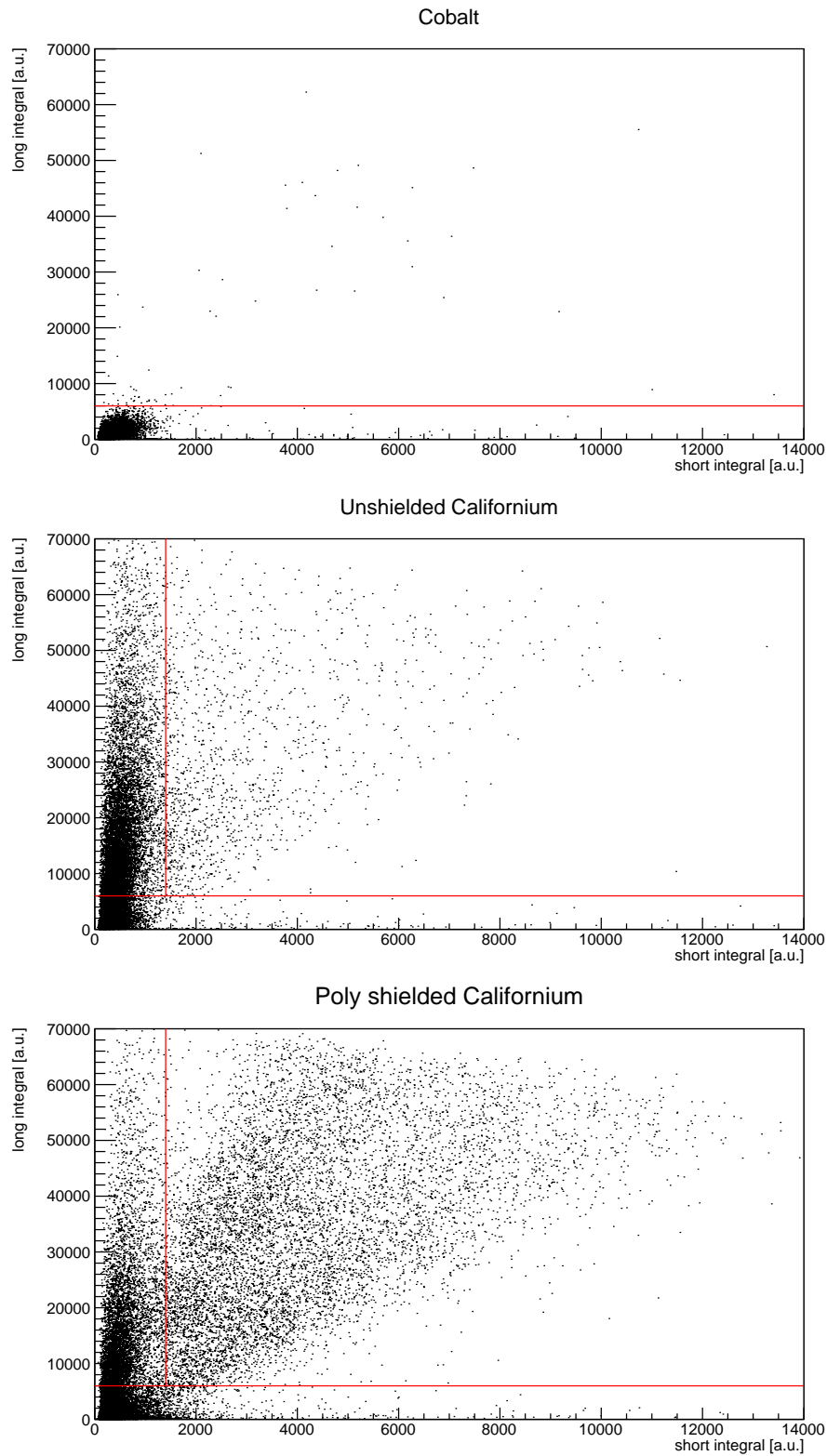
Figure 4.4: Scatter plot for a thermal neutron detector exposed to a Cobalt source (upper panel), unshielded californium source (middle panel) and the same californium source with identical geometry and exposure but shielded with polyethylene (lower panel)

4.3 Decision tree

The Decision Tree (DT) is the software module that realizes the physical interpretation of the data; energy calibration, background estimation, alarm triggering and source identification are the operations performed by the DT.

4.3.1 Energy calibration

Energy calibration of the gamma detectors is essential to perform source identification. The calibration procedure is performed assuming a linear relation between the light output and the energy. Two reference sources are used at the same time: a 9.25 kBq ^{137}Cs and a 37 kBq ^{60}Co. The conversion factors are calculated by the interpolation of the positions of the three highest peaks (662 keV from ^{137}Cs; 1173 keV and 1332 keV from ^{60}Co). The sources are weak to avoid licencing procedures during the field demonstrations and they must be placed in contact with the NaI(Tl) box during the calibration of the system.
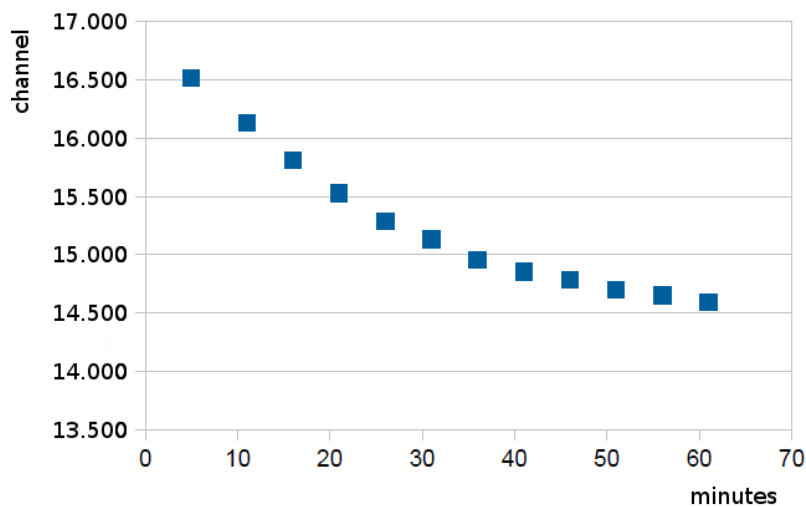
Figure 4.5: 511 keV peak position as a function of time for the NaI(Tl) detector

In addition to the main calibration procedure, a self-calibration routine has been developed to compensate for the gain drift of the NaI(Tl) assembly (Fig. 4.5). In absence of any automatic correction, this drift may result in a sensible degradation of identification performances within minutes. In order to perform this automatic correction to the calibration coefficients, a ^{40}K pulser has been placed inside the NaI(Tl) box, in the form of a KCl compound. The amount of material has been experimentally determined so that the peak is clearly distinguishable from the background even with a measurement of a few seconds. The system can compare the known energy of the pulser peak with the energy calculated with the buffer spectrum. This enables the system to correct the slope coefficient of the linear calibration, perfectly compensating for the peak shift. The presence of other sources may interfere with the process, so the self-calibration procedure is disabled in the presence of gamma ray alarms.

4.3.2 Background alarm thresholds

In MODES_SNM the normal operating mode is called "Search mode", with the system performing a continuos acquisition: every 1 seconds the total buffer counts of gamma rays,

fast neutrons or thermal neutrons are compared with the corresponding thresholds. When a threshold is passed, the associated alarm is raised.

The calculation of the thresholds is automatically performed by a procedure dedicated to the background analysis. This procedure is based on the consideration that radioactive decay follows Poisson statistics: a few basic definitions are reported here, whereas a more extensive overview of the statistics involved in the process is presented in Appendix A:

- **Detection Probability (PD)**: the probability of triggering an alarm in the presence of a real source;

- **False Alarm Rate (FAR)**: the rate of alarms triggered without sources;

- **Confidence Level (CL)**: it can be considered an index related to the reliability of the algorithm over repeated measurements.

According to the requirements, MODES_SNM system must have a maximum False Alarm Rate of 0.001, corresponding to **1 False Alarm per hour** of operation, with a Probability of Detection **PD = 0.9** at a Confidence Level **CL = 95%**.

Once that FAR and PD have been fixed and a new background measurement has been performed, thresholds can be calculated using Equation A.2 and the average counting rate for each particle family.

4.3.3   Source identification algorithm

The identification of radiation sources by means of automatic procedures is a huge challenge for every researcher in the field; taking into account the possibility to mix an arbitrary number of sources, with unknown geometry, with an unknown amount of lead and polyethylene shielding, the task is still far from receiving a definitive solution. In the worst case scenario, a certain amount of illicit and dangerous material can be successfully disguised as if it were part of a naturally, authorized radioactive cargo (NORM). This undesirable technique goes under the name of *masking*.

Nevertheless, by analyzing the operating context of a system it is possibile to make assumptions that reduce the problem to a solvable form, at least with a certain degree of reliability. The masking of an illicit source always relies on the presence of a stronger and licit emitter, so that the cargo can never pass unnoticed; a manual inspection can take place in case of any suspect. Sources may be shielded, but lead shield can be otherwise detected, e.g. by means of X-ray inspections, and the typical width of a cargo container limits the maximum amount of polyethylene shield that can be placed around a neutron emitter.

Once all the constraints related to the specific application have been evaluated, the general problem assumes a much simpler form: the system must precisely identify a small set of common sources, and notify to the operator all the other situations, providing - whenever possibile - at least some indication on the type of radiation.

The identification algorithm can now work with *source categories*, identified by the type and number of the alarms they trigger. If only gamma alarms are detected, probably it is a simple gamma source that can be identified with spectroscopic methods as described below, but it might also be Uranium. If there are neutron alarms, it is a neutron source, and if gamma alarms are very low or missing it may be an indicator of lead shielding. Finally, a

relatively intense flux of thermal neutrons can signal the presence of polyethylene or other moderating material.

Once the system has given these preliminary informations about the source family and the type of shielding (if present), two dedicated procedures can be activated for gamma ray and neutron sources, to perform a deeper analysis of the incident radiation.

Gamma source identification

During commissioning tests described in Chapter 5 xenon detectors proved to have good detection performances; however the identification process showed some instabilities at energies above 1 MeV. Due to schedule constraints it was decided to add one NaI(Tl) crystal to the system to fully meet the identificationj requirements for the prototype. The energy resolution of this additional detector is equivalent to the one measured with xenon detectors, but the full energy efficiency is larger at high energies. Therefore the identification of gamma ray sources in MODES_SNM prototype is performed analyzing the spectrum of the NaI(Tl) detector. The algorithm that has been chosen is based on the detection of photopeaks; position (energy) and resolution of the peaks are the two main parameters taken into account, while the intensity of the lines was not used since it is too much affected by geometry and shielding effects.

The first step is to create a small database of sources, each one with the number of expected peaks and their energies in keV: as an example ^{22}Na (511, 1274.5), ^{60}Co (1173, 1332), ^{137}Cs (661.7) etc. At first, this set included known gamma-ray transitions for some of the sources suggested by international standards [10]; during the commissioning of the MODES_SNM the library has been tailored on the actual performances of the system. Several issues may arise when building such a library: similar lines from different sources may mislead the algorithm; some other might be difficult to see at all; others may suffer from a fixed shift due to small non-linearities of the system. At the end of this process, the library contains only those lines that univocally identify a given source, *considering the response of the system*. This database is used a reference library for comparison with the measured spectrum.

What follows is the logical sequence for the identification algorithm:

1. the background spectrum is subtracted by the measured spectrum;

2. a peak search routine runs over the background subtracted spectrum;

3. peaks with resolutions much different from that expected at their energy are discarded;

4. a source is selected from the library;

5. for each line listed for this source, the spectrum is searched for a possible match;

6. a χ^2 value is calculated with distances between theoretical lines and their matches;

7. if the χ^2 value exceeds a threshold, or there are unmatched lines, the source is considered not present;

8. back to point 4 with another source, until the entire library has been evaluated;

9. if there is any unmatched peak in the subtracted spectrum, it is reported as unknown gamma source.
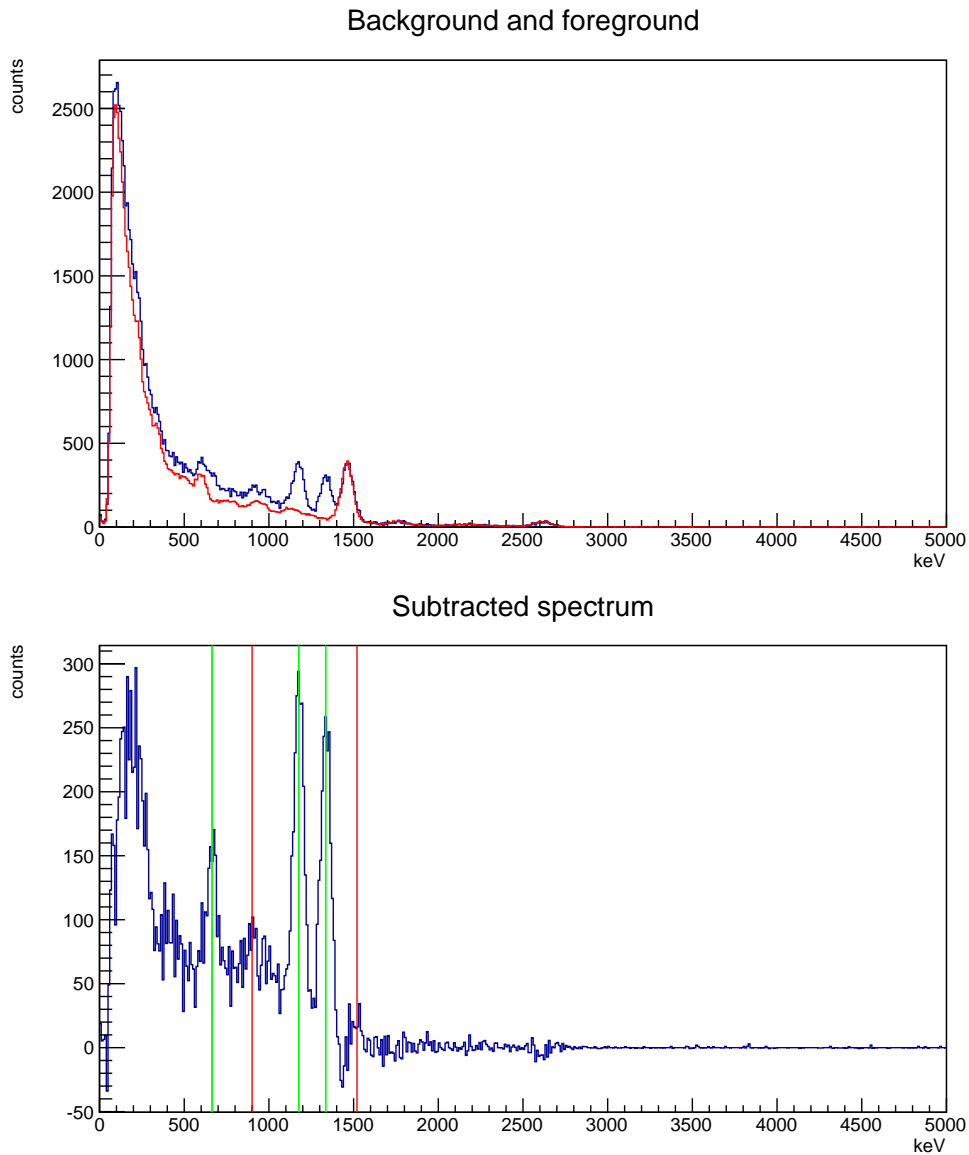
Figure 4.6: Example of identification. Starting from the Background (upper panel, red line) and Foreground (upper panel, blue) spectra, the system correctly identified a mixture of ^{137}Cs and ^{60}Co (lower panel, green lines) and discharged two structures not corresponding to any real peak (lower panel, red lines). The low intensity was achieved on purpose by increasing the distance; counting rate for this acquisition was only 1.16 times the threshold value

Fig. 4.6 shows a graphical representation of the identification steps and results. The response provided to the user is:

```
=== Identification messages ===


[11:53:02] Detected gamma radiation.
[11:53:02] Found source: 60Co
[11:53:02] Found source: 137Cs
```

Neutron source identification

At the present state of development, the information on neutron energy provided by ^{4}He detectors is very limited; therefore in MODES_SNM it is not possible to perform analysis on neutron spectra, and the identification of the neutron emitters must be based on their gamma ray emission pattern.

One possibile strategy is the so-called *full-spectrum analysis* (FSA) [42, 43]. With this method, the complete profile of the spectrum is compared with a library of spectral responses for most common sources; the best matching is proposed as the result of the identification, and can be achieved with single sources as well as arbitrary combinations. While being considered very powerful, FSA requires a very accurate preparation of the library together with a high stability of the system response; moreover, FSA is very dependent on the hardware response functions, so the library must be built using the system in its final configuration. With FSA, the exposure to sources not included in the library (as can easily happen during field tests in a real environment) may have unpredictable effects on identification performances. In addition, to take into account different shielding configurations (thickness, material, geometry) substantially increases the complexity of the algorithm.

For all these reasons, FSA has been considered incompatible with the development schedule of MODES_SNM and a more flexible approach has been used instead.

Even if the complete gamma response can not be analyzed, different families of neutron sources can be identified by looking to infomation from the energy windowing of the gamma ray emission pattern. Fig. 4.7 shows two examples of energy windowing: while the californium spectrum has a monothonic decreasing profile, americium-beryllium features some tall structures in the window between 4 and 5 MeV, characteristic of (α,n) neutron sources.

Fig. 4.7 also shows one of the advantages of the windowing method over FSA described above. MODES_SNM includes procedures for background subtraction, including the ^{40}K peak at 1462 keV emitted by the KCl pulser and used as a calibration reference; however the order between window integrals is not altered by this contamination and the identification is possible even without background subtraction. A relatively strong gamma source is required to significantly perturbate the stability of the algorithm, resulting in the impossibility to identify the family of the neutron source; in this case the system will report the presence of a strong gamma source together with an unknown neutron source, a case that protocols prescribe to be handled by a second-level inspection by human operators.

Further refinements in the identification response, e.g. exposing the presence of shielding, come from the calculation of the ratio between thermal and fast neutrons and its comparison with the expected value; this value has been experimentally determined by measuring the library sources with several configurations of polyethylene shielding.
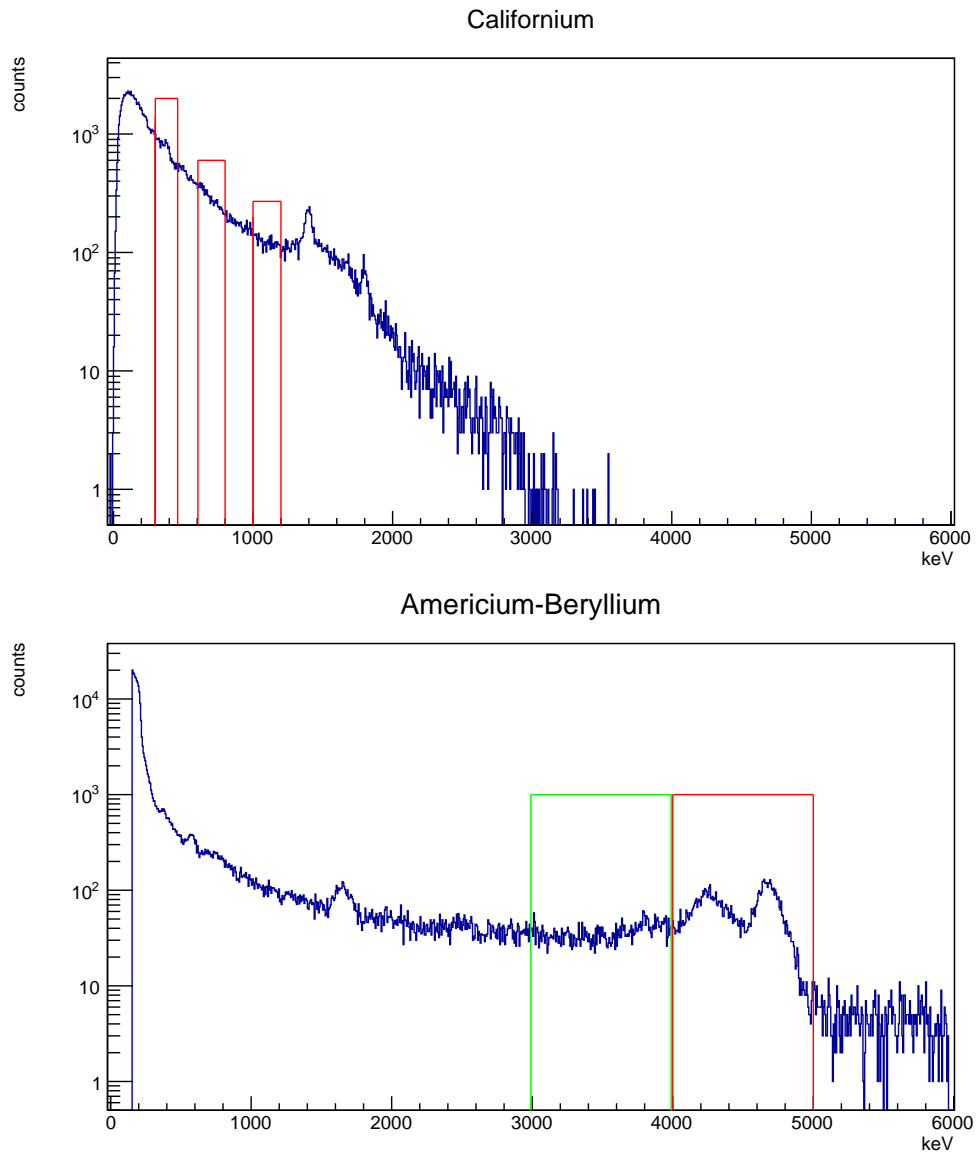
Figure 4.7: *Example of energy windowing in the gamma ray spectrum for two common neutron sources. The relations between the window integrals can be used as "fingerprints" of a source. Displayed spectra have been taken with a 125 mm × 125 mm × 25 mm NaI(Tl) detector similar to the one used in MODES_SNM; they include natural background and a contamination by ^{40}K around 1462 keV, as in the case of MODES_SNM system*

N42.42 spectroscopy standard format

ANSI/IEEE N42.42 [44] is a standard aimed to provide a unified format to share data produced by radiation measurement instruments. It is based on a XML data format that can be parsed by any compatible software, official or custom-made. These are some of the informations that can be stored in a N42.42 file:

- Date, time and GPS location;

- System description (Manifacturer, SW version...);

- Detector description;

- Calibration spectrum and coefficients;

- Background spectrum and thresholds;

- Count rates and alarm counts;

- Foreground spectrum;

- Identification results.

Data can also be grouped in sections corresponding to operating sessions, so that a single file can log the output of a system during an entire day with multiple runs.

MODES_SNM integrates a writeout module compatibile with N42.42 standard; it is called after every identification procedure, to create a comprehensive log of all the identification history of the instrument. Appendix B contains an example of a valid N42.42 file describing the measurement shown in Fig. 4.6.

4.4 Man-Machine Interface (MMI)

The Man-Machine Interface (MMI) is the part of the IS dedicated to the organization and display of all the information produced by the system, as well as the control of its operations. Developing the MMI was part of my work within MODES_SNM Work Package 4.

Fig. 4.8 shows a general overview of the MMI. Since MODES_SNM was designed to be a mobile system with the possibility to operate on battery and remote-controlled, it was decided to use a server-client configuration, with the communication handled by commercial Wireless hardware and protocols. To increase the flexibility of the system while minimizing the need for developing custom controlling application, the server and the client are developed with standard web languages and protocols; the actual interface is a web site generated by the server, and any device with Internet capabilities can connect to the private network and act as a MODES_SNM control device - also multiple connections are possibile.

MODES_SNM server program runs over the central computing unit, inside the Electronic Box. On fixed intervals (typically every 1 second for count rates and 5 seconds for slow control values) this program collects informations and updates the values of the corresponding variables; at the same time, it listens on a *socket* that communicates with the Apache web server running on the same machine. Every time the interface sends a command or requests an update, the call is redirected from the web page to the web server, and then to the
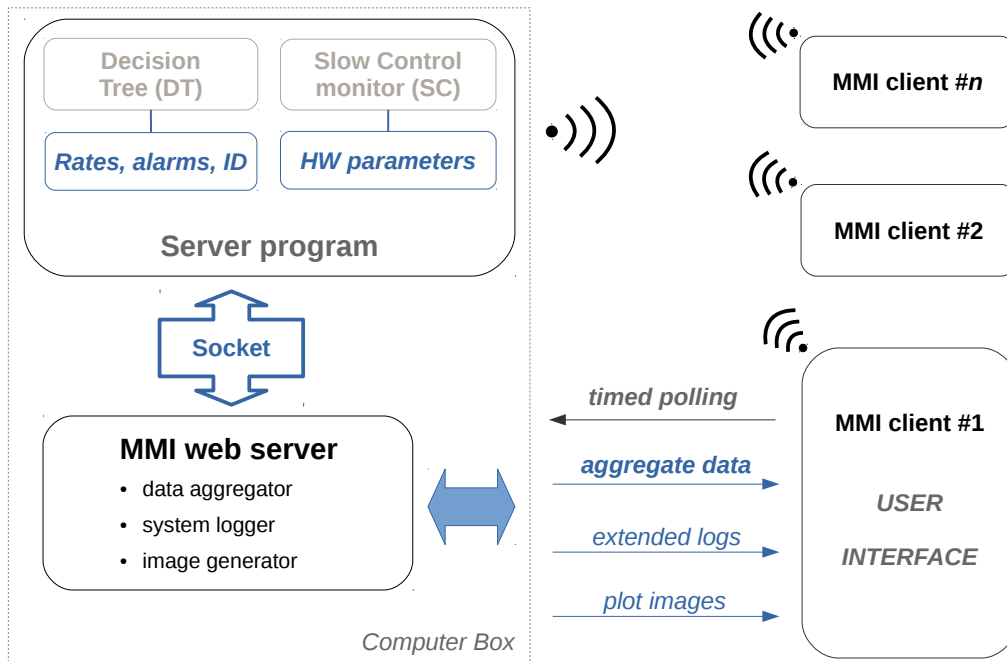
Figure 4.8: Man-Machine Interface: the client-server structure

program throught the socket; data and images related to the acquisition flow on the same path but in the opposite direction.

The core result of this part of the work can be described as a multiboard digital acquisition system that can be completely controlled and monitored by remote through a dedicated web page.

4.4.1　Main control panel

The main control panel of the system is shown in Fig. 4.9. This is the default page shown on the interface and it features all the useful controls to operate and monitor the system.

On top of the interface there are six indicators showing the status of the subsystems: the main server program (SYS), power supply (BATT), environmental parameters (TEMP), detector parameters (DET), acquisition stage (ACQ) and GPS. A "semaphore" color code is in use, where green means "ready", yellow is "warning" and red indicates a serious problem; blue is used only for ACQ while the acquisition is running. Text messages integrate the colors, providing more details in case of problems and also alerting the user when calibrations become out-of-date or a user-called procedure fails.

Under the status bar there are three main buttons, corresponding to three out of four operating modes: Energy calibration, Background estimation and Identification. Each of them has a fixed duration, and a countdown indicates the seconds left to conclusion. The fourth operating mode is called "Search mode" and is the standard operating mode of the system: a continuous acquisition that is checked for alarms every seconds.

Below the buttons there are the battery indicator, visual alarm lights and rate counters.
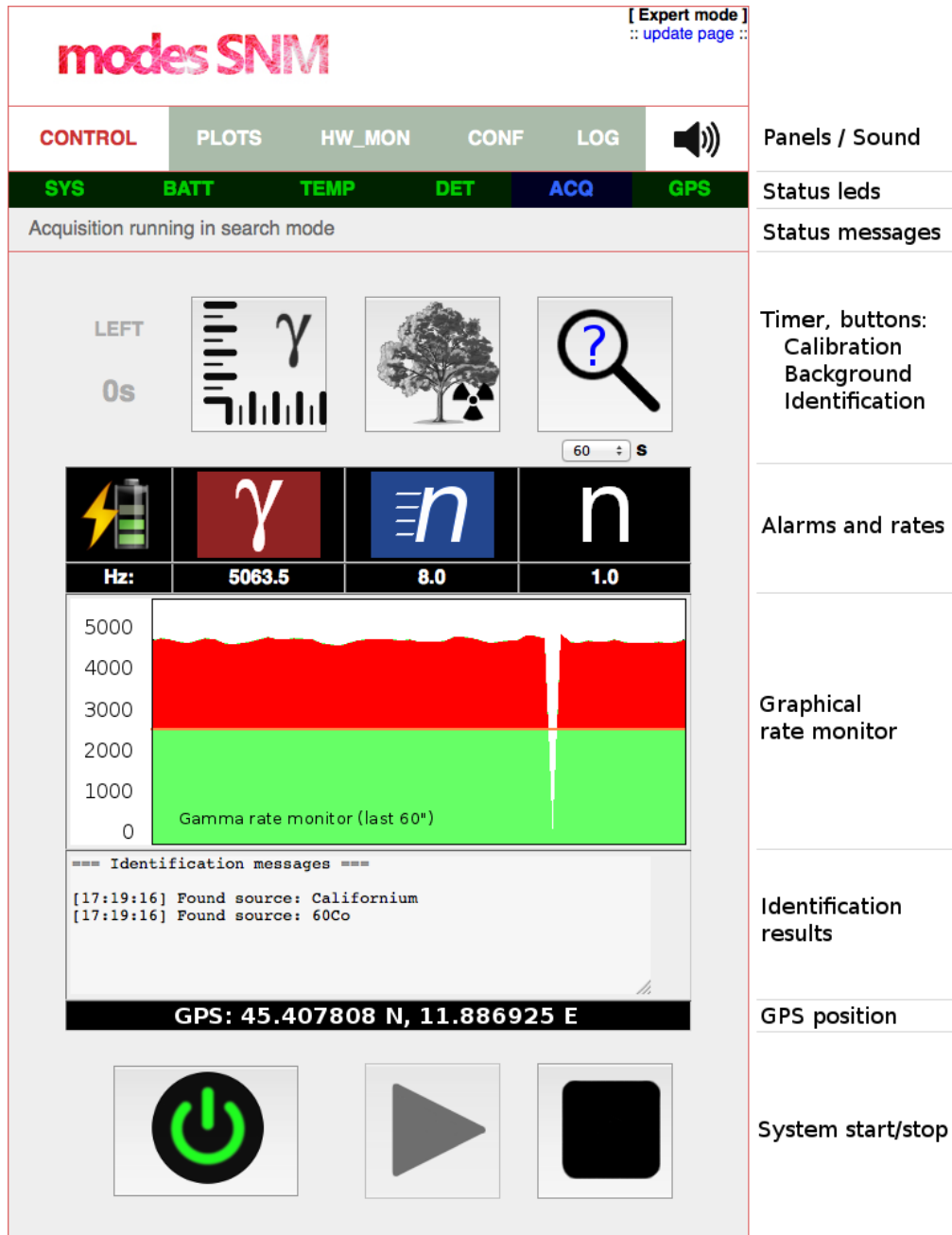
Figure 4.9: Man-Machine Interface: the main control panel

The Graphical rate monitor shows the rate dependency over time for the last 60 seconds, colouring in red/green the rates above/below the alarm threshold; it has been added after requests from the Customs personnel, to help relating a potential alarm with the recent behaviour of the instrument. The importance of this tool is evident when looking at Fig. 4.10, related to a field test in Switzerland: the apparent minima in the plot represent the effects of trucks passing by the monitoring installation, the mass of their cargo shielding the detectors from a significant ratio of the natural background. Such representations have proved to be essential to properly evaluate the significance of alarms (or the lack of).
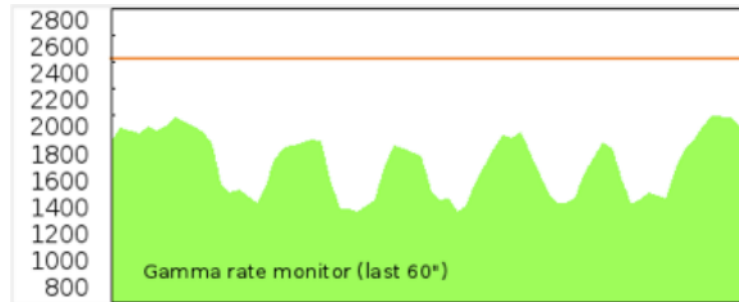
Figure 4.10: Man-Machine Interface: the Graphical rate monitor

Under the Graphical rate monitor the GPS coordinates are shown; below it lies the Identification message box that reports the results of the last identification procedure performed by the system. At the bottom of the page, there are three more buttons to restart the server and manually start/stop the acquisition in "Search mode".

4.4.2   Expert mode panels

The official MMI for the system consists of four additional panels accessibile only to "Expert users"; they give access to more detailed informations, such as detector plots and log/debug messages, and the possibility to configure the system parameters for digitizers, power supply and software algorithms. Fig. 4.11 shows an overview of these additional panels:

(a) *plot panel*: from here the user can inspect the output of any detector buffer (see Sec. 4.2.2), looking at both energy or scatter plot, in linear or log scale, with data related to the buffer or the entire acquisition;

(b) *HV monitor panel*: all the relevant parameters for the electronics and the detectors (voltage, temperature, pressure) are listed here; light will turn red in case of values out of the expected range, integrating the yellow color on the DET status led;

(c) *configuration panel*: this panel gives access to the configuration of the system;

(d) *log/debug panel*: displays all the verbose debug messages logged by the system.

In addition to the expert panels, a complete time log of all parameters displayed in the panels, as well as copies of all the detector plots and including the N42.42 identification reports, is stored in a dedicated and accessible folder; a new folder is created each time the server program is started, and a new log subdirectory is filled each time an acquisition stops.
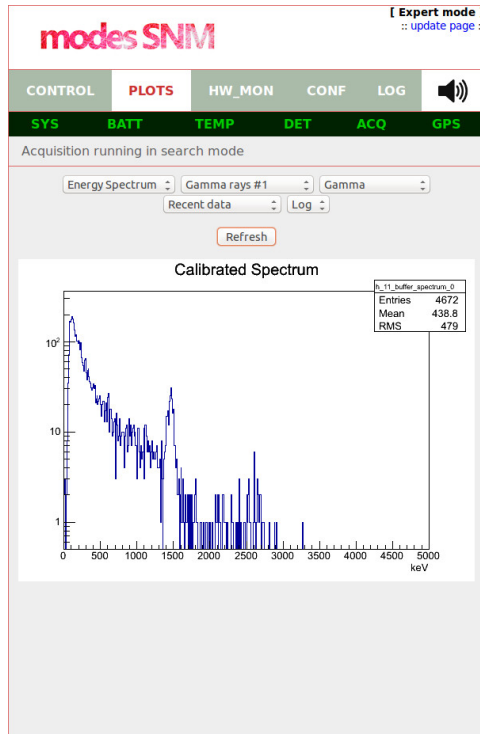
(a)
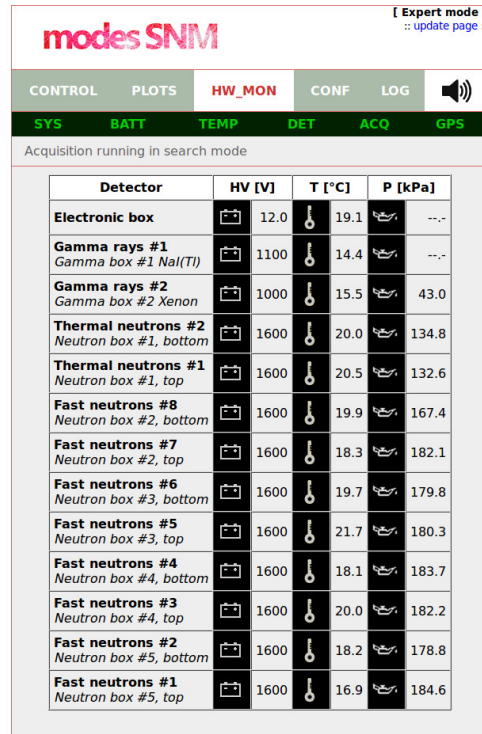
(b)
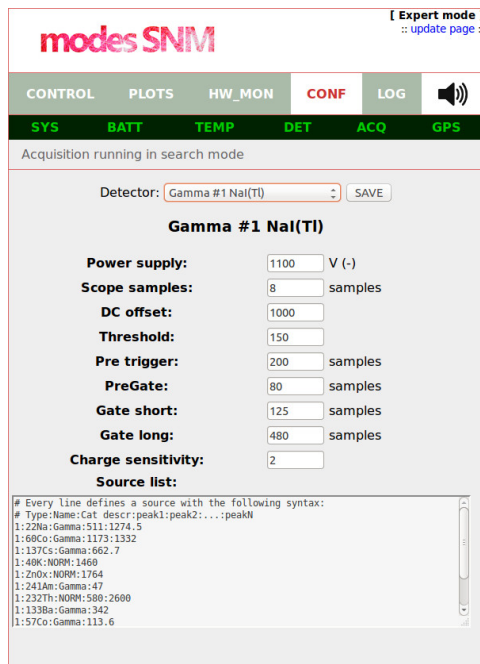
(c)
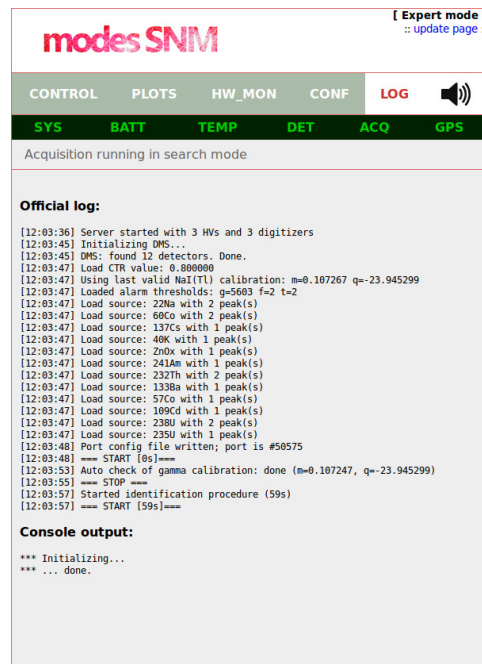
(d)

Figure 4.11: "Expert mode" control panels

Chapter 5

System integration and commissioning

5.1 System integration

At about two-thirds of the project workplan, all the subsystems separately developed by partners (detectors, electronics and IS hardware and software) were shipped to University of Liverpool for the system integration, organized in Work Package 5.

The integration included the manufacturing of the containing boxes for all system components; they are all made of Alupanel and host special waterproof connectors to ensure a reliable cabling in every condition. Table 5.1 lists the separate components of the system and their content; "A" type boxes house the electronics and the battery pack, while "B" type boxes host the detectors.

Box ID	Label	Component
B1	N1	2 high pressure ^{4}He extended scintillators for thermal neutrons
B2	N2	2 high pressure ^{4}He scintillators for fast neutrons
B3	N3	2 high pressure ^{4}He scintillators for fast neutrons
B4	N4	2 high pressure ^{4}He scintillators for fast neutrons
B5	N5	2 high pressure ^{4}He scintillators for fast neutrons
B6	G1	2 high pressure Xe scintillators for gamma rays
B7	G2	Large volume (10x10x25 cm^3) NaI(Tl) scintillator for gamma rays
A1	-	Front-end and computer
A2	-	Battery pack

Table 5.1: MODES_SNM components

5.1.1 Electronic box

A1 box hosts the electronics and has dimensions 350 mm $\times$ 450 mm $\times$ 450 mm; it is shown in Fig. 5.1. The container has two compartments; the upper is dedicated to the front-end modules and the on-board computer, while the lower hosts all the cabling. A PSU fan, powered from the computer, is installed at the one side of the electronics compartment. A

mesh aluminium panel separates the two compartments. Air ventilation grids on the top and on the side of the container ensure adequate air flow for cooling.

The back panel of the box houses power connectors, the power key switch, and a series of waterproof computer connectors; they include an Ethernet socket for connectivity and USB/VGA plugs to provide debug access to the system.
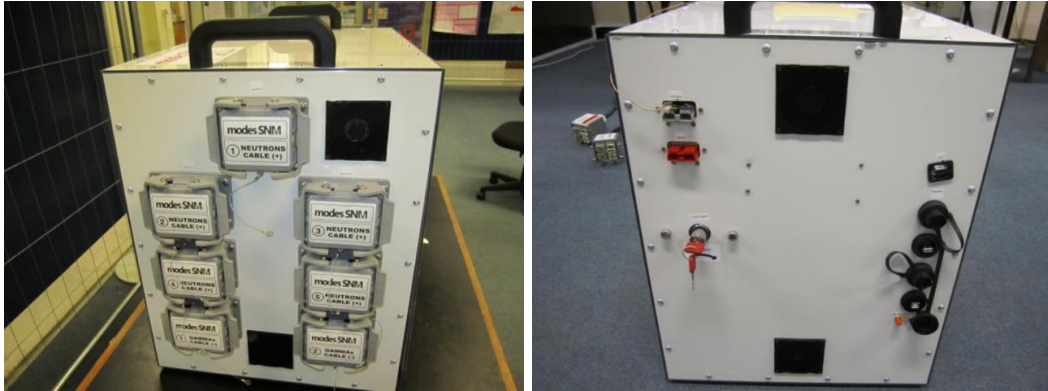
Figure 5.1: The completed electronics and computer box

5.1.2   Detector boxes

Since each box has been designed with size and connections to host two detectors, detector boxes are of two types, due to the different sizes of the gamma ray and neutron detectors. Table 5.2 summarizes their characteristics; the different box sizes are shown in Fig. 5.2.

Detector	L × H × W [mm × mm × mm]	Weight [kg]	Skin thickness [mm]	Core thickness [mm]
Neutrons	1250 × 250 × 170	4.3	0.5	5.2
Gamma rays	1000 × 300 × 170	3.9	0.5	5.2

Table 5.2: Characteristics of MODES_SNM detector boxes

The first five boxes on the front of Fig. 5.2 are the neutron boxes, with the thermal neutron box labelled in red; the two bigger, blue-labelled boxes are the gamma detector boxes. Since power supplies for xenon and ^{4}He detectors have opposite signs, the layout of the connectors has been designed to prevent a neutron box from being connected to a gamma socket and vice-versa.

5.2   Detector commissioning at NCBJ Swierk

Once the assembly was terminated, the complete system was moved to NCBJ in Swierk (Warsaw) for the laboratory characterization of the prototype. I directly partecipated to the initial tests, spending a total of two weeks working with the NCBJ group; during the first days I helped to set up the measurement equipment and understand the behaviour of the newly assembled system.

In the first phase several measurements have been carried on for all three types of detectors in order to optimize their performances and characterize the response to gamma and
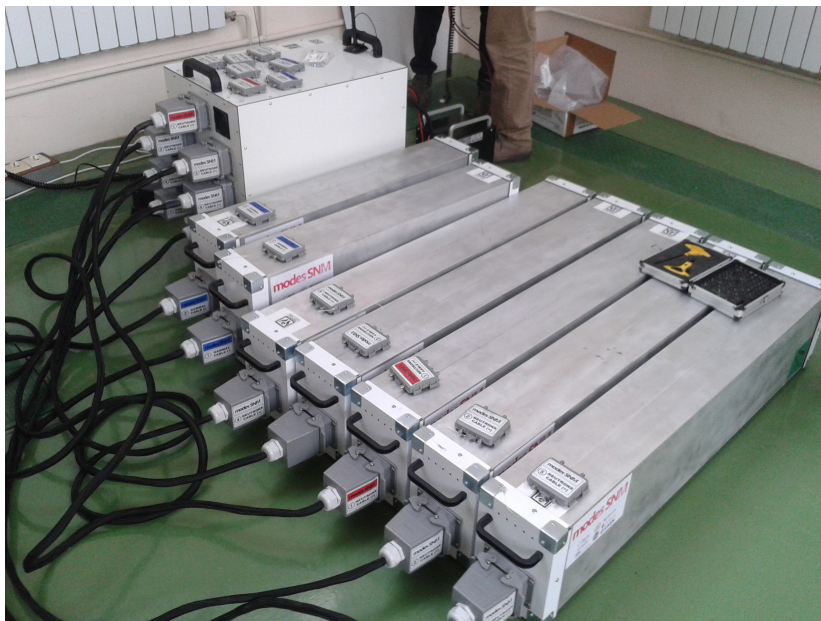
Figure 5.2: MODES_SNM detector boxes at NCBJ

neutron radiation. Further tests were then devoted to measure the False Alarm Rate, the Probability of Detection and to verify identification capabilities of various types of gamma and neutron sources.

All the measurements have been carried out in a large experimental hall to ensure a low scattering environment; the environmental conditions resembled as much as possible those defined as "Standard Test Conditions" (STC) [15]. Table 5.3 presents the environmental conditions during the PD and FAR tests. Observed humidity values are lower tha the range defined in STC specifications; given the nature of MODES_SNM detectors, this is expected to have a negligible influence on system performances.

	STC	**Measured values**
Temperature	18 °C - 22 °C	20 °C - 22 °C
Pressure	70 kPa - 106 kPa	100 kPa - 102 kPa
Humidity	50% - 75%	34% - 36%
Gamma rad. background	< 250 nSv/h	110 nSv/h

Table 5.3: STC during detection tests

Mathematical details and definitions of FAR, PD, Confidence Level (CL) and other statistical quantities are reported in Appendix A.

5.2.1 ^{4}He Fast Neutron Detectors

The response of fast neutron detectors to Pu-Be neutron source and ^{60}Co gamma-ray source was measured in order to choose optimal bias voltages and threshold settings, ensuring good neutron/gamma discrimination capability and maximum neutron detection efficiency.

Neutron/gamma discrimination in Fast Neutron Detectors (FNDs) is performed using PSD technique, as described in Sec. 4.2.3; an example of PSD discrimination plot for ^{4}He

detectors is reported in Fig. 4.3. The arrangement used for testing the FNDs is shown in Fig. 5.3.

Figure 5.3: Fast Neutron Detector tests

According to international standards and project objectives, the requirement for FNDs was to detect a ^{252}Cf source emitting a flux of 0.1 neutrons/s/cm^2 at the detector surface, with PD equal to at least 90% with CL of 95%. The FAR should be not greater than 0.001, corresponding to 1 false alarm per hour.

Each FND was raised 0.9 m above the laboratory floor and the ^{252}Cf source was placed at the same height. The distance between the detector and the source was adjusted to obtain the prescribed flux of 0.1 n/s/cm^2; for a 558 kBq source the distance equals to 228 cm. The FAR and PD tests were performed by summing the neutron events from all eight detectors available in the prototype. The cycle time was fixed to 2 s; considering a source moving at 0.5 m/s as prescribed by standards (Sec. 1.3.4) this value corresponds to a space path of 1 m, twice the active length of a single ^{4}He FND.

Detection tests consisted in 449 trials (representing a total sampling time larger than 90 minutes) with a ^{252}Cf source. The number of true positives was 448, the resulting PD being about 97.4% at CL = 95%, thus satisfying the requirements.

Detectors	Trials	Average backgr. cps	Alarm thr.	Average neutron cps	Alarms	PD
2	449	0.08	1	2.73	341	70.7%
3	449	0.13	2	4.07	341	70.7%
4	449	0.24	2	5.95	417	89.4%
5	449	0.30	2	7.57	438	94.8%
6	449	0.36	3	9.11	438	94.8%
7	449	0.41	3	11.02	446	96.9%
8	449	0.45	3	12.55	448	97.4%

Table 5.4: Results of PD for different numbers of active detectors

A typical distribution of the number of counts in the Region of Interest (RoI) defined for alarm condition is presented in Fig. 5.4. The profiles of background radiation and the source are clearly well separated.

Additional tests investigated the possibility for the system to operate with one or more FNDs powered off, exploiting the high sensitivity of the detectors. Table 5.4 presents the analysis of the counting statistics and achieved level of PD as a function of the number of active detectors. In all tested scenarios the alarm threshold was tuned to keep FAR below the level of 1/hour. At 95% Confidence Level, the requirement of PD = 90% is fulfilled even when half of the detectors are turned off.
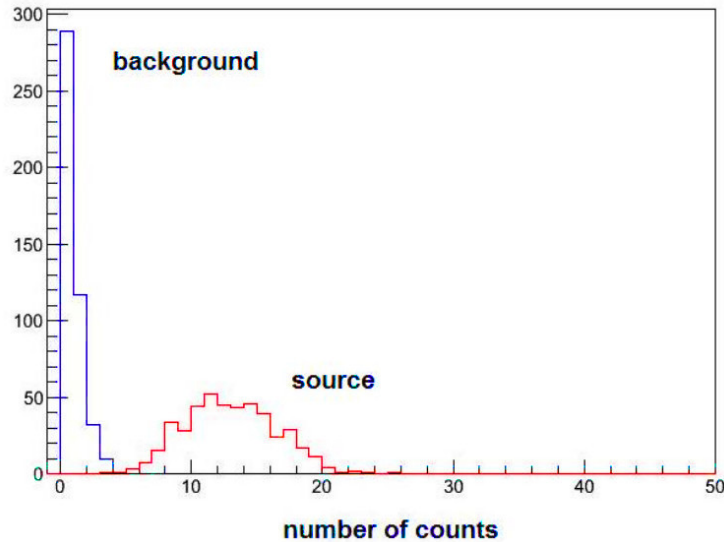
Figure 5.4: Distribution of number of counts registered with Fast Neutron Detectors for background radiation (blue line) and ^{252}Cf source (red line)

5.2.2 ^{4}He Thermal Neutron Detectors

The aim of the Thermal Neutron Detector (TND) tests was to testify their ability to provide information about the presence of a hydrogen-rich shield, as is the case of polyethylene. Measurements were performed by measuring the number of counts in the regions corresponding to the fast and thermal neutrons, with and without presence of a polyethylene shielding. A picture of the tests is reported in Fig. 5.5.

The castle surrounding the source was made up of polyethylene bricks, in a way such that all walls were 100 mm thick, with the exception of the detector-facing side that was only 50 mm thick. The distance from the source to the middle of the detector box was kept constant during all the measurements, with or without the shielding castle.

A strong increase of the number of events in the thermal neutron area of the 2D plot (see Fig. 4.4) is observed when the fission source is inserted in the shielding castle. This area is populated even when measuring the unmoderated ^{252}Cf source, probably due to scattering effects in all materials of the box. The number of the counts in the thermal neutron region with unmoderated sources represents the background for the identification of a hydrogen-rich shield; the ratio R between the fast and thermal neutron counting can be used to infere the presence of a shield and it has been studied by optimizing the cuts in the 2D plot.
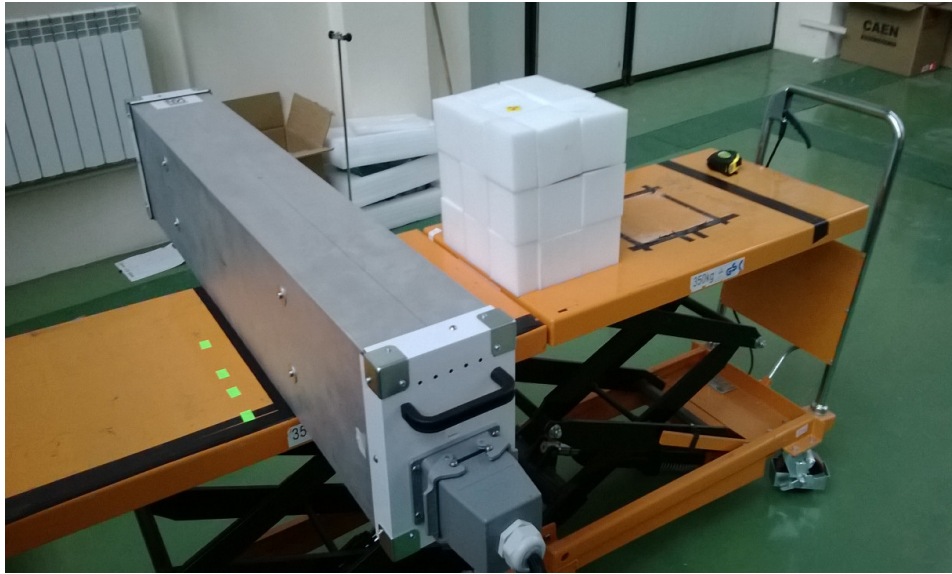
Figure 5.5: Thermal Neutron Detector tests

Considering a 60 s measurement with the ^{252}Cf source, values of this ratio were $R = 0.20 \pm 0.27\%$ without the shielding castle and $R = 3.26 \pm 0.18\%$ with the shielding in place, clearly demonstrating the possibility to identify the presence of a hydrogen-rich moderating material around a source.

5.2.3   Xenon Gamma Detectors

While neutron detectors are basically used as counters, MODES_SNM gamma detectors had to be characterized as a spectroscopic system: energy resolution, linearity, stability and efficiency. The four Gamma Detectors were labelled from 0 to 3 and separately tested; the setup is shown in Fig. 5.6.
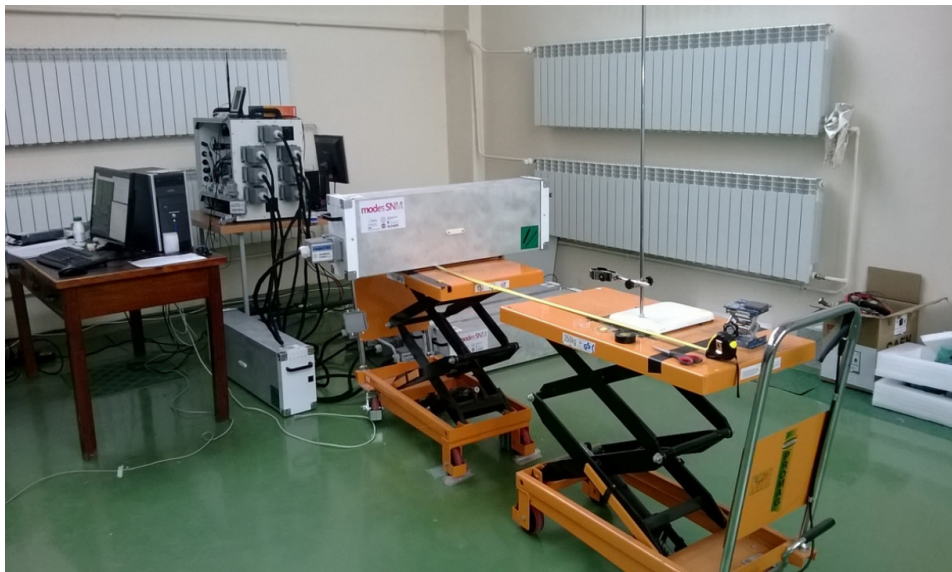
Figure 5.6: Geometry setup for testing the Gamma Ray Detectors

Threshold and gain settings

The first step was to analyze the response of the detectors to ^{241}Am and ^{137}Cs; threshold has been lowered until the ^{241}Am peak at 59.6 keV was clearly visible.
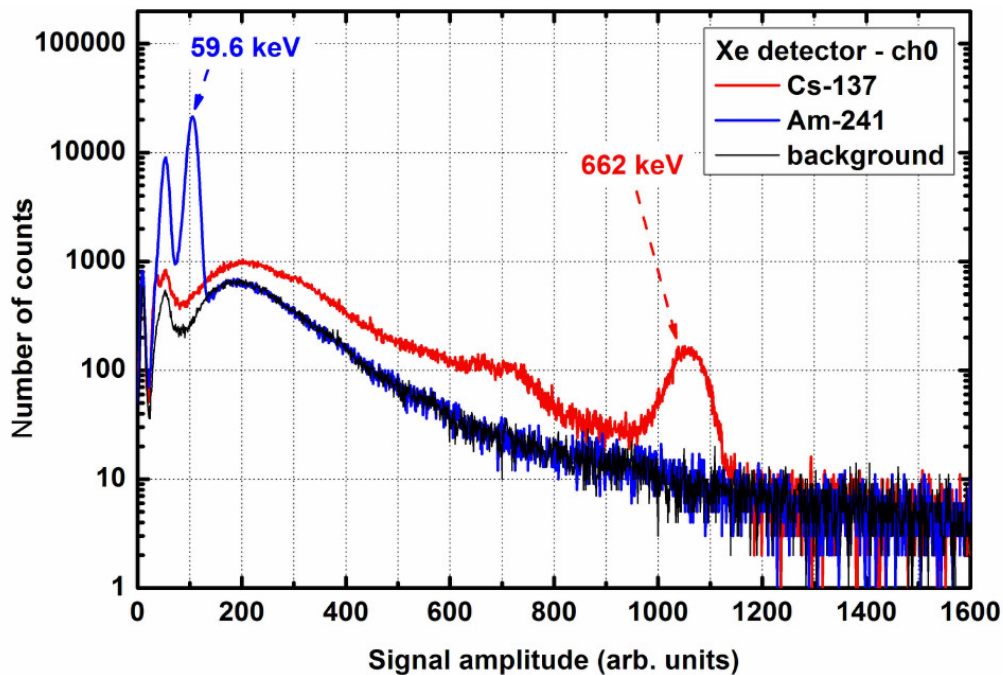
Figure 5.7: Energy spectra recorded with Gamma Detector 0 for background radiation (black line), ^{241}Am (blue line) and ^{137}Cs (red line)

An example of overlaid spectra recorded for detector number 0 with both sources superimposed to background radiation is presented in Fig. 5.7. The threshold was set at about 20 keV, a value chosen to allow for detection of americium even in the case of unexpectedly large gain drifts.

Proportionality of light yield

As most of the scintillators, xenon has a non-proportional response to gamma radiation. The deviation from proportionality was measured with a set of 10 gamma ray sources for a total of 14 different full energy peaks in the range between 50 keV and 1.5 MeV, and the amplitudes of the registered peaks were normalized to that of 662 keV gamma ray from the ^{137}Cs source.

The results, presented in Fig. 5.8, show that the scintillator response is almost linear for energies above 200 keV, whereas at low energy depositions the scintillation efficiency increases. The maximum deviation from linearity reaches 10% at about 60 keV; measurements at lower energies were restricted due to absorption phenomena in the walls of the vessels.

Energy resolution

The energy resolution of Gamma Detectors was measured with the same 10 sources mentioned above; Fig. 5.9 presents the results for Detectors 0 and 1. Energy resolution was calculated dividing FWHM of the peak by its energy. All tested channels showed energy
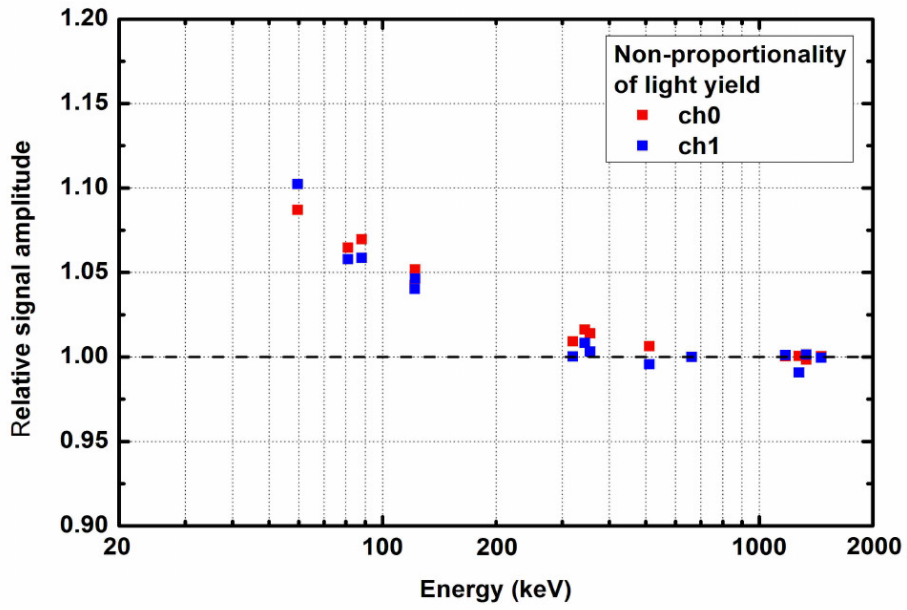
Figure 5.8: Non-proportionality of light yield for Detectors 0 and 1
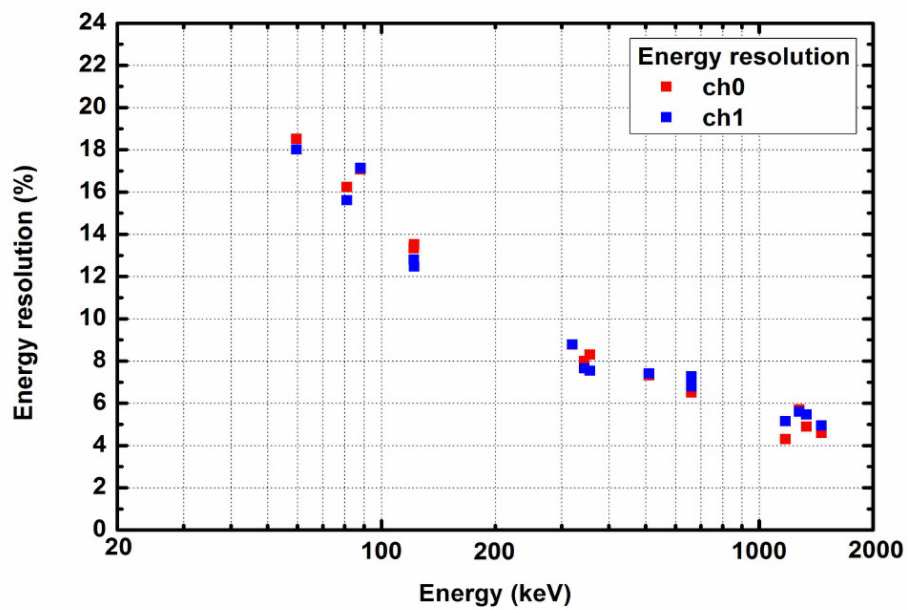
Figure 5.9: Energy resolution for Detectors 0 and 1

resolutions at 662 keV between 6.7% and 7.0%, a value close to the standard NaI(Tl) reference and suitable for spectroscopy applications.

Detection efficiency

The detection efficiency of full energy peaks was measured using the same set of 10 sources; the results are shown in Fig. 5.10. The Peak Detection Efficiency (PDE) is about 50% at about 100 keV; for lower gamma energies there is a drop down of PDE due to absorption in the gas cell container.
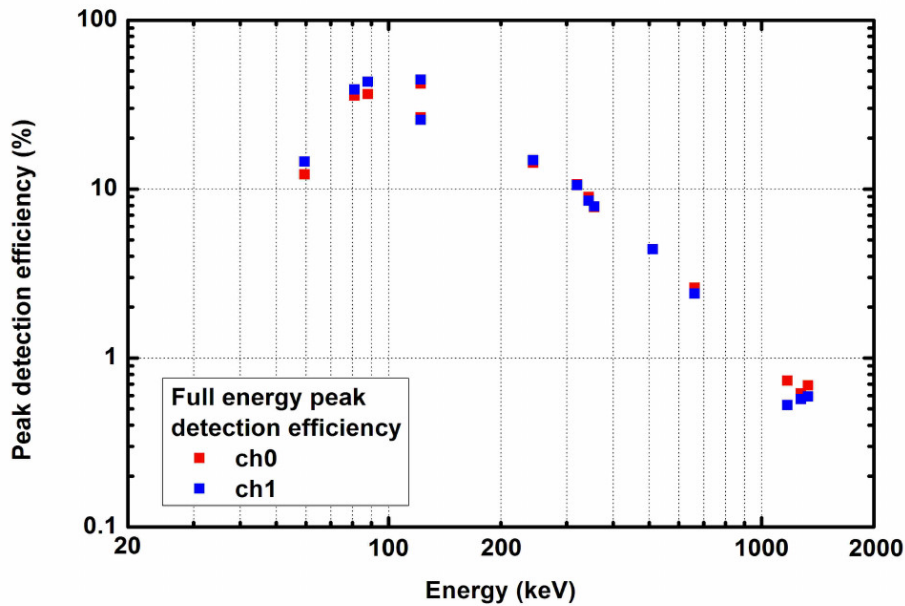
Figure 5.10: Detection efficiency of full energy peaks (PDE) for Detectors 0 and 1

PDE at 662 keV amounts to 3%; considering the time limit of 60 s prescribed by the requirements, all gamma ray sources with energies below 1 MeV are detected with sufficient efficiency to allow identification. However, at higher energies of interest, e.g. 1173 keV and 1333 keV, PDE amounts to less than 1%, which does not ensure a timely identification of ^{60}Co and other species. For comparison, a NaI(Tl) detector of similar volume (125 mm $\times$ 125 mm $\times$ 250 mm) has a PDE of 40% at 1333 keV. This reduced efficiency at high energy has an impact on identification performances of the prototype, as explained below.

Temperature stability

In principle gas detectors like the xenon tubes used in MODES_SNM are more sensitive to temperature than liquid or plastic scintillators; therefore the response of Gamma Detectors was checked upon potential fluctuations due to temperature changes in the range between 12 °C and 20 °C.

Cooling the detector resulted in an increase of the signal amplitude, but the relative change was less than 1%, a value negligible compared to the energy resolution. Fig. 5.11 presents the dependency of the signal amplitude on ambient temperature for Detectors 0 and 1, measured with a ^{137}Cs source.
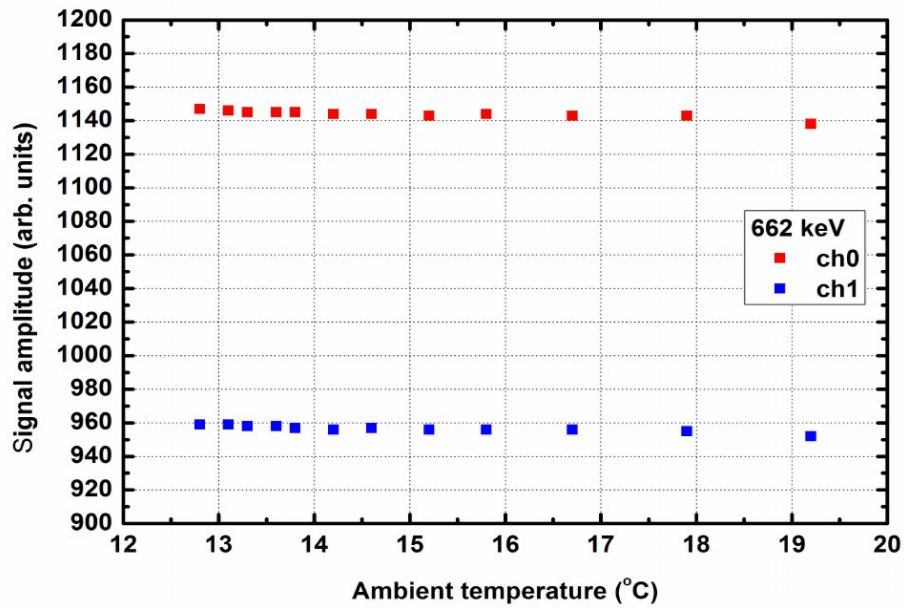
Figure 5.11: Temperature dependency of the signal amplitude for Detectors 0 and 1

The stability of the Gamma Detectors response was tested by registering 15 minutes runs of ^{137}Cs in different days; results are shown in Fig. 5.12 for Detectors 0 and 1 over 14 days of measurement. Signal amplitude was scattered by less than 2.5%.
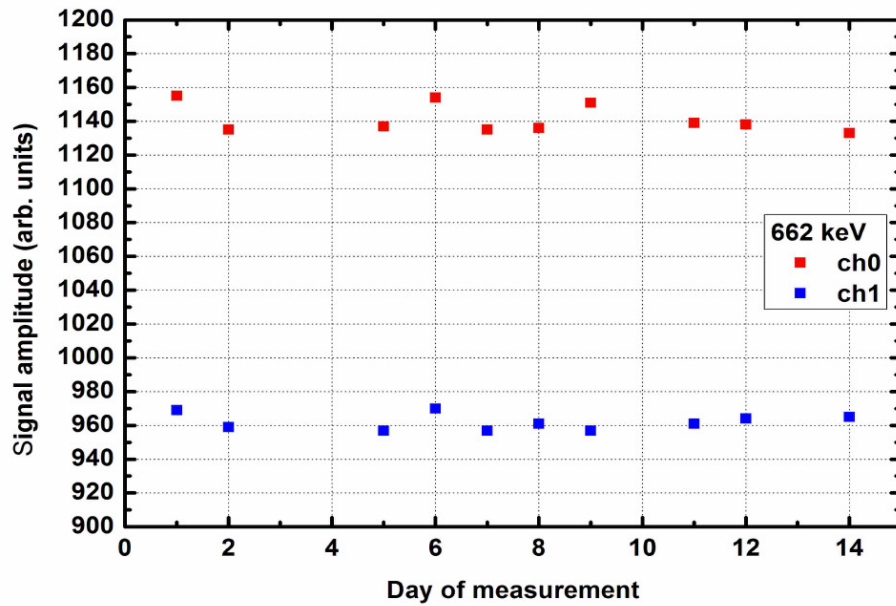
Figure 5.12: Stability of the signal amplitude for Detectors 0 and 1

Source detection performances

The requirement for the Gamma Detectors was to detect ^{241}Am, ^{137}Cs and ^{60}Co sources yielding a dose rate of 50 nSv/h on the front of the detector with PD $\geq$ 90%, CL = 95% and a maximum FAR of 0.001 (1 false alarm per hour).

The measurements were carried on in the same hall as for the Neutron Detectors. Each gamma tube was raised to 0.9 m above the floor, with three gamma sources placed at the same height (see Fig. 5.6); distances were adjusted to produce the required dose rate of 50 nSv/h. As in the case of Neutron Detectors, the cycle time was fixed to 2 s. Tests consisted in 450 consecutive cycles with each of the three sources.

Table 5.5 presents the list of used sources with their activities at the day of measurement, the distances corresponding to the prescribed dose rate and the results of the trials.

Source	Energy [keV]	Activity [kBq]	Distance for 50 nSv/h [cm]	Trials	True positives	PD
^{241}Am	59.6	18500	120	449	449	97.6%
^{137}Cs	662	641	99	450	450	97.6%
^{60}Co	1173, 1333	239	121	450	450	97.6%

Table 5.5: Gamma ray sources used for evaluation of PD and results for CL = 95%

A typical distribution for the number of counts is presented in Fig. 5.13; data were collected with background radiation and a ^{137}Cs source.
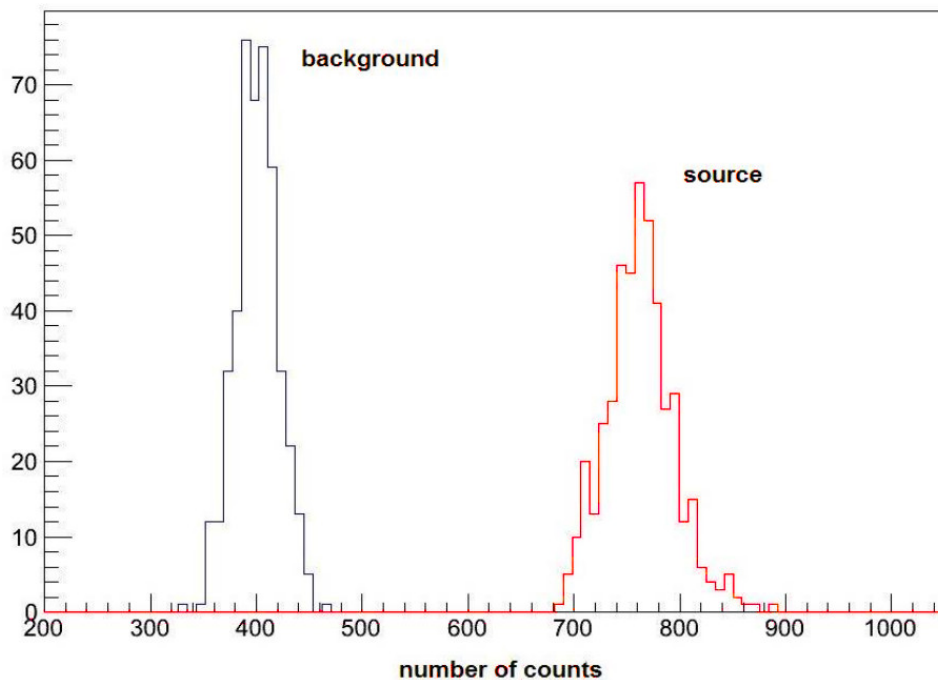
Figure 5.13: Distribution of number of counts registered with Gamma Detectors for background radiation (black line) and ^{137}Cs source (red line)

It is clear from Table 5.5 and Fig. 5.13 that the alarm requirements are easily satisfied, and the performance of the system largely exceed the international requirements for gamma source detection.

Source identification performances

After triggering an alarm the system should identify the type of the incident radiation; Table 5.6 presents the list of sources used to test the identification performances of the system, along with detector-source distances corresponding to the 50 nSv/h dose rate prescribed by the requirements.

Source	Energy [keV]	Activity [kBq]	Distance [cm]
^{241}Am	59.6	18500	120
^{57}Co	122	3622	91
^{137}Cs	662	641	99
^{22}Na	511, 1275	316	133
^{60}Co	1173, 1333	239	121
^{109}Cd	22, 88	718	80
^{133}Ba	81, 276/303*, 356/384*	979	96
^{51}Cr	320	12800	104
^{152}Eu	122, 245, 344, 779, 1408	319	89

Table 5.6: Gamma ray sources used for identification tests (* = mixed transitions)

Results of the identification tests show that the standard 60 s time interval is sufficient to identify sources yielding 50 nSv/h at the detectors, for all the sources with gamma ray energies below 1 MeV. However, at energies above 1 MeV the identification performances become unstable. Fig. 5.14 shows spectra recorded with Detector 0 and ^{241}Am, ^{133}Ba, ^{22}Na and ^{60}Co sources. In the case of ^{60}Co source, the 60 s interval was too short to identify the source, although its presence was correctly detected during the first 2 s cycle.
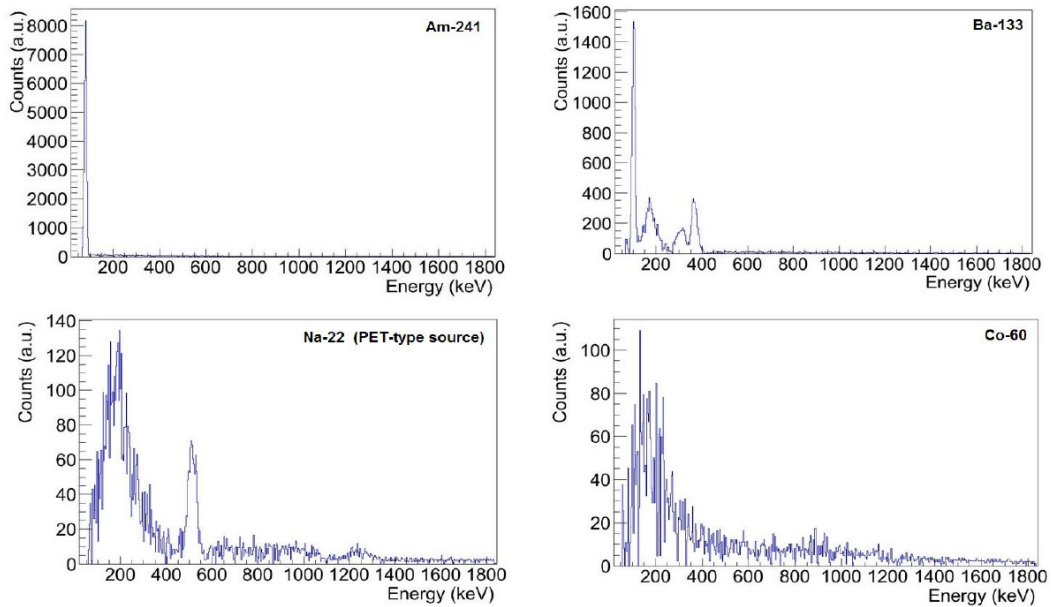
Figure 5.14: Spectra recorded with Detector 0 and ^{241}Am, ^{133}Ba, ^{22}Na and ^{60}Co sources

Since many NORM sources like ^{40}K present energy lines above 1 MeV, the sensitivity of the system had to be increased before the demonstration phase could start.

5.3 System final revision at LNL Legnaro

After the characterization campaign in Poland, the system was shipped back to INFN Legnaro National Laboratories (INFN-LNL) for the final revision.

Figure 5.15: MODES_SNM system once re-assembled at INFN-LNL

To address the issue of low sensitivity of the system at energies above 1 MeV, it was decided to replace one of the two twin xenon detectors with an existing large volume NaI(Tl) crystal (125 mm × 125 mm × 250 mm); Fig. 5.16 shows its schematics.

The energy resolution of the installed detector is equivalent to the one measured with xenon detectors but the full energy efficiency is very large at 1 MeV, approximately 40% for gamma rays incident on the 125 mm × 250 mm surface.

NaI(Tl) detectors have a very large efficiency, allowing detection of weak radioactive sources with a large detection probability (close to 99%) for dose rate of 50 nSV/h. Moreover, the energy resolution allows to detect the peaks in a 60 seconds spectrum (as prescribed by standards) and to identify the gamma ray source by comparing the identified energies with the system library. Fig. 5.17 shows a background subtracted ^{22}Na spectrum measured with the NaI(Tl) detector, at 50 nSv/h dose rate and with a 60 s measurement.

The main drawback of this detector is the presence of fluctuations in the gain, leading to a drift in the energy calibration (see Fig. 4.5). These fluctuations can significantly affect energy calibration in a short time, compromising identification performances. The problem has been addressed by placing a KCl pulser inside the detector box and compensating the drift with a dedicated software routine; this automatic self-calibration procedure is described in Sec. 4.3.1.

Detection and identification tests as the ones carried on at NCBJ in Poland have been repeated in Legnaro with the new detector layout; the first five types of sources listed in Table 5.6 have been used, adjusting the distances to the different activities.

Both detection and identification tests succeeded for all sources within the parameters required by the standards (50 nSV/h, PD ≥ 90% at 95% CL, FAR < 1/h).
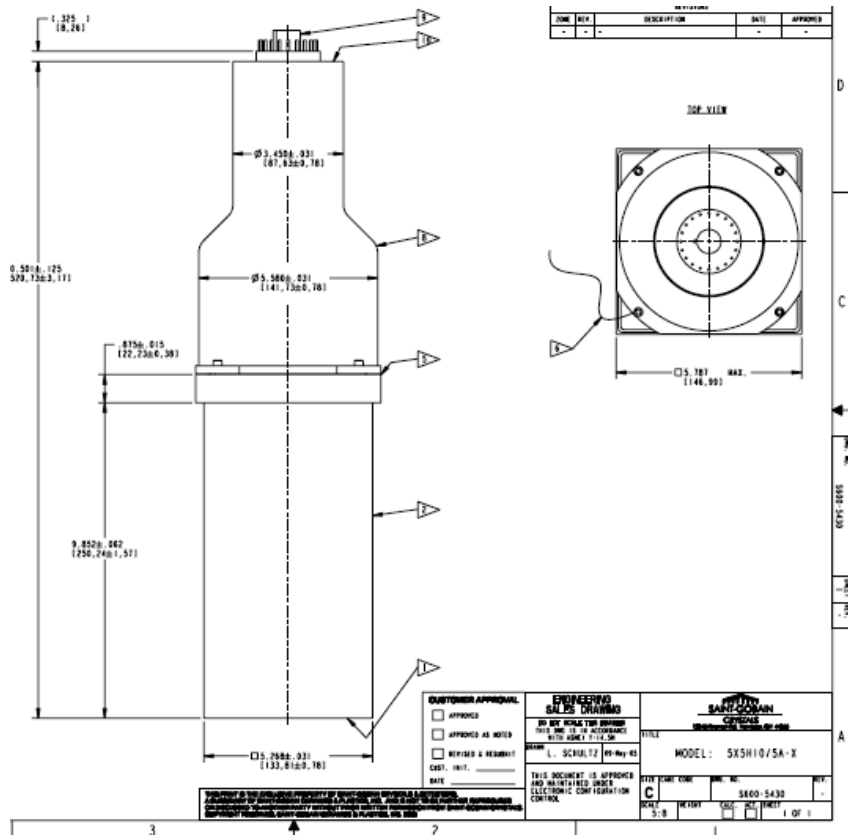
Figure 5.16: Schematics of the NaI(Tl) replacement detector
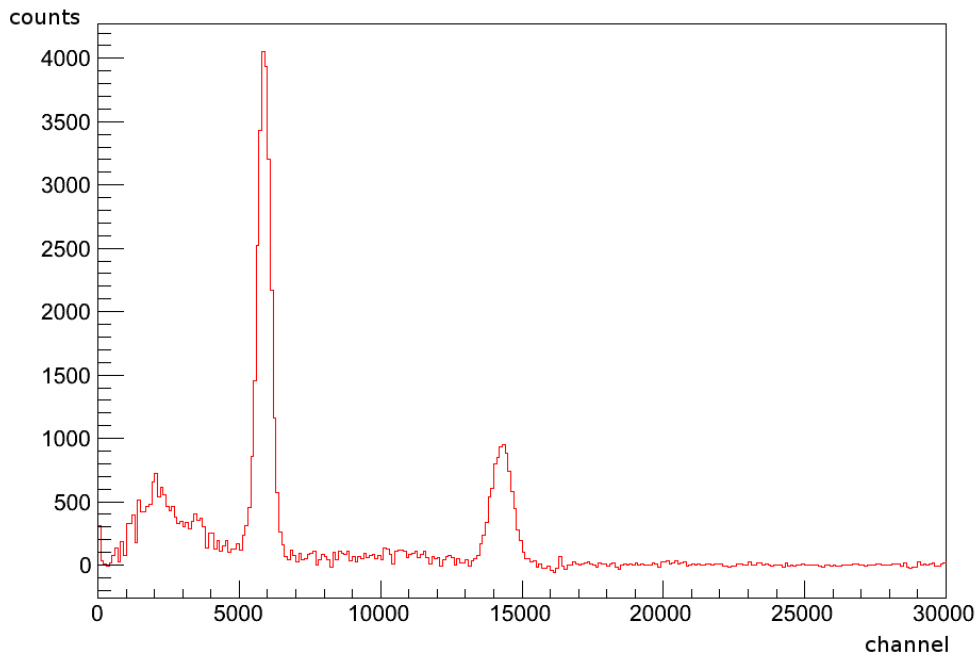
Figure 5.17: Background-subtracted spectrum for the NaI(Tl) detector, taken with ^{22}Na at 50 nSv/h dose rate and with a 60 s measurement

Figure 5.18: Different stages of MODES_SNM mounting on the chassis and inside the van: the chassis made by Uninsubria (upper left panel), testing the final position (upper right), with the system mounted view from the rear (lower left) and view from the side door (lower right)

After the tests, the system in its final configuration was mounted on a modular chassis prepared by University of Insubria; its purpose was to held all the components in place with a rigid structure suitable for being mounted inside a van for operation and transportation. The geometry of the detectors has been studied to maximize the active area once the system is mounted behind the side door of the van: neutron detectors are stacked in orizontal position on the back, while gamma detectors are vertically mounted in the front, positioned at sides to minimize shielding effects on the active volume in the middle of the neutron boxes. Fig. 5.18 shows the installation steps.

Once mounted on the chassis, the system was ready for its final exam. During the last day, the prototype was tested in the real conditions that it would face during the demonstration phase, operating on battery power from inside the moving van and being remotely controlled by the operator on the front seat (Fig. 5.19). MODES_SNM was now ready to start its journey...

Figure 5.19: MODES_SNM system operating as a real mobile inspection system

5.4   Measurements at JRC Ispra

The system left Legnaro in its definitive configuration inside the van towards JRC laboratories in Ispra. Here its performances were tested against a wider set of sources that those available at INFN-LNL, in both fixed and moving configurations. The aim of the tests was to validate detection and identification performances with all available sources, and to extend the nuclide library for the gamma identification.

5.4.1   Detection tests with moving sources

The tests at JRC were performed with moving sources to integrate static trials carried on during characterization.

According to IAEA requirements for neutron detectors [10], the prototype shall generate a neutron alarm for a ^{252}Cf source emitting 1.2×10^4 neutrons/s and moving with a speed of 0.5 m/s (1.8 km/h) at a distance of closest approach between the source and the system of

one meter. This requirement translates in a static fluence rate of 0.1 n/s/cm^2 at a distance of 1 m. Table 5.7 shows the results of the tests. While the requirements prescribe a reference speed of 1.8 km/h, our system satisfies them even for sources moving at 4.3 km/h, more than twice of the standard; detection performances are still relevant event at four times the reference speed.

Speed [km/h]	Trials	Alarms
1.8	30	30
4.3	30	28
7.9	30	23

Table 5.7: Results for dynamic sensitivity tests with neutrons

In the case of gamma ray sensitivity, both xenon and NaI(Tl) detectors are used to trigger the alarms. The requirements prescribes the generation of alarms when the ^{241}Am, ^{137}Cs and ^{60}Co gamma ray sources are moving with a speed of 0.5 m/s (1.8 km/h) at a distance of closest approach of one meter between the source and the front face of the prototype. During laboratory tests the distance of closest approach can be varied to compensate for the activity of available sources but respecting the 0.05 μSv/h dose rate requirement. Results are shown in Table 5.8. ^{241}Am, which has a very low characteristic line, is always detected at standard conditions; for higher energies the system is performing exceptionally well, with a percentage of detected source equal to 100% at all speeds, and taking into account that in the case of ^{137}Cs the dose was *one fifth* of the prescribed one.

Source	Dose [nSv/h]	Speed [km/h]	Trials	Alarms
^{60}Co	50	1.8	30	30
^{60}Co	50	4.3	30	30
^{60}Co	50	7.9	30	30
^{137}Cs	10	1.8	30	30
^{137}Cs	10	4.3	30	30
^{137}Cs	10	7.9	30	30
^{241}Am	50	1.8	30	30
^{241}Am	50	4.3	30	20

Table 5.8: Results for dynamic sensitivity tests with gamma rays

Therefore, international requirements for radiation detection can be considered fully satisfied for both neutron and gamma ray sources.

5.4.2 Identification tests

After the detection sensitivity, also the system's identification algorythm and library were intensively tested with both gamma ray and neutron sources. Table 5.9 reports the identification results, showing good performances of the prototype.

CNBM61 and CNBM93 are two Plutonium samples, both 6 g in weight, enriched in ^{239}Pu by 62.5% and 93.4%, respectively; UP8996 is a 51 g sample of 90% enriched ^{235}U. CNBM93 has a very weak gamma signature; at the distance set for the tests the intensity is close to the limit for alarm triggering, therefore affecting also identification performances.

				Source identification	
Source	Shielding	Trials	Alarms	Valid	System response
Am/Be	-	10	10	10	Am/Be
Am/Be	L + I	10	10	10	Am/Be
Am/Be	L + I + P	10	10	10	Am/Be + polyethilene
CNBM61	-	5	5	5	Pu
CNBM61	L + I	5	5	5	Pu
CNBM61	L + I + P	5	5	5	Pu + polyethylene
CNBM93	L + P	9	7	7	Pu + polyethylene
UP8996	-	5	5	5	Uranium-235
^{60}Co, 50 nSv/h	-	10	10	10	^{60}Co
^{137}Cs, 10 nSv/h	-	10	10	10	^{137}Cs
^{241}Am, 50 nSv/h	-	10	10	10	^{241}Am

Table 5.9: Results for the identification tests. Legend for shielding: L = 1 cm lead, I = 1 cm iron, P = 8 cm polyethylene, and combinations

Table 5.10 lists the sources that have been programmed inside the gamma ray identification library before leaving for the field demonstration.

Source	Class	Source	Class
ZnOx	NORM	^{57}Co	Gamma
^{40}K	NORM	^{60}Co	Gamma
^{232}Th	NORM	^{109}Cd	Gamma
^{235}U	S.N.M.	^{133}Ba	Gamma
^{238}U	S.N.M.	^{137}Cs	Gamma
^{22}Na	Gamma	^{241}Am	Gamma

Table 5.10: Sources included in the final MODES_SNM gamma ray identification library

Chapter 6

Field tests and demonstrations

MODES_SNM system has been designed to be a prototype that could lead to the development of an industrial system, with immediate applications in the fields of radiation detection and border protection. For this reason, since the beginning the two non-research European institutions were involved in the organization of the demonstration phase: Belastingdienst Douane (Dutch Customs) and the Revenue Commissioners (Irish Customs). In a later stage, the UK Border Force joined the project for the test campaign.

At the end of MODES_SNM development, and after the laboratory characterization, a series of field test was scheduled with the van-mounted prototype, to allow for a complete assessment of its present and potential performances by end users in real operating conditions.
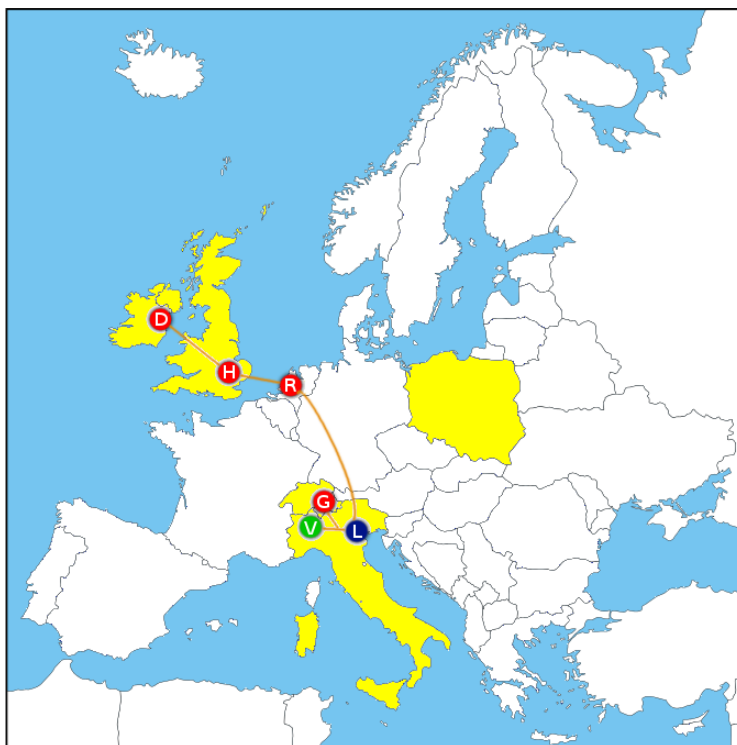
Figure 6.1: Map of locations reached by MODES_SNM van: L = INFN-LNL, V = JRC Ispra, R = Rotterdam seaport, H = Heatrow airport, D = Dublin seaport, G = Switzerland. Countries of Consortium partners are coloured in yellow

A short training course for the operators was held in Padova, following the final assembly of the system and before the transfer to Ispra. During this three-day meeting the system was presented and demonstrated in a controlled environment; I contributed to the sessions with presentations describing the analysis algorithms, the decision tree and the status of the system.

The field test campaign included operations at three different sites: Rotterdam Seaport (April, 14th - 25th), Heatrow Airport (May 2nd - 7th) and Dublin Seaport (May 9th - 16th). Then, the system went back to the Physics Department in Padova to implement some software improvements suggested by the operators and to download log data: they will be precious as a reference for future studies. Finally, another demonstration has been carried out in Switzerland in June with the updated system.

Since its final assembly at INFN-LNL in the early April, and including the tests at JRC in Ispra, the system was left mounted on the van during both transfers and operations, travelling for a grand total of nearly 6000 kilometers without suffering any damage or performance loss. Figure Fig. 6.1 shows the locations of the tests with the van-mounted system.

6.1 Training course

Following the formation of the project end-user group, a training course was organised by University of Padova during April 2nd to April 4th, 2014. Representatives from all of the consortium partners attended the meeting, together with the aforementioned end-user group and the Advisory Board (Fig. 6.2). The purpose of the training was to provide an update to all attendees on the development of the prototype system, to demonstrate the detection/identification capability of the system using the available sources at INFN-LNL, and to provide the opportunity to the end-users to become familiar with the system in advance of transport to the nominated places of demonstration. In addition, all participants were provided with a copy of the Operating Manual to assist with the familiarization.

Figure 6.2: Group photo of the partecipants of the Training Course

The Training Course was held in the same days of the system final installation inside the van. On the first day, in order to comply with radiation safety considerations, the tests involving the radiation sources were carried out by the MODES_SNM system without the chassis, inside a shielded room equipped with gamma and neutron dosimeters. The van installation was performed during the following day's meetings, and on the last day end-users had the possibility to experience the deployment and operation of the system in the final configuration.

6.2   Rotterdam seaport

The port of Rotterdam is the largest port in Europe and acts as a gateway to the EU as well as being a major global transport hub. It handles more than 12 million TEUs annually. The scanning of maritime containers to detect illicit movements of radioactive and nuclear materials is the responsibility of Dutch Customs who devote considerable resources to this task. They employ a range of fixed, mobile and hand portable detection systems in this area.

Figure 6.3: MODES_SNM performing second level inspections at Rotterdam seaport

Field trials on MODES_SNM system were performed by Dutch Customs in Rotterdam Port during April 14th to 25th, 2014. For the most part, the system was operated in the course of normal day-to-day activities, in tandem with the existing detection equipment. I partecipated to the first two days of operations, observing the startup of the system and its response to radiation sources moving in a real environment.

6.2.1   Secondary control device

On the first day, MODES_SNM system was deployed as a secondary control device; secondary inspections investigate only those cargo that already triggered an alarm on radiation portals. The tests were repated on day 4. A total of 6 containers alarmed at the fixed RPMs and were inspected with the following results:

- three containers carrying chemicals registered count rates approximately twice that of background. ^{40}K was identified in each case. However, there were 3 false thermal neutron alarms, leading to the indication of possible presence of shielded ^{252}Cf;

- a container of seaweed (Carrageenan) registered a count rate of 1850 cps and the presence of ^{40}K was indicated, but together with a false indication for ^{137}Cs;

- a container of ceramics registered 1500 cps, but identification within the set 1 minute time limit was not possible;

- a gamma alarm of 1100 cps (background 980 cps) occurred while no cargo was present. The system was deployed near to a fixed portal which alarmed too. It was concluded that a mobile container X-ray scanner with an energy of 6 MeV operating some 80 metres distant may have triggered these alarms in both MODES_SNM and the fixed portal.

6.2.2   Primary control device (static mode)

On day 2 the system was deployed in static mode as a primary control mechanism in conjunction with the fixed RPMs. The following events were recorded:

- the system alarmed for a container of live plants passing at a speed of 26 km/h;

- the system alarmed for a consignment of stoneware with a maximum reading of 1500 cps at a speed of 15 km/h;

- two gamma alarms occurred while no truck was nearby. The maximum count rate 1900 cps;

- one thermal neutron alarm occurred while no truck was nearby.

The same operations were conducted on day 3, scanning a total of 131 containers with the following results:

- one gamma alarm registering 2500 cps occurred while no truck was present;

- gamma alarms occurred in respect of 4 containers containing "NORM" materials including ceramics, minerals and chemicals.

At the end of day 3 we had enough data to begin evaluating the performances of the system. The False Alarm Rate was higher than expected, but with 8 False Alarms in 4 days, and considering 2 to 5 hours of operation per day, we were still within the requirement of 1 False Alarm per hour. These False Alarms found an explanation at the end of the field test campaign; it is briefly described in Sec. 6.6.1.

Figure 6.4: MODES_SNM deployed in static mode near fixed portals

6.2.3   "Drive by" operation mode

During days 5 to 9, when the system was prepared for the transfer to the UK, MODES_SNM was deployed in "drive by" mode to scan containers at a maximum speed of 10 km/h and at a distance of 30-50 cm from the target containers. Typical background levels varied between 950 to 1200 cps.

The following events occurred:

- a gamma alarm at 1200 cps registered for a container of groupage. After 60 seconds plutonium and a polyethylene shielded source were indicated. Following a second identification of 120 seconds duration ^{137}Cs was indicated. A new identification of 120 seconds (with van door open) was carried out. This time no neutron alarm registered and ^{40}K was identified. ^{40}K was also identified by the Dutch Customs system;

- a gamma alarm registering 1050 cps occurred with a cargo of polymers. MODES_SNM identified ^{232}Th and ZnOx, while the Customs system identified ^{232}Th;

- a container of ceramic tiles triggered a gamma alarm of 1950 cps. While a handheld device identified ^{40}K within 60 seconds, MODES_SNM did not provide an identification within 300 seconds. The calibration sources (^{137}Cs and ^{60}Co) were then introduced to the system and were identified. The system carried out a further identification on the cargo of tiles and identified ^{40}K in 60 seconds;

- with a consignment of cat litter the system registered an alarm of 2600 cps. However, it did not provide an identification within 120 seconds;

- a gamma alarm of 1300 cps occurred when passing a concrete building. ^{40}K was identified;

- When passing a quantity of stones a gamma alarm of 1150 cps occurred. After 120 seconds ZnOx and ^{137}Cs were "identified". When this test was repeated there was no nuclide identification;

- a false thermal neutron alarm lasting 1 second occurred;

- two times, in two different days, a fast neutron alarm of 1 second duration was triggered when no target was present;

- a secondary inspection of a consignment of fibre glass triggered a gamma alarm of 1260 cps. No neutron alarm occurred although after 300 seconds, a polyethylene shielded neutron source and californium were "identified".

When driving the system across the container terminals numerous gamma alarms occurred, with a maximum of 1250 cps (less than 10% above threshold) indicating variation in backgrounds levels arising from differing materials used in the construction of the terminal surface.

During all these tests, natural background variations proved to have a significant impact on the behaviour of a mobile system like MODES_SNM. This effect has long being recognized and it is still being studied [45, 46]; its importance justifies further efforts in its assessment.

6.2.4 Tests with radioactive samples

A number of tests were then carried out on day 6 using a variety of locally held known radioactive sources:

- a ceramic plate containing a Uranium glaze was held close to the door aperture of the MODES_SNM van. No alarm occurred. However, when held close to the NaI(Tl) detector, a gamma alarm of 1500 cps was triggered and ^{235}U was identified in 60 seconds;

- a gas mantle containing ^{232}Th was held at a distance of 15 cm from the detector. A gamma alarm of 1500 cps was triggered and after 60 seconds ^{232}Th was correctly identified and ^{133}Ba was also indicated (the ^{232}Th decay chain contains also a gamma line close to the relevant one in ^{133}Ba);

- about 20 g of zirconium sand contained in a glass vial were held at a distance of 30 cm from the detector. Following a gamma alarm of 5500 cps, ZnOx was identified, but the operators also expected the identification of ^{226}Ra; it did not happen because at the time ^{226}Ra was not present in the source library. The test with zirconium sand was repeated, this time in "drive by" mode at a distance of 1 metre, at speeds of 10 km/h and 5 km/h. A gamma alarm of 1250 cps occurred at 5 km/h, no alarm occurred at 10 km/h;

- the system was driven past a lead shielded Am/Be neutron source placed on a tripod at 10 km/h at a distance of 1 m without alarming. This was repeated at 5 km/h resulting in a fast neutron alarm of 1.5 cps and identification of "shielded neutron source". The test was repeated with the lead shielding removed from the source. Gamma and fast neutron alarms were triggered and both Am/Be and ^{241}Am were identified;

- a ^{133}Ba source was mounted on a tripod and a gamma alarm of 1490 cps at 10 km/h at a distance of 1 metre occurred. ^{133}Ba was identified.

Identification performances proved to be satisfactory and Customs personnel were impressed by the level of MODES_SNM prototype. There were also a few glitches in the algorithms, mostly regarding neutron sources; they are commented at the end of this chapter.

6.3 Heatrow airport

The next stage of the tests involved the transfer of the system in the United Kingdom, to be operated in the cargo area of one of London's airports. Heathrow Airport is the busiest UK airport and acts as a major international hub handling large volumes of passengers and cargo. Cargo arriving at Terminals 1, 3, 4, and 5 is transported to the Heathrow Cargo Terminal for scanning by fixed RPMs; the cargo is transported in trucks and vans.

Field trials on the MODES_SNM system were performed by the United Kingdom Border Force (UKBF) in Heathrow Cargo Terminal during May 2nd to 7th, 2014. The system was operated in the course of normal day-to-day activities, in tandem with the existing detection equipment.

Figure 6.5: MODES_SNM operating in static mode at Heatrow airport.

During the five days of operations, the system was deployed in static mode for most of the time. A total of 635 cargo carrying vehicles were scanned, passing at speed of 8-16 km/h. The system behaved as follows:

- the system returned a gamma alarm for a consignment of medical isotopes; over multiple tentatives, the system once proposed identification was "Am/Be shielded neutron source", but a definitive identification was not possible. That isolated misidentification is considered the result of one false thermal neutron alarm combined with the presence of isotopes not included in the source library;

- one gamma alarm was generated as a vehicle passed;

- the False Alarm number was around 30, still close to the 1 FA/hour requirement;

- the system successfully identified two ^{60}Co sources shielded by stainless steel after 60 seconds.

In addition MODES_SNM system drove past a container known to contain ^{60}Co contaminated metal products. At a passing speed of 8-16 km/h and at a distance of 15 metres from the source the system alarmed and performed a correct source identification.

6.4   Dublin Customs

Dublin Port is the largest port in Ireland and handles a variety of containerized, bulk and car ferry traffic. The Dublin field tests were carried during May 9th to 16th, 2014. In addition to the continuance of evaluating the technical capability of the MODES_SNM system, the

Figure 6.6: MODES_SNM inspecting an airport cargo truck

assessment of the potential for its deployment in a variety of operational scenarios was an important consideration in this phase of the field testing.

As weather conditions were generally favourable during the tests, it was possible to carry out all of the scanning with the side door of the van open. The temperature range during the tests was $8 \div 20$ °C.

6.4.1 Static mode operations

On the first day, MODES_SNM scanning was conducted in conjunction with an X-ray scanning operation at container compound in Dublin Port. No difficulties were encountered in setting up the system. The MODES_SNM system was deployed in static mode approximately 50 metres distant from the Nuctech 6 MeV mobile X-ray scanner, without experiencing any interference. The Nuctech scanner incorporates an integrated R/N detection system which operates in tandem with the X-ray scanning. A total of 9 inward bound maritime containers, as well as 1 vehicle were scanned. No real alarms were triggered.

The following day, scanning took place at a car ferry compound where a total of 74 inward bound trailers and vehicles were scanned. No real alarms were triggered although 3 gamma alarms occurred when no target was in range.

On day 6, MODES_SNM was deployed in static mode in a container compound and scanned 2 inward bound containers which had been profiled as containing "NORM" materials. Gamma alarms were triggered by both containers, one of which contained ceramic tiles, and the second contained clay pots. Gamma alarms were also triggered on the container X-ray scanner. In the case of the clay pots, MODES_SNM gave an erroneous identification of Am/Be source.

The last day, MODES_SNM scanned some 40 outward bound trailers and 20 inward

bound trailers at a car ferry compound, without triggering any alarm.

6.4.2   Tests with radioactive samples

On the third day, MODES_SNM system was brought to University College Dublin for testing
with a sealed Pu/Be source. The source was transferred from its storage area to a smaller
paraffin-filled drum which was placed in a Customs van. During testing, the van containing
the Pu/Be neutron source was driven past the MODES_SNM SNM van, which was deployed
in stationary mode. Measured neutron dose at 1 m from the shielded drum, as determined
with an EG&G Berthold LB6411 neutron probe, was 5 - 6 μSv/hr. The corresponding figure
for gamma dose rate, measured with an EG&G Berthold LB1236 proportional counter, was
about 1 μSv/hr.

Figure 6.7: MODES_SNM tests with a moving Pu/Be neutron source at University College

Passing with a speed of approximately 8 km/h and at a stand-off distance of 1 metre from
the van, the source triggered gamma, fast neutron and thermal neutron alarms. The passing
speed was increased to 20 km/h and the distance to 4 metres, which were the maximum
values permitted by the site conditions, and on each occasion all three alarms were triggered.

6.4.3   "Drive mode" operations

Scanning loose or bulk materials is often problematic. For example, there is significant trade
in exporting "end of life" vehicles and equipment to Africa which are not always suitable
for scanning by fixed detection systems. MODES_SNM was therefore deployed to scan this
type of cargo in an open compound in Dublin Port in mobile or "drive by" mode. No alarms
were triggered by this cargo, although a number of gamma alarms, caused by variation
in background levels (and confirmed by elevated readings on a handheld device) occurred.

MODES_SNM was again deployed (static mode) in proximity to the X-ray container scanner, this time at a distance of approximately 30 metres, and a gamma alarm occurred.

The system was then deployed, again in "drive by" mode, at a warehouse where a variety of goods are stored. The van screened cargo within the warehouse passing along the aisles between the racks. No alarms were triggered. It was then moved to the adjoining compound and screened a variety of vehicles, containers, tankers, machinery and equipment. No alarms were triggered except for elevated background alarms which occurred from time to time in various regions of the compound.

6.5 Swiss Heavy Goods Traffic Center and Customs

At the end of operations at Dublin seaport, the system was brought back to Padova to check the system and receive some software updates. The updated MODES_SNM system was field tested at the Swiss border in Basel, Switzerland, on June 2nd, and at the Heavy Goods Traffic Center in Uri, Switzerland, on June 17th.

Figure 6.8: MODES_SNM at Heavy goods traffic center in Uri

At the Swiss Customs controls in Basel, the MODES_SNM system was tested at two different sites to see the different Concept of Operations (CONOPS) involved. One site was on the border at Freiburgerstrasse where a mobile container X-ray scanner is deployed. In case of suspicion (for example from the analysis of the truck's papers), a truck is accompanied by a special vehicle and guided to the inspection area. Throughput is therefore not high and the speed of the trucks is approximately 8 km/h. During 90 minutes, 8 vehicles passed the MODES_SNM van. No alarm was triggered. The background was around 1.8-2 kHz, falling to 1.2-1.5 kHz when a truck passed through. The system behaved as expected.

Then the MODES_SNM van was moved to the customs in Weil am Rhein. It was placed right after one of the customs check points. 30 vehicles passed the van; no alarm occurred but it was clearly visible the influence of the trucks to background shielding (see Fig. 4.10).

Finally MODES_SNM van was moved between trucks stationed at the parking lot in Weil am Rhein and measurements were performed while driving. No alarm occurred, but the background had to be recalibrated once.

On the second day, operations were held at Heavy goods traffic center in Uri (Fig. 6.8). The center is located in front of the Gotthard tunnel in Switzerland. Roughly 1300-1500 trucks (about 75% of all trucks driving through Switzerland) pass through the heavy goods traffic center in Uri every day. The center is operated by the Police; two out of three lines were closed so that the MODES_SNM van could measure out all trucks passing through the control center within a 2.5 h window. Another confirmation of the high variability of background count rates is that gamma background in Uri was about twice as high compared to the values registered in Zürich during the system transfer.

218 trucks passed by the MODES_SNM van at a speed between 5 km/h and 25 km/h. Four alarms occurred during all operations, all of which happened when no truck was present. By looking at the gamma rate display these false alarms could be traced back to the same issue: a firmware bug. The problem was later identified and corrected, as described in Sec. 6.6.1.

Source identification was performed three times without alarms, and ^{232}Th and ^{40}K were identified during a 60 s measurement window.

6.6   Feedbacks from the Field test campaign

MODES_SNM prototype system was generally well liked by the end-users, particularly on account of its versatility and mobility. Set up time was minimal and the high level of availability of the system during the tests was considered excellent. The fact that the system suffered no adverse effects from long distance travel indicated a high standard of design and construction. The operator interface was clear and simple to use, and the ability to be controlled from a remote device proved useful. The system also performed very well in terms of sensitivity and analysis times within the opportunities available during the tests.

The physics algorithms for detection and identification behaved fairly well, but some flaws have emerged during the four weeks of tests. They have been analyzed at the end of the campaign; here I will comment the most relevant ones, together with the solutions implemented.

6.6.1   Investigation on the False Alarm Rate

A recurring problem was the high level of False Alarms in absence of cargos and materials; while the FAR was still within the requirements, we expected the system to have better performances. A detailed study was put in place, with night-long measurements and additional log routines. All the gamma FA events had one thing in common: a particularly dependency of the counting rate versus time, a small peak with very short duration and the shape of a shark fin (Fig. 6.9). The frequency of these peaks had an average of one every 1-2 hours.

We traced back the problem to errors of unknown origin in the data transfer between the front-end and the computer. These errors are relatively rare but constant in effect, switching a particular bit of the event structure and altering the timestamp of the affected events. For the 4 seconds after the problem occurred, these wrong timestamps prevented the data buffers from being properly flushed, leading to an overestimation of the counting rate up to 150%. This issue affected both gamma and neutron countings and can explain the FAR observed during field tests.
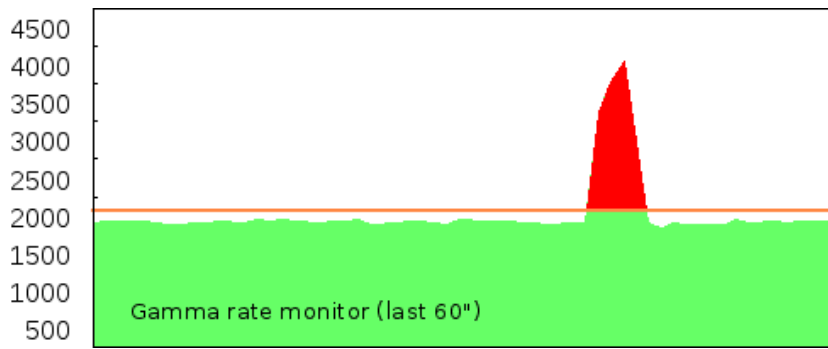
Figure 6.9: Anomalous counting rates leading to False Alarms

The problem has been software compensated, and the system proved to operate for more than 10 consecutive hours without any false alarm. We now consider strong background fluctuations as the only source of False Alarms.

6.6.2 Erroneous identification of gamma sources

The gamma identification procedure proved to be extremely precise at times, but it didn't always perform as expected. There are many factors contributing to these performances:

- the gain drift of the NaI(Tl): even if a self-compensation procedure is in place (see Sec. 4.3.1) it does not operate continuously, and can be safely used only when there are no gamma alarms, to ensuring that the reference peak of the KCl will be clearly visible. Therefore, not only it does not completely eliminate gain fluctuations, but it becomes ineffective when the alarm condition lasts for more than a few minutes;

- background fluctuations: when a mobile detection system is used while moving, background levels can rapidly change up to a factor of two, depending on the nature of the terrain or the presence of artificial manufacts. To improve identification performances, as well as the False Alarm Rate, a better background estimation strategy would be required;

- completeness of the source library: to add a source to the identification library is not simply a matter of loading the emission lines into the software. For each source with an emission spectrum more complex than those of ^{137}Cs or ^{22}Na, the system response to each line must be carefully studied, analyzing possible detection conflicts with other sources, and evaluating the impact of the resolution, drifts and other non-linearities.

6.6.3 Erroneous identification of neutron sources

The neutron identification algorithm is triggered by the two neutron counting alarms, then it analyzes both the neutron counting and the gamma ray spectrum. False Alarms like those described in Sec. 6.6.1 could have forced this analysis to be performed on background spectra, leading to the identification of neutron sources with or without shielding. This behaviour should have been corrected together with the False Alarm issue described above.

In two different occasions, a wrong neutron identification resulted from identification procedures with non-standard duration (other than 60 s). This is explained by a software error in the renormalization of event counting: the system has been designed and tested

with a standard identification time of 60 s as described by international requirements, while the possibility to change this duration was implemented as an experimental feature during the first day at Rotterdam seaport. This issue has now been addressed.

Chapter 7

Project results

Project MODES_SNM concluded with full success on June 30th, 2014. Not only all the project milestones were achieved, but the prototype was completed on time and showed good performances. The technical requirements defined at the beginning of the project have been fulfilled, and during the demonstration tour the end users showed great appreciation to the final result of the work, to the satisfaction of all the Consortium partners. This chapter summarizes the various results achieved by the project.

7.1 Fulfillment of the requirements

The requirements for MODES_SNM demonstrator are described in Sec. 1.3.4; they have been extensively tested at the NCBJ, INFN-LNL and JRC facilities (see Chapter 5). The results can be summarized as follows:

- **probability of detection (PD) and False alarm rate (FAR):** performances of the prototype largely exceeded these requirements (Table 5.4 and Table 5.5). The prescribed value for PD in the case of neutron sources is respected even when half of neutron detectors are turned off. One single source of false alarms has been traced back at the end of the field test campaign (Sec. 6.6.1) further lowering the FAR well below the threshold level;

- **gamma sensitivity:** results shown in Table 5.8 evidence that all sources are always detected at standard conditions. As the energy of the source increases the system performs better and better: in the case of ^{137}Cs it has percentage of detection equal to 100% at *four times* the reference speed and *one fifth* of the prescribed dose;

- **neutron sensitivity:** the prototype performs as expected even at more than twice the reference speed (Table 5.7);

- **single nuclide identification:** the system in its final configuration was able to detect all the library nuclides (Table 5.10) in a time smaller or equal of the prescribed time (Sec. 5.3 and Table 5.9);

- **multiple nuclide identification and masking:** identification of multiple sources performed well in laboratory set-ups. Field tests gave a wider spectrum of results, providing valuable feedback from actual operating conditions (Sec. 6.6);

- **radiation interference:** in all the trials which involved strong gamma radiation and neutron source it has been testified that strong gamma sources do not trigger neutron alarms by their own presence, while the system continues to respond to actual neutrons as prescribed.

International requirements for radiation detection can be considered fully satisfied for both gamma ray and neutron sources, either standing or in motion.

7.2   Official evaluation by the EU

On August 19th, 2014 the Final Review Meeting was held in Bruxelles. Representatives of Consortium partners presented the results of this 30-month work to the EU Project Officer and the team of experts, which later issued their Final Report. The project has been positively evaluated by EU officials, from the point of view of both the organization and the results.

The following are excerpts from the official Final Review Report clearly showing the level of appreciation that MODES_SNM Consortium has gained during its activities:

> *the objectives of the project has been achieved thanks to a well organised and effective work of the consortium. [...] All Deliverables were delivered on time or within reasonable delay [...] and all have good to excellent quality.*

The outcomes of the R&D effort have also been considered successful by the reviewers:

> *the obtained results are relevant from a scientific and technical viewpoint. New advances have been produced in Detector Physics and Nuclear Electronics. And still there is room for improvements [...] The final result is a friendly instrument that can be used by a wide range of users to detect SNM and distinguish it from the natural background mostly compound of gamma radiation.*
> ***The objectives of the project have been achieved.***

And as a conclusion:

> *The project is certainly of innovative character and is very attractive for the general public. The scientific results are relevant and of interest in several scientific and technical fields. As said before, the project has a significant impact on the EU safety politics.*

7.3   Publications

MODES_SNM activities have originated a number of publications and presentations, describing either one specific research result or the project as a whole. This is a selection of the oral presentations given by Consortium members:

- G. Viesti, *MODES_SNM Modular Detection System for Special Nuclear Material* 5th meeting of the C2013 Customs Detection Technology expert group Mestre/Venice (Italy) June 26-27, 2012;

- G. Viesti, *Development of a mobile modular system for the detection of Special Nuclear Material (MODES_SNM)* 10th Latin American Symposium on Nuclear Physics and Applications Montevideo (Uruguay) December 1-6, 2013;

- M. Caccia, *Silicon photomultiplier readout of a scintillating noble gas detector for homeland security* ANIMMA - Advancement in Nuclear Instrumentation Measurement Methods and their Applications Marseille (France), June 22-27, 2013;

- R. Santoro, *Integration of SiPM in a high-pressure noble gas scintillation detector for homeland security* 13th Topical Seminar on Innovative Particle and Radiation Detectors (IPRD13) Siena (Italy), October 7-10 2013.

The appearance of MODES_SNM on scientific literature as to January 2015 has been limited due the schedule of the project itself. A dedicated and comprehensive paper describing the entire project and its outcomes is currently in preparation by the Consortium; it is expected to be published during 2015. These are the scientific papers published so far:

- M. Caccia et al., *Silicon Photomultiplier readout of a scintillating noble gas detector for homeland security* ANIMMA - Advancement in Nuclear Instrumentation Measurement Methods and their Applications Marseille (France), June 22-27, 2013, DOI: 10.1109/ANIMMA.2013.6727974;

- F. Resnati et al., *Suitability of high-pressure xenon as scintillator for gamma ray spectroscopy* Nuclear Instruments and Methods in Physics Research Section A, Volume 715, 1 July 2013, Pages 87-91.

In addition, as part of the Dissemination activities incouraged by the EU policy, the project has made some appearances on specialized journals, such as *Border Security Matters*, the official magazine of Borderpol, on May 2014.

7.4 Industrial developments

The exploitation of either single technologies or the complete MODES_SNM system has been studied during WP9, exploring the potential of the original concept both from a security and a commercial points of view.

After the conclusion of the project, Arktis Radiation Detectors Ltd. decided to continue the development of MODES_SNM at an industrial level; the system is now part of the Company's catalogue [47]. In November 2014, Arktis and Padova University reached a licence agreement for the commercial use of the software written within the University's participation to the project. This collaboration is still in place and open to future developments.

Chapter 8

Other studies on detectors and materials

While working at MODES_SNM project I also dedicated many efforts in widening my knowledge of detectors and materials, with a focus on those used in security applications. With our group I have studied the performances of a non toxic reference liquid detector (Eljen Technologies EJ-309, Sec. 8.3), the use of a flat panel PMT much less affected by magnetic fields (Hamamatsu H8500, Sec. 8.5, and a new plastic scintillator with PSD capabilities (Eljen Technologies EJ-299-33, Sec. 8.4).

8.1   PSD corrections at high neutron energies

In order to validate PSD discrimination methos, tail-to-total ratios are supposed to depend on the signal shape and thus only on the particle type (with the exclusion of the noisy, low energy region). This has proven to be not completely true, since there are additional effects that may affect the distributions.

First effect is saturation of the ADC. If a pulse of high energy is higher than the dynamic range of the ADC, the associated waveform will have a truncated peak and the tail-to-total ratio would be overestimated, resulting in a greater PSD value. The statistic impact of saturation effects increases with the energy, resulting in an gradual and upward bending of the two populations in the PSD plot. Since high energy events are a minority in most applications, the impact of saturation on FOM estimations is rather low, and, if needed, these events can easily be filtered out checking the pulse heights.

A second effect is the slow decrease of the neutron PSD value as the energies increase, as is clearly confirmed in Fig. 8.10. Fig. 8.1 from [40] reports the average shapes of the neutron events for different cuts in total light output; the average shapes of the signals are normalized to the signal minima. The relative role of the delayed component, determining the value of the PSD parameter, is very clear. A clear reduction is observed from Fig. 8.1 for the tail component, causing the decrease of the PSD parameter value. This fact was already outlined in [52]. The origins of these phenomena have not yet been completely estabilished, and must be found in the physics of the scintillation mechanisms. One possibile explanation is that the emission of delta electrons increases with the energy of the recoil proton. In this case, an increasing portion of the recoil proton kinetic energy is dissipated by delta
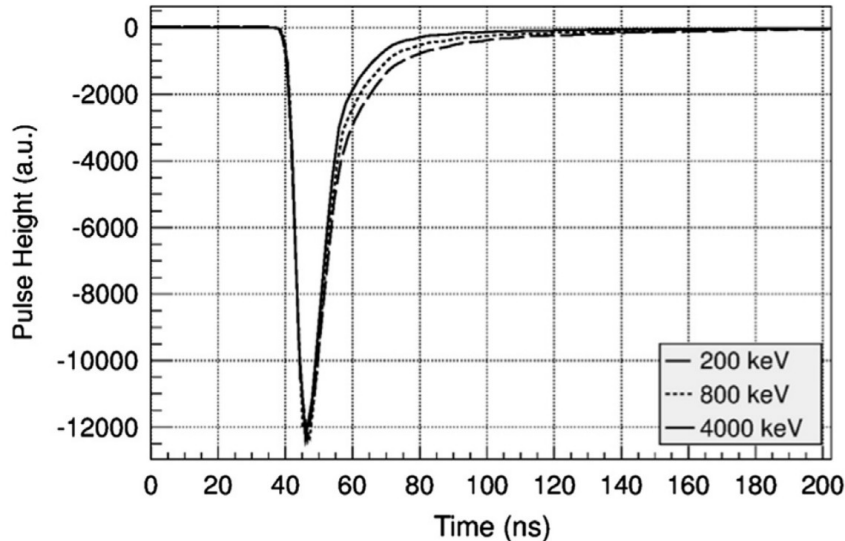
Figure 8.1: Average signal shapes for neutron events having average total light output of 200, 800 and 4000 keVee. The spectra are normalized to the pulse minima

electrons that are not contributing to the signal tail. In any case, the observed decrease means that the PSD parameter for neutrons is not a constant with the total light output and this reflects on the capability of discrimination between gamma rays and neutrons in an extended dynamical range.

8.2   Gamma energy calibration in organic scintillators

In the case of inorganic scintillators like NaI(Tl) calibration procedures are rather simple: since the spectra are characterized by one or more full-energy peaks, their calibrations can be reduced to a linear fit of the positions of at least two full-energy peaks. Typical calibration sources include pure ^{22}Na or a combination of ^{60}Co and ^{137}Cs. Further refinements may include subtraction of the Compton background or using more than two sources to perform a quadratic fit; however, for most applications the linear calibration already provides satisfactory results.

Calibration of organic scintillators is more complicated due to the special characteristics of these types of detector. First, the yield of the scintillation light depends on the ionizing particle (electron, proton...) being the light output for electrons not linear below 40 keV and beyond 1.6 MeV [28]. Moreover, the low average atomic number of the solute implies that photons emitted by typical radioactive sources interact almost exclusively by Compton scattering. In this case the nominal energy of the Compton Edge is well known; however, the finite pulse resolution of the scintillation detector implies that the position of the maximum in the Compton events distribution is shifted to lower energies, and the intensity of this shift depends on the detector pulse resolution.

In order to solve this problem, some empirical prescriptions have been developed in the past and simulations by Monte Carlo methods are commonly used to determine the shift value by fitting the experimental distribution.

In my works I have used a simplified method, fully described in [49]. The algorithm starts by constructing the expected distribution of the Compton events using the Klein-Nishina

formula:

$$\frac{dN}{dE}(E) = \frac{\pi r_e^2}{m_e c^2 \beta(E)} \left(2 + \frac{\beta(E)^2}{\alpha^2 \left(1 - \beta(E)\right)^2} + \frac{\beta(E)}{\left(1 - \beta(E)\right)} \left(\beta(E) - \frac{2}{\alpha} \right) \right)$$

where $\alpha = E_0/m_e c^2$, $\beta(E) = E/E_0$, r_e is the classical electron radius and m_e the electron mass.

The overall pulse height resolution of the detector is then reproduced by a Gaussian smearing of the predicted distribution [50, 51].

As an example, the effect of the Gaussian smearing corresponding to width values of σ = 5, 10, 15 and 25 keV is compared in Fig. 8.2 with the theoretical distribution. It appears, as expected, that the maximum in the Compton distribution moves to a lower energy value by decreasing the pulse height resolution.
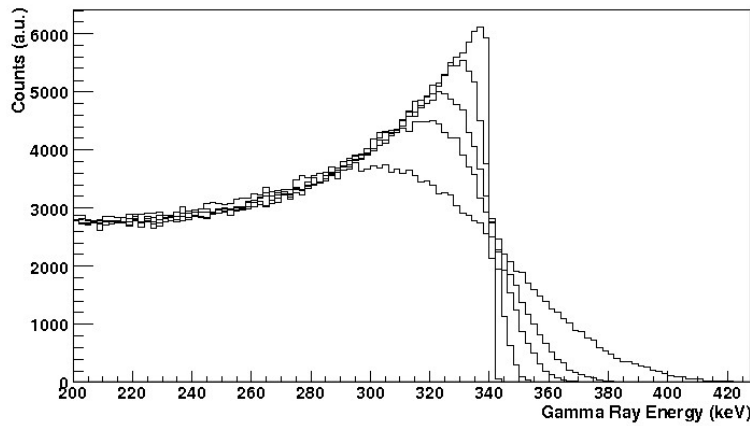
Figure 8.2: The effect of different gaussian smearings over a theoretical Compton Edge

The energy calibration of the organic scintillator is performed by the following steps:

1. measuring with high statistics the pulse height distribution using a non-monochromatic gamma ray source;

2. producing a set of theoretical Compton distributions for the expected energy lines (e.g. 511 and 1275 keV in the case of ^{22}Na) with Gaussian smearings for different values of the width;

3. determining, by a χ^2 analysis, the width that better reproduces the experimental distribution. The best-fit width value determines directly the energy shift of the nominal Compton Edge that is then used to calibrate the spectra.

An example of the above procedure is reported in Fig. 8.3 for a ^{22}Na spectrum measured by an EJ-228 plastic scintillator. The result of the spectrum analysis is also shown. In this case it is found that the best fit values for the width of the Gaussian smearing are σ = 36 keV (σ = 64 keV) for the 511 keV (1275 keV) photon, respectively. This resolution values imply shifts of 52 keV and 89 keV for the two maxima in the spectrum respect to the nominal Compton Edge energies. The precision of this method is typically 10% of the σ value.

Figure 8.3: Example of fitting an experimental Compton Edge

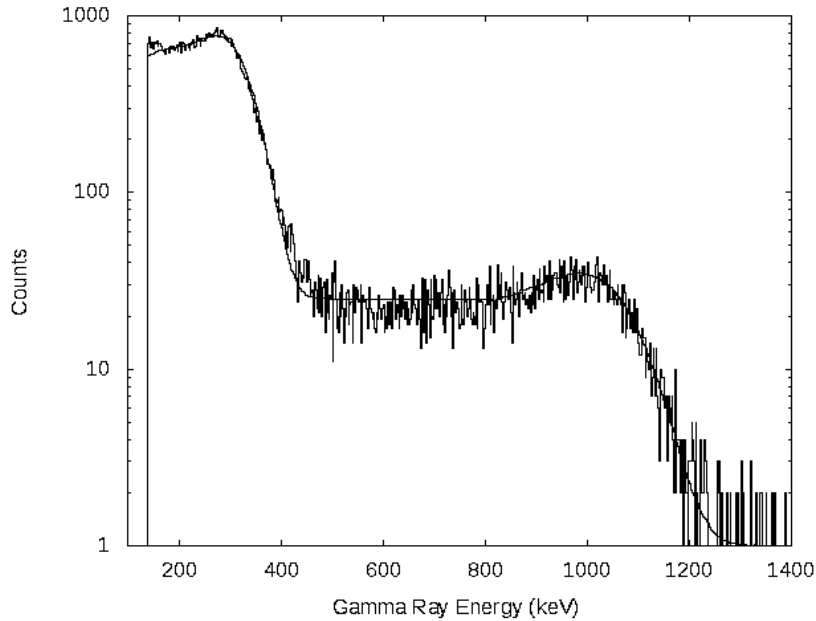## 8.3   Characterization of EJ-301 and EJ-309

Organic liquid scintillators are commonly used for fast neutron detection thanks to their PSD capability used to separate neutrons from the gamma-ray component of the radiation field. Being the liquid scintillator a standard tool in basic research, such detectors have found a rather marginal use in nuclear security applications since many operational contexts prohibit these liquids because of their toxicity and flammability. Moreover liquid scintillators detect neutron above a low energy threshold (usually few hundred keV) and exhibit a good gamma-ray efficiency so that such detectors are normally characterized by a modest gamma-ray rejection capability, a property that is required to identify weak neutron source in a strong gamma-ray background [55].

New liquid scintillation materials have become recently available as the EJ-309 type [56] from Eljen Technology, which is characterized by low toxicity and high flash point (144 °C) compared to the more traditional EJ-301 (flash point 26 °C) which is equivalent to the well known NE-213.

In 2012 our group has studied the performances of both EJ-301 and EJ-309 when exposed to neutrons in a high gamma ray background [57]. The detectors studied consist of 2" × 2" liquid scintillator cells coupled to an H1949-51 HAMAMATSU photomultiplier (PMT) through an EJ-560 silicon rubber interface. The PMT anode signals were analyzed with a CAEN V1720 12 bit 250 MS/s digitizer.

Fig. 8.4 reports the spectra measured with the two scintillators: they are very similar. The calibration procedure described in Sec. 8.2 allows one to estimate of the detector pulse height resolution by determining the spreading width s needed to reproduce the Compton Edge structures. The energy resolution is defined as σ/L where L is the energy value of the Compton Edge. The energy resolution derived in this case for the two liquid scintillators is $\sigma/L \sim 6.0\%$ for the Compton Edge of the 1275 keV gamma-ray ($\sigma/L \sim 8.2\%$ for the Compton Edge of the 511 keV gamma ray). This figure is slightly better with respect to those reported
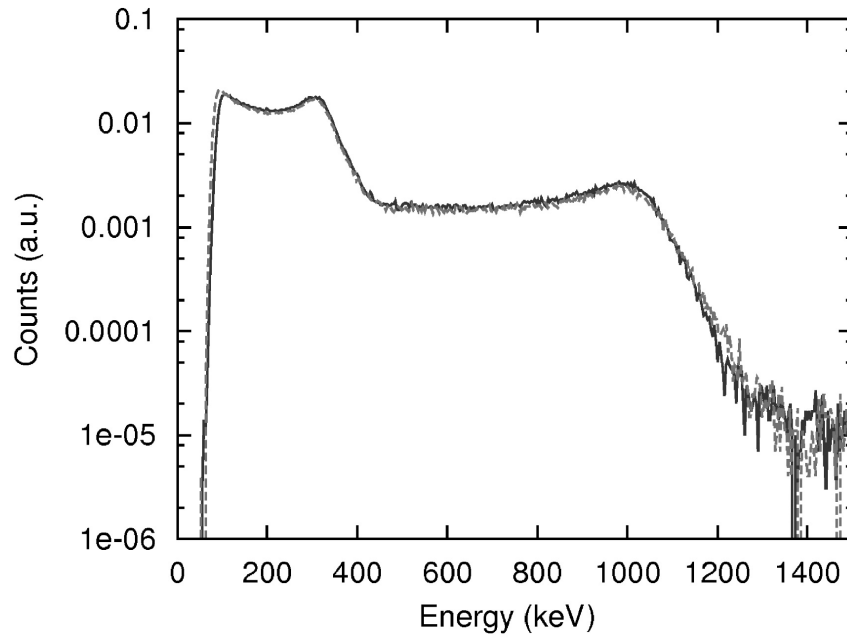
Figure 8.4: Calibrated ^{22}Na pulse height distribution for EJ-301 (full line) and EJ-309 (dashed line) detector.

in [49] for a 2" × 2" EJ-228 plastic scintillator processed with standard NIM electronics. The low energy detection threshold, as determined from the spectra in Fig. 8.4, results to be about 60 keV.

The response of the different scintillators was studied using a weak ^{252}Cf source (0.7×10^4 neutron/s) placed at about 15 cm from the detector front face. Typical PSD versus energy scatter plots are shown in Fig. 8.5. In this representation the neutron and gamma regions can be separated by a cut at PSD = 0.09 for the EJ-301 and PSD = 0.16 for the EJ-309 for energies larger than 300 keV.
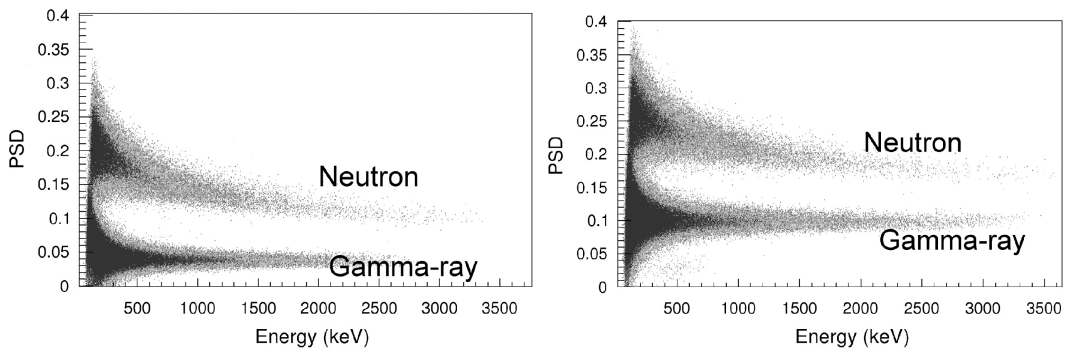
Figure 8.5: Scatter plot PSD versus energy of a ^{252}Cf source measured with the EJ-301 detector (left) and EJ-309 (right)

A number of PSD spectra have been produced by varying the low energy threshold and analyzed. Extracted FoM values are reported in Fig. 8.6 for the two detectors explored in this work as a function of the low energy threshold. It is seen from Fig. 8.6 that the FoM increases, improving the discrimination, with the low energy threshold reaching values of FoM = 1.5 for thresholds of about 300 keV. This threshold value corresponds to about 1.5 MeV in proton energy by using the response functions provided in [58]. The slightly lower

pulse shape capability of the EJ-309 with respect to the EJ-301 is also confirmed, although the measured FoM values for the two detectors are fairly closed.
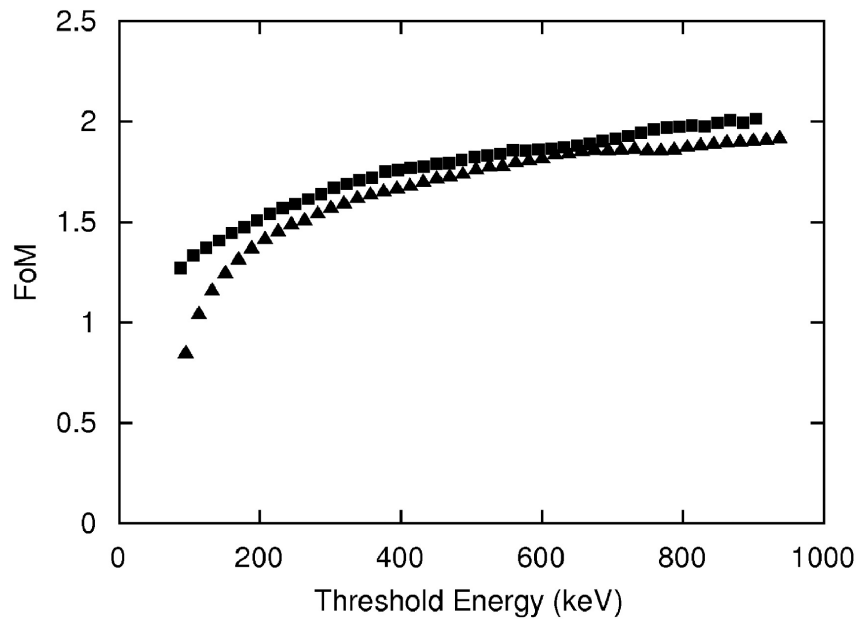
Figure 8.6: Figure-of-Merit parameter (FoM) as a function of the low energy threshold for EJ-301 (squares) and EJ-309 (triangles) detectors. The statistical uncertainties are within the point size

8.4   New plastic scintillator with PSD: EJ-299-33

The possibility to use plastic scintillator in the field of neutron detection has always stimulated the attention of researchers; unfortunately the quest went on for years without much success. In 1960, Brooks discovered that discrimination of fast neutrons from gamma rays could be obtained by doping a standard plastic scintillator (e.g., polystyrene + p-terphenyl + POPOP) with a so-called "secondary solvent" (herein 4-isopropylbiphenyl) [48]. He developed a prototype named "Plastic 77", later marketed as NE-150; by a few months however, physical alterations appeared on the samples and the product was discarded.

Since then the research continued unsuccessfully, until in 2012 a new experimental detector appeared on the market. It was developed by Zaitseva [59, 29] and manifactured, probably with some modifications, by Eljen Technologies under the name of EJ-299-33. It is composed from highly concentrated 2,5-diphenyloxazole (PPO) and a wavelength shifter (optional), 9,10-diphenylanthracene (DPA), in polyvinyltoluene (PVT). Later, Blanc et al. further investigated the chemical composition for PSD plastic scintillators starting from Brooks' works [60]; at last they were able to reproduce the successful combination, albeit with slightly worse performances than the commercialized material. Scintillators with sizes up to 1 liter have been manifactured, without sensible physical alterations after one year of exposure to light and radiation.

In 2014 I partecipated to the characterization of a detector equipped with EJ-299-33 [61], and the results have been compared to other scintillators as listed in Table 8.1. All detectors tested were equipped with the same volume of scintillator: a right cylinder of 50 mm diameter × 50 mm height. Pulse height resolution, time resolution and PSD capability
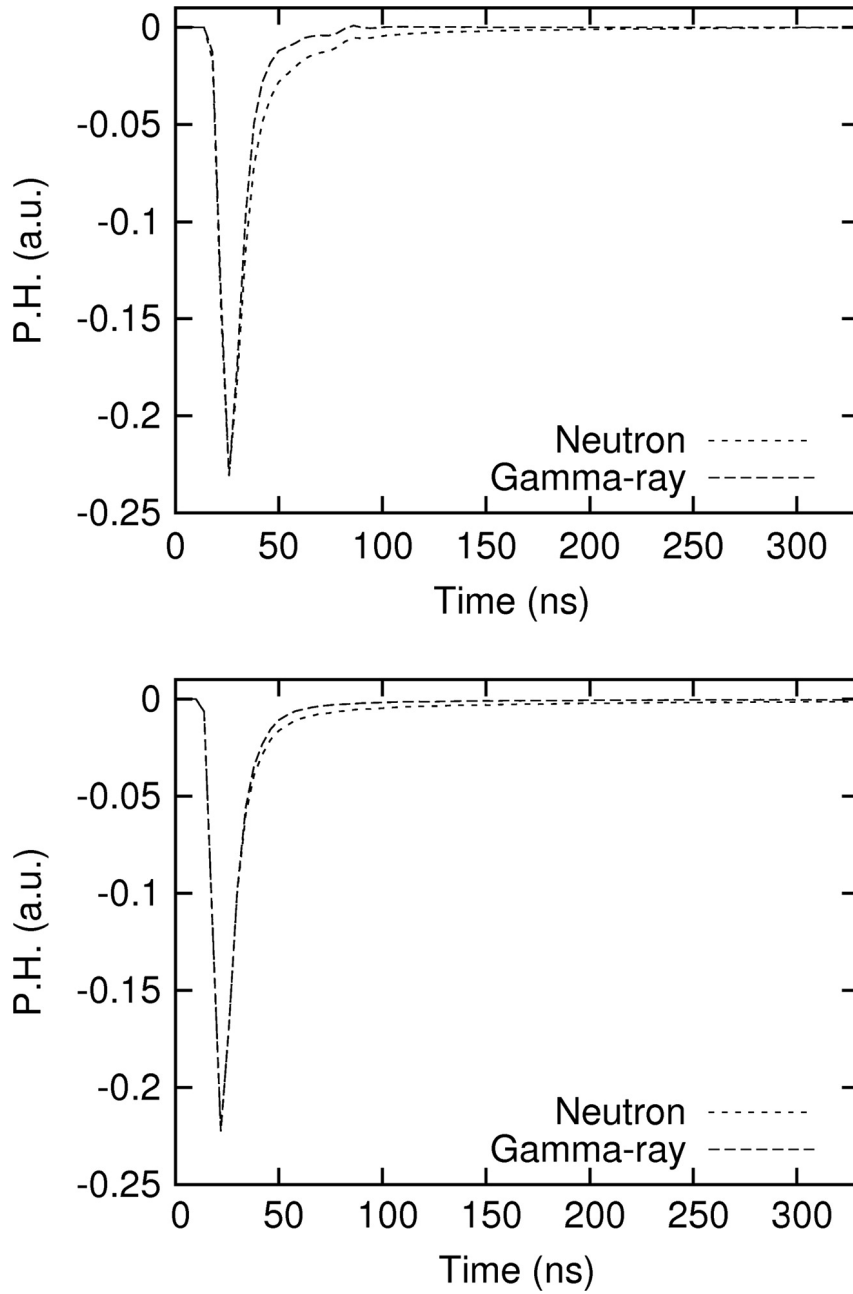
Figure 8.7: Samples of pulses from neutrons and gamma rays in EJ-301 (upper panel) and EJ-299-33 (lower panel)

have been measured for each scintillator.

Scintillator	Description	Density [g/cm^3]
EJ-228	Plastic without PSD capability	1.023
EJ-299-33	New plastic with PSD capability	1.08
EJ-301	Liquid equivalent to NE213	0.874
EJ-309	New liquid with lower hazard	0.95

Table 8.1: Liquid and plastic scintillators compared in this section

In Fig. 8.7 the examples of signal shape for neutron and gamma ray pulses in the standard liquid scintillator EJ-301 and the new EJ-299-33 are reported. One can see from Fig. 8.7 that the difference between neutron and gamma signals is larger for the standard liquid scintillator than for the new one.

A typical pulse height distribution obtained with EJ-299-33 irradiated with a ^{22}Na source is reported in Fig. 8.8, showing clearly the two Compton Edges relative to the 511 keV and 1275 keV gamma rays. The pulse height distributions can be analyzed by the method described in [63] to extract the pulse height resolution σ/E at the Compton Edge of the 511 keV gamma rays.
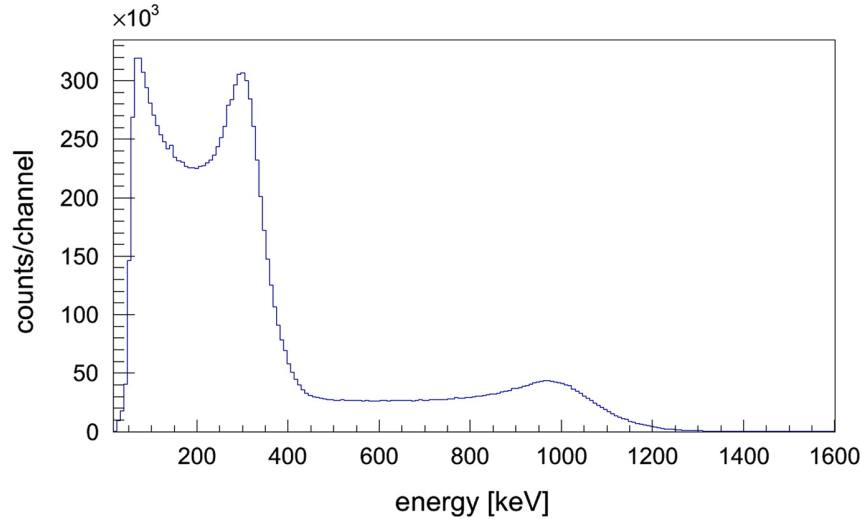
Figure 8.8: Typical pulse-height spectrum of a ^{22}Na source with EJ-299-33 detector

Table 8.2 shows the expected correlations between the measured pulse height resolution and the scintillation efficiency for the three detectors coupled to the same PMT.

Model	PMT	Scintillation efficiency [photons/MeV]	Energy resolution [σ/E %]	Decay time [ns]	Time resolution [ns]
EJ-299-33	H1949-51	8600	10.0 ± 0.8	-	0.44 ± 0.01
EJ-228	XP2020	10200	11.0 ± 0.8	1.4	0.42 ± 0.01
EJ-301	H1949-51	12000	8.0 ± 0.5	3.2	0.43 ± 0.01
EJ-309	H1949-51	11500	8.0 ± 0.5	3.5	0.51 ± 0.01

Table 8.2: Summary of the measured values for 2"x 2"scintillators. Energy resolutions refer to the 511 keV Compton Edge. Time resolutions are related to a low energy threshold of 150 keV

The time resolution has been studied by collecting gamma-gamma coincidences between the detector under test and a reference EJ-228 - XP2020 assembly with the ^{22}Na source placed at about 6 cm from each detector face. The photomultiplier signals were analyzed with a 1 GS/s digitizer and processed off line by the virtual constant fraction discriminator as described in [63]. Coincident events were then selected to build the time distribution reported in Fig. 8.9. The contribution to the resolution of the reference fast plastic was determined in a measurement using two identical EJ-228 - XP2020 assemblies and then scaled from the measured overall time resolution. The data reported in Table 8.2 are relative to a low energy threshold of 150 keV. The measured time resolution of the new plastic material compares well with standard plastic EJ-228 that is recommended for fast timing applications.
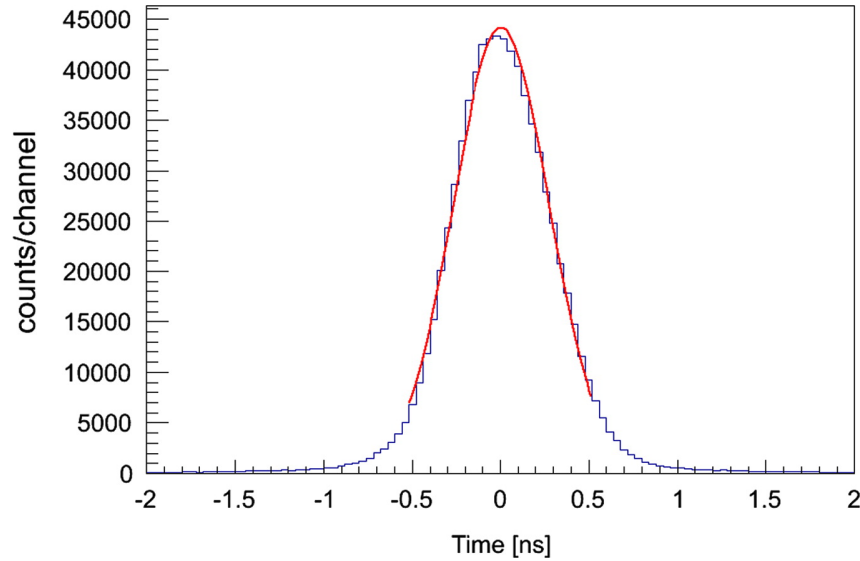

Figure 8.9: Time distribution of coincidence events between the EJ-299-33 and the reference EJ-228 detectors. The gaussian fit between -0.5 ns and +0.5 ns yields an overall time resolution of about 610 ps (FWHM)

The discrimination between gamma ray and neutrons was studied using a weak ^{252}Cf source (about 0.8×10^4 neutrons/s) placed at 17 cm from the front faces of the EJ-301 and the EJ-299-33 detector assembly. Raw PSD scatter plots for the two detectors obtained in a first measurement using standard parameters for the on-line DPP analysis are reported in Fig. 8.10.

The new plastic detector is certainly capable of discriminating neutrons from gamma rays but the discrimination capability is clearly poorer compared to that of EJ-301. DPP parameters were tuned in order to optimize the discrimination capability, following the same procedure described in [57], nevertheless the final parameters (and the PSD capability) did not improve significantly the initial results. As an example Fig. 8.11 reports the PSD scatter plot obtained with optimized DPP parameters and with an energy threshold of 300 keVee.

In this case the regions of gamma rays and neutrons are completely separated with a rather linear response in terms of PSD vs. total light. For a more quantitative comparison of the discrimination capability, several PSD distributions of the EJ-299-33 detector assembly were obtained using different energy thresholds between 100 and 1000 keVee. The FoM values extracted from the PSD distributions are reported in Fig. 8.12 and compared to the results of EJ-301 and EJ-309 from [57]. It is clear that the FoMs of EJ-299-33 are much
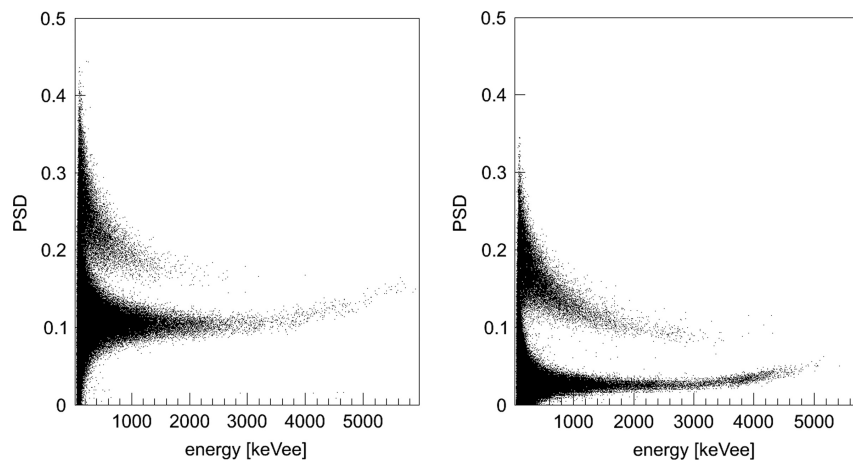
Figure 8.10: Comparison of the PSD vs. total light for EJ-299-33 (left panel) and EJ-301 (right panel) scintillators
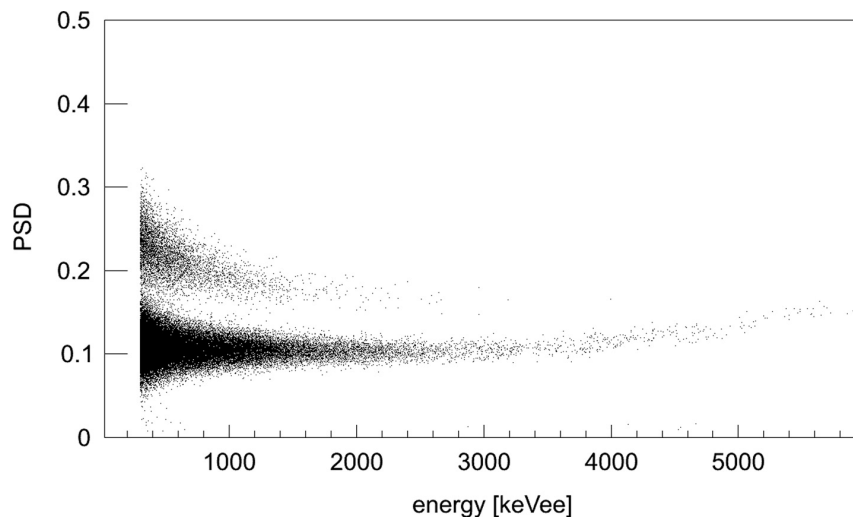

Figure 8.11: PSD plot for EJ-299-33 with optimized parameters and 200 keVee energy threshold

lower compared to the liquid scintillator detectors, with FoM values in the range 0.8-1.0 for thresholds in the range 200-400 keVee. It is interesting to notice that a threshold of 200 (400) keVee corresponds to a reduction of the events statistics by 50% (75%) for a ^{252}Cf source.
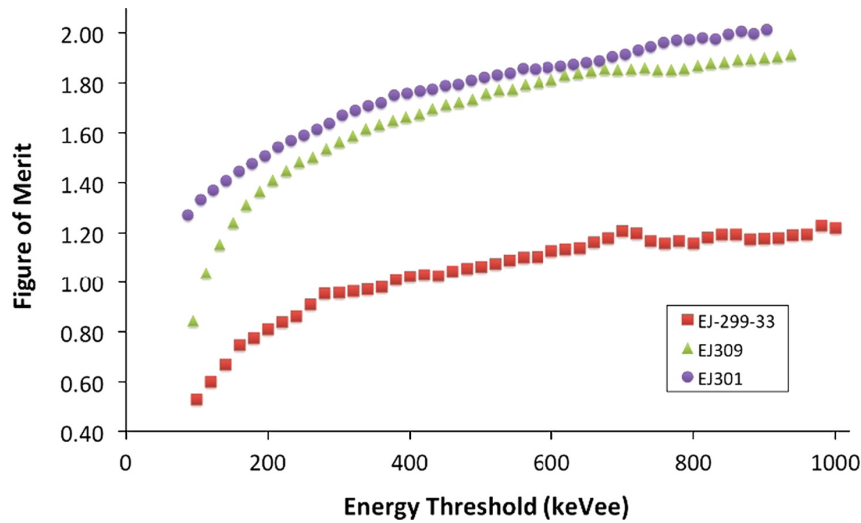

Figure 8.12: FOM plot for EJ-299-33 with optimized parameters and 200 keVee energy threshold

Results from the plastic scintillator show that energy and time resolutions are very similar to those obtained with liquids, but the pulse shape discrimination capability is markedly lower, becoming critical at low energy where neutron and gamma ray are hardly separated. However, the general characteristics of this prototype certainly support the possibility of its use in applications where large active volumes/areas are required.

8.5 Use of flat panel photomultiplier

Photomultipliers (PMTs) belong to the category of light sensors: they act as converting devices from visibile light into electric signals. Their use in radiation detection is necessary to bring the very weak light emitted by a scintillator to a form that can easily be analyzed to extract physical information.

Two key aspects dominates the operations of a PMT: the conversion efficiency and the linearity in the multiplication process. The former is a function of the material chosen as a photocatode, the latter depends on the internal structure of dynodes. Both have been greatly improved over the years and the performances of standard PMTs are weel suited for the use with most common scintillators.

One issue can rise when operating PMTs in special environmental conditions: the sensitivity to external magnetic fields. The multiplication process is based on a sequence of perfectly tailored accelerating electric fields; external magnetic fields can bend the trajectories of the electrons, causing them to miss the electrodes and resulting in a drop of the amplification factor.

The problem of sensitivity of PMTs to external magnetic fields can be addressed by manufacturing so-called "flat panel" PMTs: these are PMTs that operate on the same principles as standard PMTs, but are designed to minimize the length of the multiplication

stage, and thus reducing the path of the electrons and the possibility that they are deviated away from the dynode electrodes. The compact design also has the advantages of reduced power consumption, making it suitable for use inside low-power instrumentation, at a cost comparable to that of standard PMTs.

In a recent work from our group [54], we studied the properties of EJ-309 liquid scintillator, comparing its performances with a standard PMT to whose when coupled to a Flat Panel PMT. Two detectors have therefore been studied, consisting of two cylindrical EJ-309 liquid scintillator cells 50 mm diameter × 50 mm length. One cell was coupled to an H1949-51 HAMAMATSU linearly focused 12 dynodes photomultiplier (PMT) through an EJ-560 silicon rubber interface. This will be referred to as Detector A in the following. A second cell was coupled also through an EJ-560 interface to an H8500 HAMAMATSU flat panel position sensitive photomultiplier (Fig. 8.13) referred to as Detector B. The PSPMT has a square active area of about 50 mm × 50 mm which is divided in 64 independent anodes (pixels). In our application all anodes' outputs were connected together so that the position capability was not used.
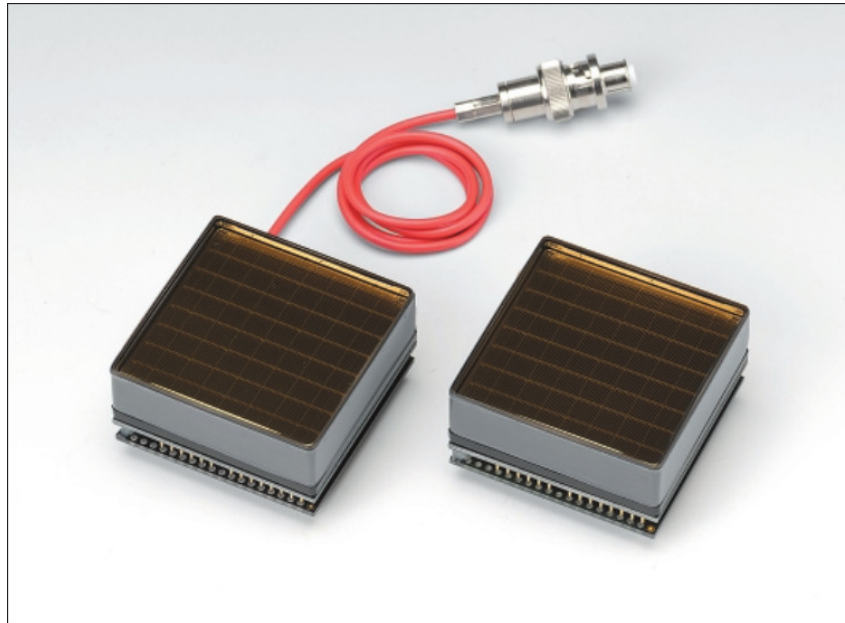
Figure 8.13: Hamamatsu H8500 PSPMT. Left: HV cable input type; right: HV pin input type

Table 8.3 compares the major technical features of the two detectors:

	Detector A	Detector B	
PMT	H1949-51	H8500	
Max diameter	75	75	[mm]
Total length	320	127	[mm]
Total weight	900	490	[g]
Operating voltage	-1600	-1050	[V]
Divider current	0.80	0.20	[mA]

Table 8.3: Comparison between Detector A and B major features

The energy calibration of the scintillation light was based on the procedure described in Sec. 8.2. The calibration procedure made it possible to extract the detector pulse height

resolution by determining the spreading width σ needed to reproduce the Compton Edge structures. The energy resolution, defined in the following as σ/L where L is the energy value of the Compton Edge, is shown in Table 8.4.

	Detector A	**Detector B**	
σ/L @ 511 keV	8.8	8.2	[%]
σ/L @ 1275 keV	5.0	4.7	[%]

Table 8.4: Energy resolutions of the two assemblies

The slightly better energy resolution obtained with the H8500 PSPMT is most probably related to the size of the photocathode (460 mm diameter for the H1949-51) and the slightly larger photocathode quantum efficiency of the PSPMT (>20% in the range 300-400 nm) compared to that of the H1949-51 assembly (<20% in the same wavelength range).

The pulse shape discrimination (PSD) of the two detectors was studied using a weak ^{252}Cf source (0.7×10^4 neutron/s) placed about 15 cm from the detector front face. Typical PSD versus energy scatter plots are shown in Fig. 8.14. It is worth noting that Detector A exhibits an increase of the PSD parameter for gamma pulses having energy larger than 2000 keVee, probably because of saturation phenomena in the PMT.

PSD spectra reported in Fig. 8.15 have been produced by setting an energy window of (480 ± 75) keVee. The FoM of Detector A is 1.87, slightly better than the value 1.73 obtained with Detector B. Since we hard-wired 64 independent pixels of Detector B to obtain a single signal, the shape of the analog sum suffers from the time jitter contributed by each pixel, thus explaining the small difference in FoM with respect to Detector A.

The detectors have then been tested while operating in a magnetic field. Gamma ray spectra from a ^{22}Na source were measured with the detectors positioned in the proximity of a dipolar electromagnet. The magnetic field value at the detector position was measured by a Hall probe (LABORATORIO ELETTROFISICO model DG4080 with a Hall probe FW BELL model STD 58-0404). The spectra measured with Detector A and B for different magnetic field values are reported in Fig. 8.16, respectively in the upper and lower panel. The gain of Detector A's photomultiplier decreases as the magnetic field increases, with a corresponding deterioration of the energy resolution. As an example, the pulse height corresponding to the 1275 keV Compton Edge is reduced by 70-80% at about 60 Gauss, with an increase of σ/L from 5% to 11%. The behavior of Detector B is rather different, the reduction of the Compton Edge position is within 20% when the field is about 250 Gauss with a consequent deterioration of σ/L of the same order. This effect is certainly related to the larger distance between adjacent dynodes in the linearly focused PMT, while in the Flat Panel design the dynode structure is much more compact. The lowering of the final gain is due to magnetic deflection of electrons which is much less severe for the shorter PSPMT.

Further tests were performed by measuring gamma-gamma coincidences with a ^{22}Na source using a fast plastic scintillator (EJ-228 2" × 2" coupled to a XP2020 PMT) as a reference detector, to determine the time resolution for both PMTs. The contribution to the overall time resolution of the fast plastic was experimentally determined by running two such detectors in coincidence. Data were acquired with the DT5751 digitizer and the time correlation between coincident signals was reconstructed using a Digital Constant Fraction Discriminator (DCFD) [62, 63].

Results are reported in Fig. 8.17 where the time resolutions of single detectors (fast

a

b
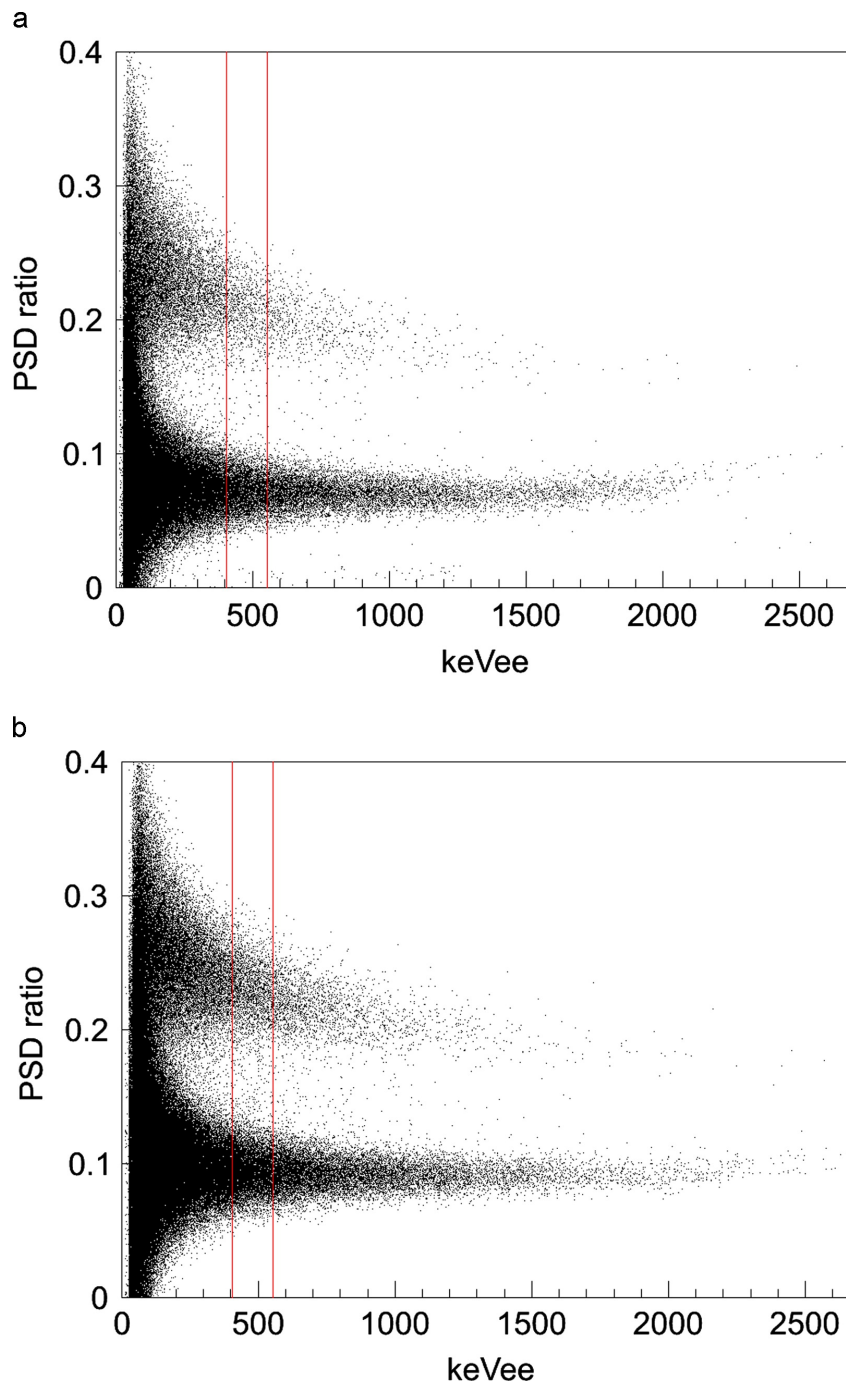
Figure 8.14: PSD plots: left panel Detector A, right panel Detector B
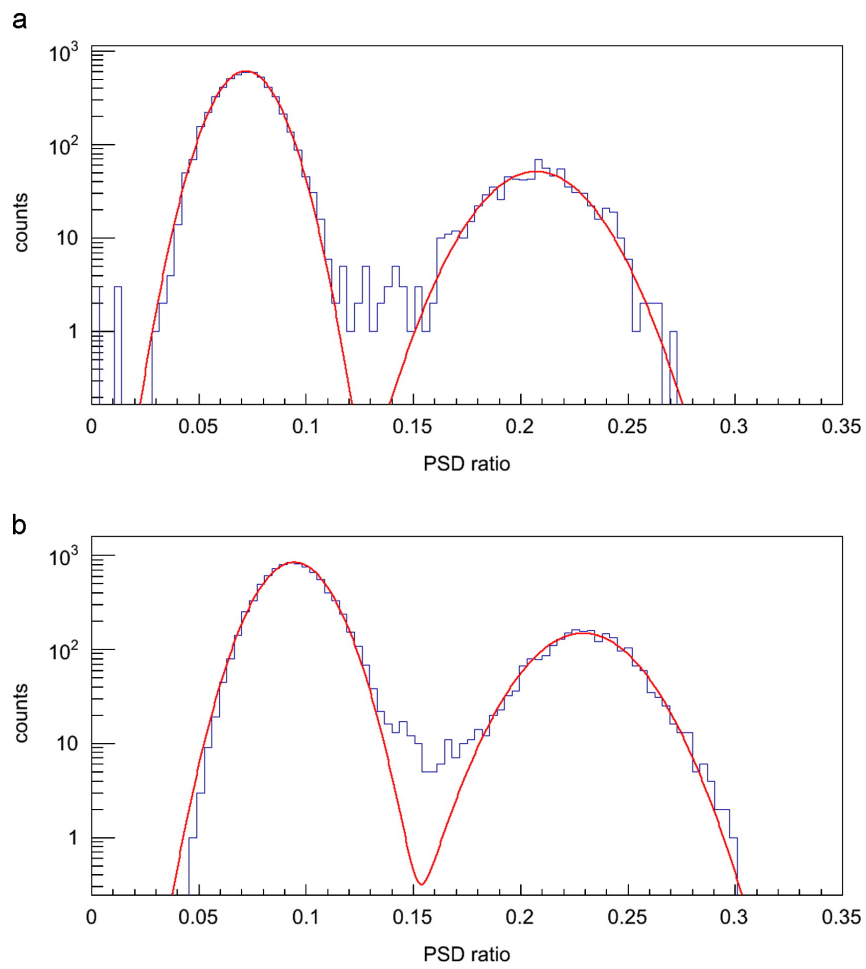
Figure 8.15: Pulse shape spectra for (480 ± 75) keVee energy window: left panel Detector A, right panel Detector B
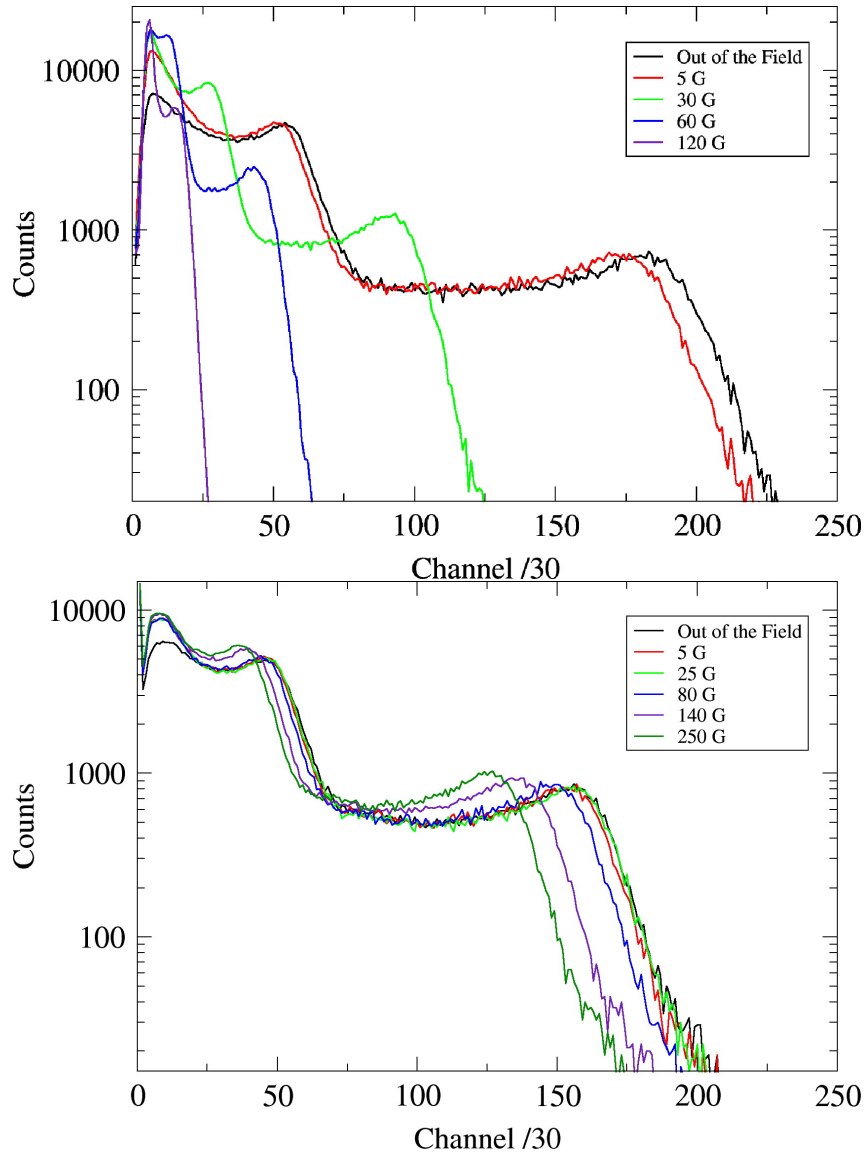
Figure 8.16: Pulse height distributions measured for different magnetic field values: upper panel Detector A, lower panel Detector B

plastic EJ-228, Detectors A and B) are reported as a function of the energy threshold in the DCFD. It appears that hard-wiring all the anodes of the H8500 PSPMT results in a worsening of the time resolution with respect to that obtained with a linearly focused PMT. However, it is worth mentioning that a sub-nanosecond time resolution is obtained even at 100 keV low-energy threshold, well within the needs of several applications. As a conclusion, Flat panel PMTs proved to have performances comparable to those of standard PMTs, but with an exceptional stability while operating in high magnetic fields.
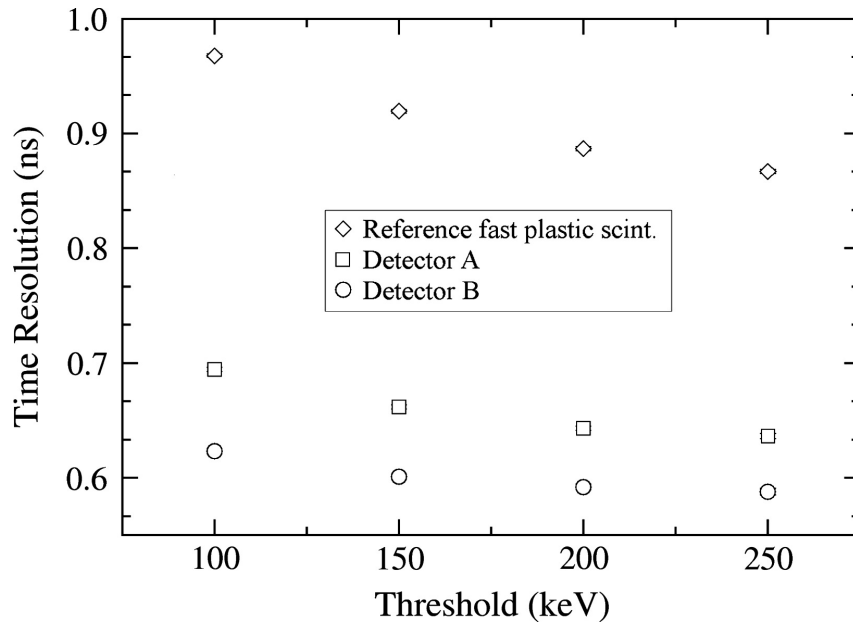
Figure 8.17: *Time resolution of a single scintillation detector as measured with a ^{22}Na source as a function of the DCFD energy threshold. Circles, squares and diamonds refer to the reference fast plastic detector, Detector A and Detector B, respectively*

Bibliography

[1] R.A. Falkernrath et al., *America's Achilles Heel*, 1998, Cambridge, MA: The MIT Press

[2] Reuters, *Race against time to prevent nuclear terror*, November 9, 2004

[3] S. Fetter et al., *Detecting nuclear warheads*, Science & Global Security, 1990, vol. 1, 225

[4] R. Chandra et al., *Fast neutron detection in homeland security applications*, IEEE NSS CR, 2010

[5] T.E. Valentine, *Evaluation of Prompt Fission Gamma Rays for Simulating Nuclear Safeguard Measurements*, Report ORNL/TM-1999/300

[6] http://ec.europa.eu/research/index.cfm

[7] P. Buzhan et al., *Silicon photomultiplier and its possible applications*, Nucl. Instr. Meth. A 504 (2003) 48-52

[8] B. Dolgoshein et al., *Status report on silicon photomultiplier development and its applications*, Nucl. Instr. Meth. A 563 (2006) 368-376

[9] M. Caccia et al., *Silicon Photomultiplier readout of a scintillating noble gas detector for homeland security*, ANIMMA - Advancement in Nuclear Instrumentation Measurement Methods and their Applications Marseille (France), June 22-27, 2013, DOI: 10.1109/ANIMMA.2013.6727974

[10] IAEA, *Technical and Functional Specifications for Border Monitoring Equipment*, NUCLEAR SECURITY SERIES NO. 1 TECHNICAL GUIDANCE, 2nd edition

[11] ANSI N42.34-2006, *Performance Criteria for Hand-Held Instruments for the Detection and Identification of Radionuclides*

[12] US Domestic Nuclear Detection Office (DNDO), *Technical Capability Standard for Handheld Instruments Used for the Detection and Identification of Radionuclides*

[13] US Domestic Nuclear Detection Office (DNDO), *Technical Capability Standard for Vehicle Mounted Mobile Systems*

[14] M. Voytchev, P. Chiaro, R. Radev, *Development of international standards for instrumentation used for detection of illicit trafficking of radioactive material*, Radiation Measurements 44 (2009) 1-5

[15] IEC 62244, *Radiation protection instrumentation - Installed radiation monitors for the detection of radioactive and special nuclear materials at national borders*

[16] IEC 62327, *Hand-held instruments for the detection and identification of radionuclides and additionally for the indication of ambient dose equivalent rate from photon radiation*

[17] G.W. Phillips, D.J. Nagel and T. Coffey, *A Primer on the Detection of Nuclear and Radiological Weapons*, Center for Technology and National Security Policy National Defense University, July 2005

[18] G.F. Knoll, *Radiation detection and measurements*, 2000, John Wiley & Sons

[19] J. B. Birks, *The Theory and Practice of Scintillation Counting*, Pergamon Press Ltd., 1964

[20] Scionix, *Crystal Properties*, http://www.scionix.nl/crystals.htm (retrieved 12/12/2014)

[21] R.A. Austin, *High-pressure xenon detector development at Constellation Technology Corporation*, Nucl. Instr. Meth. A 579 (2007) 58

[22] V.V. Dmitrenko et al., *High-pressure xenon detectors for gamma-ray spectrometry*, Applied Radiationand Isotopes 52 (2000) 739-743

[23] F. Resnati et al., *Suitability of high-pressure xenon as scintillator for gamma ray spectroscopy*, Nucl. Instr. Meth. A 715 (2013) 87-91

[24] T. Nakagawa, H. Kawasaki and K. Shibata, *Curves and tables of neutron cross section in JENDL-3.3 (Part I and II)*, JAERI-Data/Code 2002-02, 2002.

[25] L.J. Wittenberg, E.N. Cameron, G.L. Kulcinski, S.H. Ott, J.F. Santarius, G.I. Sviatoslavsky, I.N. Sviatoslavsky, H. Thompson, *A review of helium-3 sources and acquisition for use as fusion fuel*, WCSAR-TR-AR3-9107. Fusion Technology, Special Issue on DHe3 Fusion, 21(4), (1991) pp. 2230-2253

[26] R.T. Kouzes, *The 3He supply problem*, Technical Rpt. PNNL-18388Pacific Northwest National Laboratory, Richland, WA (2009)

[27] R.T. Kouzes et al., *Neutron detection alternatives to 3He for national security applications*, Nucl. Instr. Meth. A 623 (2010) 1035-1045

[28] H. Klein and F.D. Brooks, *Scintillation detectors for fast neutrons*, 2006, Proceedings of Science (FNDA2006) 097

[29] N. Zaitseva, et al., *Plastic scintillators with efficient neutron/gamma pulse shape discrimination*, Nucl. Instr. Meth. A 668 (2012) 88

[30] C. Matei, et al., *Proton light output function and neutron efficiency of a p-terphenyl detector using a ^{252}Cf source*, Nucl. Instr. Meth. A 676 (2012) 135

[31] *Production of Stilbene for Fast Neutron Detection*, Inrad Optics white paper (2012), `http://www.inradoptics.com/optics-resources/white-papers/` (last accessed 13/12/2014)

[32] Eljen Technology, *EJ-299-33 Data Sheet*, http://www.eljentechnology.com/

[33] R.Chandra et al, *Fast neutron detection with pressurized ^{4}He scintillation detectors*, 2012 Journal of Instrumentation 7 C03035 doi:10.1088/1748-0221/7/03/C03035

[34] CAEN White Paper: *Digital Pulse Processing in Nuclear Physics*, 2011; available at www.caen.it under "Document library"

[35] CAEN Guide: *Introduction to Digitizers*, 2014; available at www.caen.it under "Document library"

[36] L. Stevanato et al., *Neutron detection in a high gamma-ray background with EJ-301 and EJ-309 liquid scintillators*, Nucl. Instr. Meth. A 690 (2012) 96-101

[37] P. Blanc et al., *Neutron/gamma pulse shape discrimination in plastic scintillators: Preparation and characterization of various compositions*, Nucl. Instr. Meth. A 750 (2014) 1-11

[38] C.E. Shannon, *Communication in the Presence of Noise*, Proceedings of the Institute of Radio Engineers 37 (1949) 10

[39] F. Belli, et al., *A study on the pulse height resolution of organic scintillator digitized pulses*, Fusion Engineering and Design 88 (2013) 1271

[40] D. Cester et al., *Pulse shape discrimination with fast digitizers*, Nucl. Instr. Meth. A 748 (2014) 33-38

[41] CERN ROOT website, http://root.cern.ch

[42] P.H.G.M. Hendriks et al., *Full-spectrum analysis of natural gamma-ray spectra*, J. Environ. Radioactivity 53 (2001) 365-380

[43] B.R.S. Minty et al., *Multichannel processing for airborne gamma-ray spectrometry*, Geophysics 63 (1999)

[44] IEEE, *American National Standard Data Format for Radiation Detectors Used for Homeland Security*, 2012

[45] A. Nicholson et al., *Day to Day Variations in Neutron and Gamma Ray Background Radiation*, IEEE Transactions on Nuclear Science

[46] A. Iyengar et al., *Systematic measurement of fast neutron background fluctuations in an urban area using a mobile detection system*, Nucl. Instr. Meth. A 773 (2015) 27-32

[47] http://www.arktis-detectors.com/products/security-solutions/

[48] F.D. Brooks, R.W. Pringle, B.L. Funt, *Pulse shape discrimination in a plastic scintillator*, IRE Trans. Nucl. Sci. NS-7 (1960) 35-38

[49] L. Stevanato, et al., *Light output of EJ228 scintillation neutron detectors*, Applied Radiation and Isotopes 69 (2011) 369

[50] N. Kudomi, *Energy calibration of plastic scintillators for low energy electrons by using Compton scatterings of γ rays*, 1999, Nucl. Instr. Meth. A 430, 96-99

[51] E.R. Siciliano et al., *Energy calibration of gamma spectra in plastic scintillators using Compton kinematics* 2008, Nucl. Instr. Meth. A 594, 232-243

[52] C. Guerrero, et al., *Analysis of the BC501A neutron detector signals using the true pulse shape*, Nucl. Instr. Meth. A 597 (2008) 212

[53] Hamamatsu Photoniks K. K., *Photomultiplier Tubes: Basics and Applications*, 2007

[54] D. Cester et al., *A compact neutron-gamma spectrometer*, Nucl. Instr. Meth. A 719 (2013) 81-84

[55] R. C. Runkle, *Neutron sensors and their role in nuclear nonproliferation*, Nucl. Instr. Meth. A 652 (2011) 37-40

[56] Eljen Technologies, *EJ-309 Data Sheet*, http://www.eljentechnology.com/

[57] L. Stevanato, et al., *Neutron detection in a high gamma-ray background with EJ-301 and EJ-309 liquid scintillators*, 2012, Nucl. Instr. Meth. A 690, 96-101

[58] N.V. Kornilov et al., *Total characterization of neutron detectors with a ^{252}Cf source and a new light output determination*, Nucl. Instr. Meth. A 599 (2009) 226-233

[59] N. Zaitseva, L. Carman, A. Glenn, S. Hamel, S.A. Payne, B.L. Rupert, PCT Patent Application WO2012142365, 2012

[60] P. Blanc et al., *Neutron/gamma pulse shape discrimination in plastic scintillators: Preparation and characterization of various compositions*, Nucl. Instr. Meth. A 750 (2014) 1-11

[61] D. Cester at al., *Experimental tests of the new plastic scintillator with pulse shape discrimination capabilities EJ-299-33*, Nucl. Instr. Meth. A 735 (2014) 202-206

[62] A. Fallu-Labruyere et al., *Time resolution studies using digital constant fraction discrimination*, Nucl. Instr. Meth. A 579 (2007), 247-251

[63] L. Stevanato, et al., *High rate read-out of LaBr(Ce) scintillator with a fast digitizer*, Nucl. Instr. Meth. A 678 (2012) 83.

[64] Gilliam, Leigh, Rukhin and Strawderman, *Pass-Fail Testing: Statistical Requirements and Interpretations* 2009, J. Res. Natl. Inst. Stand. Technol. 114, 195-199

[65] Johnson, Kotz and Kemp, *Univariate Discrete Distributions*, 2005, John Wiley & Sons

Appendix A

Statistical foundations of background analysis

As described in 4.3.2, International standards request any instrument to have a certain value of PD (Probability of Detection) to reduce as much as possible the PFA (Probability of False Alarm). In addition, these two values must be defined and experimentally testified for a certain Confidence Level (CL) [64].

According to the requirements, MODES_SNM system must respect the following parameters:

- having a maximum False Alarm Rate of 0.001 (corresponding to 1 False Alarm per hour of operation)

- 90% Probability of Detection

- 95% Confidence Level

This Appendix gives more detailed definitions of FAR, PD and CL, and derives the formula for calculating the thresholds.

A.1 Probability of Detection (PD)

The Probability of Detection is the probability of triggering an alarm in the presence of a real source. The measured variable is the counting of a detector; in the following paragraphs, one event corresponds to one single count (one particle).

Radioactive decays follow Poisson statistics. Poisson distribution is a discrete probability distribution that express the probability for n events to realize in a given time, providing that their medium number is λ. This distribution is also known as "rare event's law"; it is defined as

$$P(n) = e^{-\lambda} \frac{\lambda^n}{n!}$$

for any n belonging to naturals. Once the medium number of background events is known, for a given threshold n Poisson distribution gives the probability to detect n events in a new measurement of the same duration.

	Source present	**No source**
Alarm raised	True Positive (TP)	False Positive (FP)
No alarms	False Negative (FN)	True Negative (TN)

Table A.1: Possible outcomes of source detection

Assuming that the detector produces a normal distribution of responses, two normal distributions are expected as the output, depending on the absence or presence of radioactive sources; they are shown in Fig. A.1.
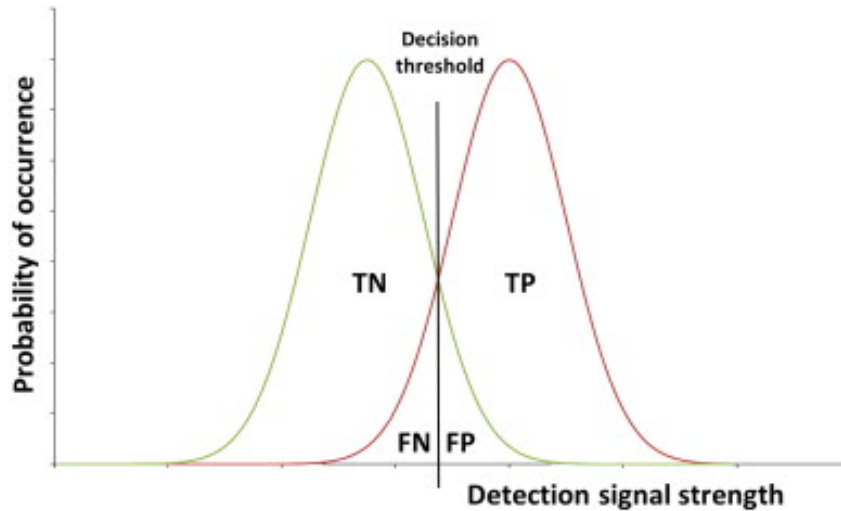

Figure A.1: Probability distribution for countings in absence/presence of sources

Table A.1 describes the four possibile outcomes for a detection system, while Table A.2 defines some practical quantities that directly measure system performances.

Acronym	**Quantity**	**Definition**
TPR	True Positive Rate	TP/(TP+FN)
TNR	True Negative Rate	TN/(TN+FP)
FAR	False Alarm Rate	FP/(FP+TN)

Table A.2: Variables used to measure system performances

In Fig. A.1 the threshold has been set to the value that minimizes misclassifications *on both sides*. This is a rather poor choice for a system like MODES_SNM; since in most operational procedures instrument alarms are followed by manual cargo inspection, international standards tend to limit the FAR and maximize the TPR.

A.2   Confidence Level (CL)

For any number of trials n, the Confidence Level fixes the minimum number of successes m needed to verify a given Probability of Detection. Therefore it represents an estimation of the reliability of the analysis over repeated measurements, and is used to check the performances of a system. This section describes how to calculate the reference value m for a given combination of (CL,n,PD).

PD	0,9	0,8	0,7
PFA	0,1	0,2	0,3
n=2	*	*	*
n=3	*	*	*
n=4	*	*	*
n=5	*	*	*
n=6	*	*	*
n=7	*	*	*
n=8	*	*	*
n=9	*	*	0
n=10	*	*	0
n=11	*	*	0
n=12	*	*	0
n=15	*	0	1
n=20	*	0	2
n=25	*	1	3
n=30	0	2	4
n=40	0	3	6
n=50	1	5	9
n=60	1	6	11

Table A.3: Maximum number of failures for various PD/PFA and attempts n

To begin with the statistical analysis of CL, the Binomial Discrete Density Function $b(m, n, p)$ has to be defined; it is the basis of following definitions:

$$b(m, n, p) = (Pr(BIN(n, p)) = m) = \frac{n!}{m!(n-m)!} p^m (1-p)^{n-m}$$

where $m = 0.1, \ldots, n$ is the number of successful events in the search for hidden materials, in n independent attempts with $p = PD$ (see [65]). PD is here intended as the probability to succeed in finding hidden sources.

Cumulative function $CL(m, n, PD)$, for a given series of n measurements and a number m of successes with a fixed PD, is defined as:

$$CL(m, n, PD) = \sum_{j=0}^{m-1} b(j, n, PD)$$

With $x = 0.1, \ldots n, 0 \leq p \leq 1$, Binomial Cumulative Distribution Function ($BINCDF$) can also be defined as follows:

$$BINCDF(x, n, p) = Pr(BIN(n, p) \leq x) = sum_{k=0}^{x} \binom{n}{k} p^k (1-p)^{n-k}$$

To find the maximum number of identification m_c with a given PD and a desired CL the upper equation must be reversed:

$$BINCDF(m_c - 1, n, PD) \geq CL$$

BINCDF is a discrete step-function in the x variable, hence does not have a continuous inverse function. m_c must be intended as the first integer for which $BINCDF(mc-1, n, PD)$ is greater than CL.

$$m_c = INVBINCDF(CL, n, PD) + 1$$

This reverse function can be found ready-to-use inside statistical function of many spreadsheet, eventually under other names. Some of them do not return the maximum number of positive identification, instead they calculate the maximum number of failures (M_c); in this case we speak of Probability of False Alarm (PFA). The greater the ratio $\frac{M_c}{n}$, the lower will be the PFA. The two quantities are connected by the relation:

$$m_c + M_C = n$$

At this point it is possible to calculate the maximum acceptable number of wrong results for a given PD or PFA with a fixed CL. As an example, for standards requiring a Confidence Level of 95%, Table A.3 contains the maximum number of failures for various PD/PFA and different values of the number of attempts n.

Working with a PD of 90% and at a CL of 95% at least 29 consecutive positive tests are needed to satisfy requirements. The formula $a = \frac{\log(CL)}{\log(PD)}$ returns immediately the required number of consecutive positive results as a function of CL and PD.

Figure A.2: Number of attempts in function of PD and CL
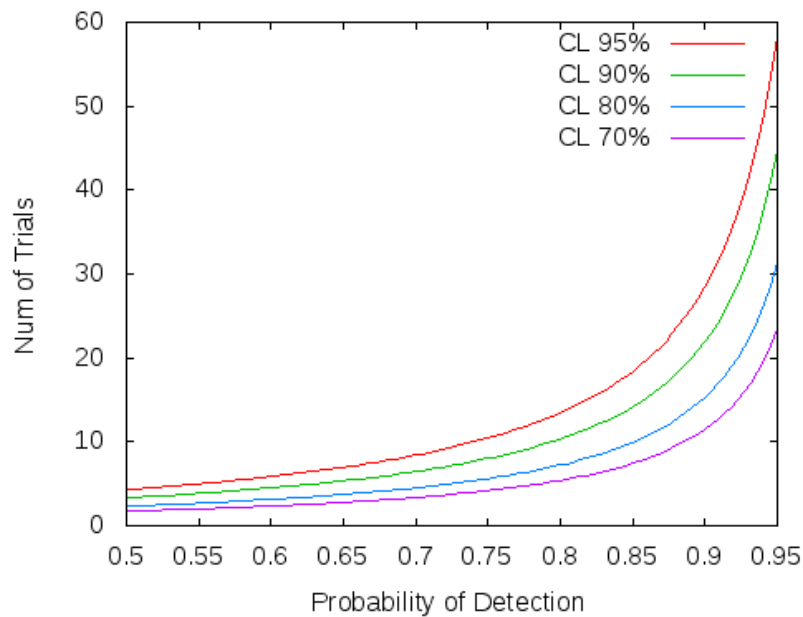
The number of attempts will be the smaller integer greater than a. Fig. A.2 shows the dependance of a as a function of PD for different values of CL.

A.3   Threshold calculation

Once a background measurement of the proper duration has been carried on, and it is known the average number of background events λ, it becomes possibile set a treshold that

satisfies the standards. Given the requirement of 1 False Alarm per hour, and considering a sampling time of 2 seconds, the False Alarm Rate must not exceed $PFA = 0.0\bar{5}\%$ of the total background events. Therefore the corresponding threshold must be set in correspondence of $I_t = 99.9\bar{4}\%$ of the integral of Poisson Distribution; this integral can be expressed as

$$I = \frac{\Gamma(n+1, \lambda)}{n!} \tag{A.1}$$

where $\Gamma(x, y)$ is the *upper* incomplete gamma function and n belongs to natural positive numbers.

Considering Equation A.1, when $I > 1 - PFA$ the first integer n is set as threshold. This condition can be translated as

$$t = \inf\{n | n \in \mathbb{N}, \gamma(n+1, \lambda) > I_t\} \tag{A.2}$$

where $\gamma(x, y)$ is *normalized lower* incomplete gamma functio, λ is the average counting rate during a measurement of standard duration and $I_t = 1 - PFA$. In MODES_SNM the alarms are checked over data samples with a duration of 2 seconds and the background procedure lasts 120 seconds, containing 60 independent intervals; λ is the average counting rate of each of these intervals.
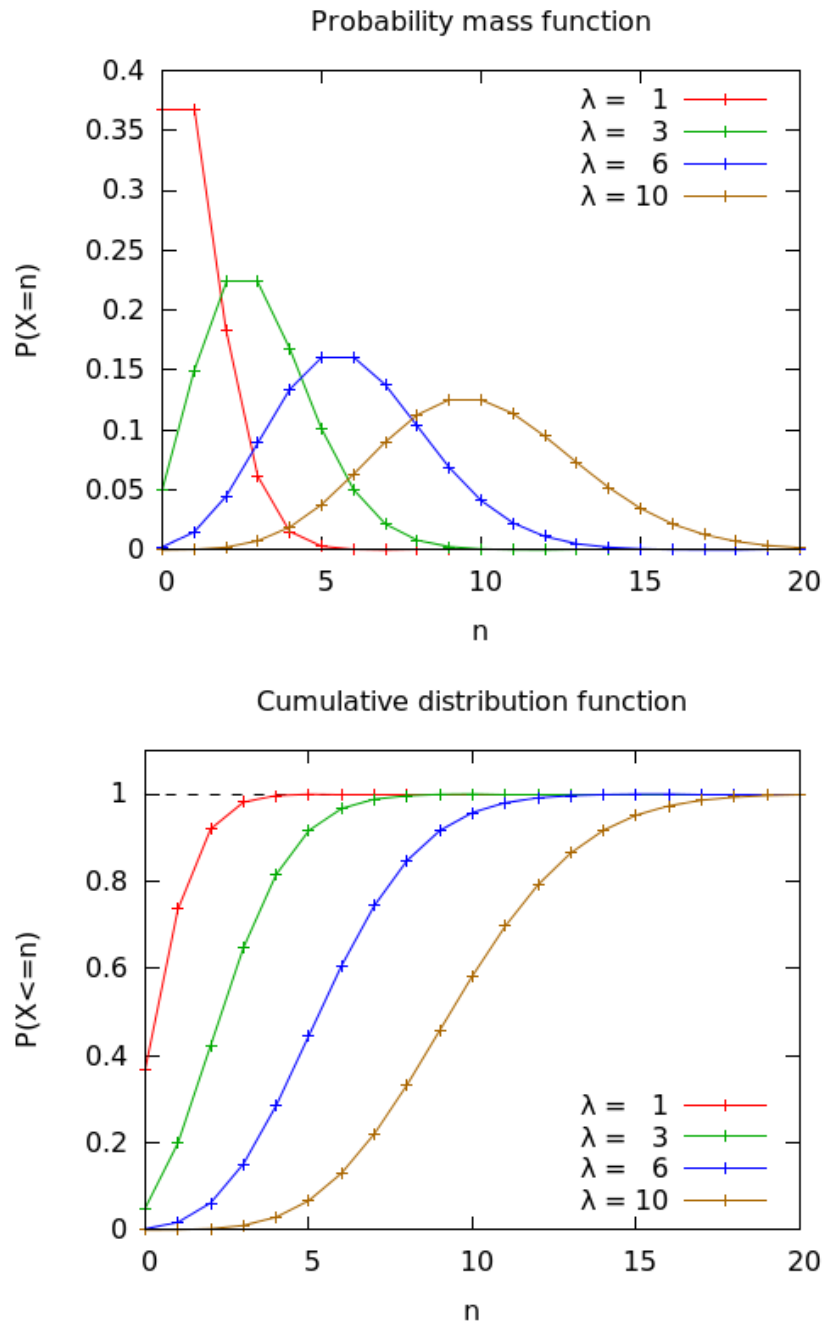
Figure A.3: Poisson Probability Distribution Functions (left panel) and Cumulative Distribution Function (right panel) for different values of the average value λ

Appendix B

N42.42 XML example

```
<?xml version="1.0"?>
<?xml-model href="http://physics.nist.gov/N42/2011/schematron/n42.sch"
type="application/xml" schematypens="http://purl.oclc.org/dsdl/schematron"?>
<RadInstrumentData xmlns="http://physics.nist.gov/N42/2011/N42"
                   xmlns:xsi="http://www.w3.org/2001/XMLSchema-instance"
                   xsi:schemaLocation="http://physics.nist.gov/N42/2011/N42
                                       http://physics.nist.gov/N42/2011/n42.xsd">

  <RadInstrumentInformation id="RadInstrumentInformation-1">
    <RadInstrumentManufacturerName>MODES_SNM
      Consortium</RadInstrumentManufacturerName>
    <RadInstrumentModelName>MODES_SNM</RadInstrumentModelName>
    <RadInstrumentClassCode>Radionuclide Identifier</RadInstrumentClassCode>
    <RadInstrumentVersion>
      <RadInstrumentComponentName>Software</RadInstrumentComponentName>
      <RadInstrumentComponentVersion>2.0</RadInstrumentComponentVersion>
    </RadInstrumentVersion>
  </RadInstrumentInformation>

  <RadDetectorInformation id="RadDetectorInformation-1">
    <RadDetectorCategoryCode>Gamma</RadDetectorCategoryCode>
    <RadDetectorKindCode>NaI</RadDetectorKindCode>
  </RadDetectorInformation>

  <EnergyCalibration id="EnergyCalibration-1">
    <CoefficientValues>-23.9453 0.107291 0</CoefficientValues>
  </EnergyCalibration>

  <RadMeasurement id="RadMeasurement-1">
    <MeasurementClassCode>Calibration</MeasurementClassCode>
    <StartDateTime>2014-10-01T11:46:53+0200</StartDateTime>
    <RealTimeDuration>PT60S</RealTimeDuration>
    <Spectrum id="RadMeasurement-1Spectrum-1"
        radDetectorInformationReference="RadDetectorInformation-1"
        energyCalibrationReference="EnergyCalibration-1">
```

```
<LiveTimeDuration>PT60.0S</LiveTimeDuration>
<ChannelData compressionCode="None">
  808 156 112 96 42 39 59 167 429 1169
  2213 3510 4113 4359 4510 4300 4165 3850 3674 3406
  3223 3103 2809 2632 2578 2455 2307 2136 2201 2100
  1948 1738 1599 1479 1403 1352 1276 1258 1133 1076
  1089 1130 1120 989 940 893 718 703 667 643
  578 615 560 570 616 547 563 583 522 539
  553 544 512 486 435 489 431 453 458 524
  553 599 553 607 527 487 414 376 323 320
  314 297 273 287 299 284 272 285 320 287
  251 296 256 242 278 244 238 249 268 228
  198 224 239 236 224 240 239 266 294 269
  280 274 271 268 276 262 216 216 228 230
  175 192 176 154 158 168 165 153 179 165
  192 209 191 194 207 189 181 163 193 175
  172 155 145 130 150 134 148 131 125 109
  123 84 108 107 89 99 90 93 93 88
  86 90 111 136 136 164 225 286 352 458
  531 615 675 682 614 601 474 419 341 244
  154 102 97 69 63 55 51 52 47 51
  45 48 50 47 27 41 34 35 25 46
  29 33 46 47 55 51 61 58 43 51
  63 42 40 53 36 30 37 41 26 26
  23 14 19 27 18 18 19 20 25 17
  13 14 13 11 9 18 9 16 21 7
  9 17 15 18 23 20 23 30 29 16
  32 16 21 27 26 21 24 22 31 22
  20 27 15 30 22 23 17 14 20 10
  15 14 15 11 8 11 16 4 12 15
  12 9 10 4 11 11 14 21 9 11
  9 15 8 7 15 6 13 24 14 14
  37 39 44 50 63 66 59 58 48 64
  50 54 40 54 38 23 23 16 12 11
  10 4 2 1 2 2 1 0 2 1
  1 0 0 0 0 0 0 0 0 2
  0 2 0 1 0 0 2 0 1 0
  0 0 0 0 0 1 0 1 0 1
  1 0 0 0 0 1 0 0 1 0
  0 0 0 2 0 0 0 0 0 0
  0 0 0 1 0 1 0 0 0 1
  0 1 1 0 0 1 0 0 0 0
  0 0 0 0 0 0 0 1 0 1
  0 0 0 0 0 0 0 0 0 0
  0 0 1 0 0 1 0 0 0 0
  1 0 0 0 0 0 0 2 1 0
  1 0 0 1 0 1 0 1 0 0
  0 0 1 0 1 0 0 0 0 0
  2 0 0 0 0 0 0 1 0 0
```

```
        0 0 0 0 0 0 0 0 0 0
        0 0 0 0 0 0 0 0 0 0
        0 0 2 1 1 0 0 0 0 0
      </ChannelData>
    </Spectrum>
</RadMeasurement>


<RadMeasurement id="RadMeasurement-2">
  <MeasurementClassCode>Background</MeasurementClassCode>
  <StartDateTime>2014-10-01T11:33:44+0200</StartDateTime>
  <RealTimeDuration>PT120S</RealTimeDuration>
  <Spectrum id="RadMeasurement-2Spectrum-1"
      radDetectorInformationReference="RadDetectorInformation-1"
      energyCalibrationReference="EnergyCalibration-1">
    <LiveTimeDuration>PT120.0S</LiveTimeDuration>
    <ChannelData compressionCode="None">
      224 127 85 151 699 2114 4940 8181 10117 10432
      10250 9609 9272 8528 7893 7195 6811 6418 5950 5610
      5234 5086 5089 4681 4151 3588 3345 3212 3063 2903
      2771 2499 2512 2564 2449 2294 1941 1833 1623 1554
      1443 1415 1399 1345 1289 1322 1315 1198 1266 1236
      1245 1193 1149 1079 1064 1016 1181 1165 1300 1302
      1253 1274 1063 972 814 691 655 627 636 667
      595 655 627 658 641 662 629 619 631 637
      609 563 506 514 525 503 511 545 534 591
      612 630 649 637 612 582 570 566 546 469
      412 387 393 384 372 371 353 400 399 429
      486 439 442 460 440 412 422 393 367 326
      326 327 294 330 289 290 279 263 230 216
      226 229 214 213 174 216 245 287 282 424
      544 725 946 1199 1462 1525 1629 1431 1250 1041
      802 558 359 263 190 147 130 129 102 104
      107 120 95 80 75 77 69 93 75 85
      85 109 109 150 134 129 143 156 127 103
      91 92 77 71 72 44 65 50 59 53
      39 37 38 31 38 35 35 27 40 33
      26 41 30 42 47 36 37 49 42 50
      44 69 66 59 54 57 58 72 54 58
      67 61 51 46 37 52 34 39 35 29
      40 30 37 27 26 33 25 17 29 22
      22 29 21 31 29 28 22 24 26 29
      18 31 36 45 53 67 95 95 112 136
      136 123 138 148 138 80 79 76 50 40
      33 22 17 7 10 1 3 4 1 6
      1 1 3 2 3 0 1 1 0 0
      1 1 1 1 3 3 1 0 1 1
      0 0 0 1 2 0 1 1 0 0
      1 0 0 2 0 0 2 0 1 1
      2 1 0 0 0 2 0 0 1 0
```

```
        0 1 0 1 0 0 0 0 2 0
        0 0 0 0 0 1 0 1 3 1
        2 0 0 0 0 1 0 1 0 1
        0 1 1 0 0 0 0 1 1 0
        0 0 1 0 0 0 0 0 1 0
        0 1 0 0 0 1 0 0 0 1
        0 1 0 0 0 3 1 1 2 1
        0 0 0 0 0 0 1 0 0 0
        0 0 0 2 0 1 0 0 0 0
        0 0 0 0 1 1 1 0 0 0
        0 0 1 2 0 0 1 1 1 0
        2 1 1 0 0 0 1 0 3 0
        2 0 0 0 1 0 2 0 1 0
        0 0 0 0 0 2 1 0 0 0
        0 0 0 0 1 0 0 1 0 1
        0 1 0 0 0 0 1 1 0 2
        0 0 0 0 0 1 0 0 0 1
      </ChannelData>
    </Spectrum>
  </RadMeasurement>


  <RadMeasurement id="RadMeasurement-3">
    <MeasurementClassCode>Foreground</MeasurementClassCode>
    <StartDateTime>2014-10-01T11:52:33+0200</StartDateTime>
    <RealTimeDuration>PT29S</RealTimeDuration>
    <Spectrum id="RadMeasurement-3Spectrum-1"
        radDetectorInformationReference="RadDetectorInformation-1"
        energyCalibrationReference="EnergyCalibration-1">
      <LiveTimeDuration>PT29.0S</LiveTimeDuration>
      <ChannelData compressionCode="None">
        73 36 27 46 135 560 1317 2144 2603 2617
        2655 2518 2482 2308 2158 1918 1936 1776 1717 1571
        1484 1526 1401 1367 1229 1060 966 975 895 818
        791 712 683 714 673 630 573 496 521 457
        456 424 420 445 367 419 387 377 387 327
        377 352 330 343 322 307 317 345 390 382
        416 374 363 338 337 324 304 322 304 248
        247 223 230 227 217 217 231 182 228 216
        210 187 188 208 174 207 185 204 226 219
        250 238 250 210 193 205 223 224 182 181
        179 147 153 149 141 155 112 142 142 160
        179 171 198 261 275 330 377 389 357 348
        283 214 167 124 115 101 106 95 152 183
        201 256 295 310 274 299 219 186 152 132
        140 178 203 259 339 377 376 380 305 272
        210 150 103 98 59 45 30 28 32 31
        20 22 31 28 18 13 23 8 27 15
        30 22 23 32 22 33 40 30 22 37
        30 19 23 21 14 14 13 8 17 19
```

```
        14 7 13 20 11 13 6 12 6 5
        10 10 6 8 15 13 9 11 8 16
        11 14 16 13 14 18 8 15 23 15
        14 13 14 10 13 11 13 15 11 8
        8 7 6 10 10 8 6 4 6 8
        6 9 2 8 9 7 3 7 5 7
        3 9 12 7 9 24 25 12 25 26
        27 24 24 38 26 25 15 19 12 13
        12 7 1 5 1 2 1 2 0 0
        1 0 0 1 0 1 1 1 0 0
        0 0 1 0 0 0 0 0 1 0
        1 0 0 0 1 0 0 0 0 0
        1 0 0 0 0 0 0 0 0 0
        0 1 0 0 0 0 0 0 0 0
        0 0 0 0 0 0 0 1 0 0
        0 0 0 0 0 0 1 1 0 0
        0 0 2 1 0 0 0 0 0 1
        0 0 1 0 0 0 0 0 0 1
        0 0 0 0 0 0 0 0 0 0
        1 0 1 3 0 0 0 0 0 0
        0 0 0 1 0 0 0 0 0 0
        0 0 0 0 0 0 0 0 0 0
        0 0 0 0 0 0 0 0 0 0
        0 0 0 0 0 0 0 0 0 0
        0 1 0 0 0 0 0 0 0 0
        0 0 1 0 0 0 0 0 0 0
        0 0 0 0 0 2 0 0 0 0
        0 0 0 0 0 0 0 0 0 0
        0 0 0 0 0 0 0 0 0 0
        0 0 0 1 0 0 0 1 0 0
        0 0 0 0 0 0 1 0 0 0
      </ChannelData>
    </Spectrum>
  </RadMeasurement>

  <NuclideAnalysisResults>
    <Nuclide>
      <NuclideName>60Co</NuclideName>
      <NuclideCategoryDescription>Gamma</NuclideCategoryDescription>
    </Nuclide>
    <Nuclide>
      <NuclideName>137Cs</NuclideName>
      <NuclideCategoryDescription>Gamma</NuclideCategoryDescription>
    </Nuclide>
  </NuclideAnalysisResults>

</RadInstrumentData>
```

Acknowledgements